

Research Articles: Neurobiology of Disease

Tip60's novel RNA-binding function modulates alternative splicing of pre-mRNA targets implicated in Alzheimer's Disease

<https://doi.org/10.1523/JNEUROSCI.2331-22.2023>

Cite as: J. Neurosci 2023; 10.1523/JNEUROSCI.2331-22.2023

Received: 21 December 2022

Revised: 8 February 2023

Accepted: 13 February 2023

This Early Release article has been peer-reviewed and accepted, but has not been through the composition and copyediting processes. The final version may differ slightly in style or formatting and will contain links to any extended data.

Alerts: Sign up at www.jneurosci.org/alerts to receive customized email alerts when the fully formatted version of this article is published.

**Tip60's novel RNA-binding function modulates alternative splicing of
pre-mRNA targets implicated in Alzheimer's Disease**

Akanksha Bhatnagar¹, Keegan Krick²⁺, Bhanu Chandra Karisetty¹⁺, Ellen M. Armour¹,
Elizabeth A. Heller², Felice Elefant^{1*}

¹ Department of Biology, Drexel University, Philadelphia, PA 19103, USA

² Department of Systems Pharmacology and Translational Therapeutics, University of Pennsylvania,
Philadelphia, PA 19104, USA

+ K.K. and B.K. contributed equally to this work and are co-second authors.

* Correspondence should be addressed to Dr. Felice Elefant, Department of Biology, Drexel University,
3245 Chestnut Street, PISB 312, Philadelphia, PA 19104. E-mail: fe22@drexel.edu.

Number of pages: 42

Number of figures: 14

Number of main tables: 6

Number of extended tables: 6

Number of words for abstract: 250

Number of words for introduction: 643

Number of words for discussion: 1499

Competing Interests: Authors declare no competing interests.

Acknowledgements: The research was supported by the National Institutes of Neurological
Disorders and Stroke of the NIH under Award Number R01NS095799 to F.E. We thank Dr. Ann
Ehrenhofer-Murray for generously contributing the *Drosophila*-Tip60 antibody. We also thank Dr.
Harini Sreenivisappa for overseeing microscopic imaging at Drexel University's Cell Imaging
Center.

25

26 **ABSTRACT**

27 The severity of Alzheimer's Disease (AD) progression involves a complex interplay of
28 genetics, age, and environmental factors orchestrated by histone acetyltransferase (HAT)
29 mediated neuroepigenetic mechanisms. While disruption of Tip60 HAT action in neural gene control
30 is implicated in AD, alternative mechanisms underlying Tip60 function remain unexplored. Here, we
31 report a novel RNA binding function for Tip60 in addition to its HAT function. We show that Tip60
32 preferentially interacts with pre-mRNAs emanating from its chromatin neural gene targets in
33 the *Drosophila* brain and this RNA binding function is conserved in human hippocampus and
34 disrupted in *Drosophila* brains that model AD pathology and in AD patient hippocampus of either
35 sex. Since RNA splicing occurs co-transcriptionally and alternative splicing (AS) defects are
36 implicated in AD, we investigated whether Tip60-RNA targeting modulates splicing decisions and if
37 this function is altered in AD. Replicate multivariate analysis of transcript splicing (rMATS) analysis
38 of RNA-Seq data sets from wild-type and AD fly brains revealed a multitude of mammalian-like AS
39 defects. Strikingly, over half of these altered RNAs identified as bona-fide Tip60-RNA targets that
40 are enriched for in the AD-gene curated database, with some of these AS alterations prevented
41 against by increasing Tip60 in the fly brain. Further, human orthologs of several Tip60-modulated
42 splicing genes in *Drosophila* are well characterized aberrantly spliced genes in human AD brains,
43 implicating disruption of Tip60's splicing function in AD pathogenesis. Our results support a novel
44 RNA interaction and splicing regulatory function for Tip60 that may underly AS impairments that
45 hallmark AD etiology.

46

47

48

49

50 **SIGNIFICANCE**

51

52 Alzheimer's Disease (AD) has recently emerged as a hotbed for RNA alternative splicing (AS)
53 defects that alter protein function in the brain yet causes remain unclear. Although recent findings
54 suggest convergence of epigenetics with co-transcriptional AS, whether epigenetic dysregulation in
55 AD pathology underlies AS defects remains unknown. Here we identify a novel RNA interaction and
56 splicing regulatory function for Tip60 histone acetyltransferase that is disrupted in *Drosophila* brains
57 modeling AD pathology and in human AD hippocampus. Importantly, mammalian orthologs of
58 several Tip60-modulated splicing genes in *Drosophila* are well characterized aberrantly spliced
59 genes in human AD brain. We propose that Tip60 mediated AS modulation is a conserved critical
60 post-transcriptional step that may underlie AS defects now characterized as hallmarks of AD.

61

62

63

64

65

66

67 **INTRODUCTION**

68 Alzheimer's Disease (AD) is a chronic late-onset neurodegenerative disorder characterized
69 by an accumulation of amyloid plaques and neurofibrillary tangles, memory impairment and
70 cognitive decline (DeTure and Dickson, 2019;Knopman et al., 2021). The severity of AD progression
71 is dependent in large part, by epigenetic histone acetylation mediated neural gene control
72 mechanisms (Sanchez-Mut and Gräff, 2015;Killin et al., 2016;Nativio et al., 2018). Reduced histone
73 acetylation resulting from decreased histone acetyltransferase (HAT) and/or increased histone
74 deacetylase (HDAC) activity causes chromatin packaging alterations in neurons with concomitant
75 transcriptional dysregulation that is a key initial step in AD etiology (Francis et al., 2009;Graff et al.,
76 2012;Peixoto and Abel, 2013;Lu et al., 2014). In this regard, we previously identified a
77 neuroprotective role by the Tip60 HAT in AD (Zhu et al., 2007;Pirooznia et al., 2012;Johnson et al.,
78 2013;Pirooznia and Elefant, 2013;Xu et al., 2014;Xu et al., 2016;Panikker et al., 2018;Karnay et al.,
79 2019;Zhang et al., 2020;Beaver et al., 2021;Bhatnagar et al., 2023). Increasing Tip60 HAT levels in
80 the brains of *Drosophila* that model AD-associated neurodegeneration protects against AD associated
81 neuroepigenetic deficits that include reduced Tip60 and enhanced HDAC2 chromatin enrichment and
82 concomitant transcriptional dysregulation and ameliorates multiple AD-associated phenotypes
83 including A β plaque accumulation, neural apoptosis, synaptic plasticity, learning/memory, and
84 longevity. Intriguingly, recent insights reveal that histone modifying enzymes, such as HDACs, not
85 only determine which genes are expressed but also how the transcribed RNA is ultimately spliced
86 (Luco et al., 2011;Rahhal and Seto, 2019;Agirre et al., 2021). Thus, while the role of Tip60 HAT
87 activity in chromatin mediated gene expression is well established, it remains to be studied if Tip60
88 has the ability to modulate alternative splicing decisions that may in part contribute towards its
89 neuroprotective abilities.

90

91 In addition to the catalytic HAT domain, Tip60 also contains an N-terminus chromodomain
 92 that acts as a code reader that recognizes distinct methylated-lysine histone tails (Sun et al.,
 93 2009;Kim et al., 2015). Elegant studies have shown that chromodomains within certain proteins have
 94 the ability to directly interact with RNA that likely aids in chromosomal recruitment and targeting
 95 (Akhtar et al., 2000;Bernstein and Allis, 2005;Morales et al., 2005;Bernstein et al., 2006;Shimojo et
 96 al., 2008;Ishida et al., 2012;Akoury et al., 2019). Interestingly, a closely related HAT belonging to
 97 the same MYST superfamily as Tip60, MOF, is dependent on its chromodomain-RNA binding for
 98 integration into chromosomal complexes and dosage compensation (Akhtar et al., 2000). Tip60
 99 chromodomain has also been shown to be critical for its recruitment to chromatin-rich regions in
 100 human cell lines as chromodomain mutations cause Tip60 mislocalization (Sun et al., 2009;Kim et
 101 al., 2015). Additionally, chromatin-interacting Heterochromatic Protein 1 (HP1) has been recently
 102 shown to modulate alternative splicing decisions via its direct RNA binding function (Rachez et al.,
 103 2021). However, it remains to be elucidated if Tip60 has RNA binding capabilities and if so, whether
 104 Tip60-RNA binding aid in chromatin recruitment and/or splicing modulation.

105
 106 Here, we uncover a novel RNA binding function for Tip60 HAT that underlies RNA
 107 alternative splicing (AS) regulation in the brain. Genome-wide RNA immunoprecipitation (RIP) and
 108 sequencing of Tip60-bound RNA from *Drosophila* brain reveal Tip60 specifically targets RNAs
 109 enriched for critical neuronal processes implicated in AD. Strikingly, Tip60 targets pre-mRNA
 110 emanating from its chromatin gene targets and this function is conserved in human hippocampal
 111 tissues and disrupted in both *Drosophila* AD-brains that model AD pathology and in AD patient
 112 hippocampal samples. Over half these Tip60 interacting RNAs from AD fly brains exhibit a
 113 multitude of mammalian-like AS defects enriched for in the AD-gene curated database. Notably,
 114 some splicing alterations are partially protected against by increasing Tip60 in the AD fly brain,
 115 suggesting that Tip60 modulates AS decisions for AD-associated RNA targets. Our results support

116 an RNA splicing regulatory function for Tip60 that modulates AS decisions for its unspliced pre-
 117 mRNA targets and that disruption of this Tip60 function in the AD brain may underly AS
 118 impairments that hallmark AD etiology.

119

120 **METHODS**

121 **Fly stocks and crosses**

122 All fly lines were raised under standard conditions at 25°C with 12-hr light/dark cycle on yeasted
 123 *Drosophila* media (Applied Scientific Jazz Mix *Drosophila* Food, Thermo Fischer Scientific). The
 124 w¹¹¹⁸, pan-neuronal driver *elav*^{C155}-*Gal4*, transgenic UAS lines carrying human APP695 isoform
 125 (*UAS-APP*⁶⁹⁵), and Tip60-RNAi mediated knockdown (*UAS-Tip60 RNAi*) were all obtained from
 126 Bloomington Drosophila Stock Center (Bloomington, IN). Generation and characterization of the
 127 double-transgenic *UAS- APP*⁶⁹⁵; *Tip60*^{WT} fly lines are described in (Pirooznia et al., 2012). The
 128 *elav*^{C155}-*Gal4* driver line was crossed with either w¹¹¹⁸ (wild type control), *UAS-APP*⁶⁹⁵ (APP
 129 model), *UAS- APP*⁶⁹⁵; *Tip60*^{WT} (APP; Tip60 model) or *UAS-Tip60 RNAi* (Tip60 RNAi model). For
 130 all experiments, transgene expression levels for APP and/or Tip60 in each UAS fly lines were
 131 revalidated using a quality control qPCR strategy with RNA extracted from the same pooled larval
 132 brains used for RIP-Seq or RIP-qPCR experiments. Although all transgenic fly lines have been well
 133 characterized with appropriate controls, we do not rule out the unpredictable physiological changes
 134 associated with addition of P[w+] transgene for generation of fly lines.

135

136 **Homology modeling and molecular visualization**

137 3D protein structure of *Drosophila* Tip60 chromodomain was generated using SWISS-MODEL
 138 automated protein structure homology modelling server (Waterhouse et al., 2018). X-ray crystallized
 139 structure of *Homo sapiens* Tip60 chromodomain (PDB: 4QQG, chain A) with 79% coverage was

140 used as a modeling template. Post energy-minimization with YASARA Energy Minimization Server
 141 (Krieger et al., 2009) and stereochemical quality checks with ProCheck server (Laskowski et al.,
 142 1993), the resultant *Drosophila* Tip60 chromodomain model was exported as a PDB file. All
 143 visualization and molecular alignments were performed using PyMOL molecular viewing software
 144 (DeLano, 2002).

145

146 ***In silico* RNA target predictions**

147 Tip60's RNA interaction probabilities were calculated using the RNA-protein interactions prediction
 148 (RPISeq) server (Muppirala et al., 2011). RNA sequences of key genes involved in synaptic plasticity
 149 were obtained from the NCBI database. Input protein sequences containing either only the
 150 chromodomain region or the full protein *Drosophila* Tip60 protein (Q960X4) were submitted. Each
 151 interaction was scored between 0 to 1 using support vector machine (SVM) classifier.

152

153 **Multiple sequence alignment and secondary structure prediction**

154 Protein sequences of Esa1 in *Saccharomyces cerevisiae* (Q08649) and Tip60 from *Drosophila*
 155 *melanogaster* (Q960X4), *Homo sapiens* (Q92993), *Pongo abelii* (Sumatran orangutan) (Q5RBG4),
 156 *Mus musculus* (Q8CHK4), and *Rattus norvegicus* (Q99MK2) were obtained from UniProt
 157 Knowledgebase (Consortium, 2020). Protein sequences were aligned using Clustal Omega multiple
 158 sequence alignment tool (Sievers et al., 2011) with default parameters. Alignment results were
 159 visualized using Jalview bioinformatics software (Waterhouse et al., 2009). Secondary structure
 160 predictions were performed using protein sequence alignment of yeast Esa1 and *Drosophila* Tip60 on
 161 the 'Easy Sequencing in PostScript' (ESPrpt) program (Robert and Gouet, 2014).

162

163 **Polytene chromosome squashes, staining and imaging**

164 Polytene chromosomes were prepared from wildtype third instar larvae and were fixed and stained
 165 according to conventional squash technique using acid fixation as previously described (Johansen et
 166 al., 2009). For RNase treatment, salivary glands were incubated in PBS with 0.4% PBT for 5 minutes
 167 and RNase (500µg/ml, Thermo Scientific EN0531) for 15 minutes before proceeding with fixation.
 168 Primary antibodies used were guinea-pig anti-dTip60 (1:5,000; from (Schirling et al., 2010)), mouse
 169 anti-RNA polymerase-II (1:400, Sigma: 05-623), and rabbit anti-acetyl-Histone H3 Antibody (1:400,
 170 Sigma 06-599). Secondary antibodies used were Alexa Flour 488, 568 and 633 (Invitrogen) at 1:200.
 171 DNA on chromosomes was counterstained using DAPI dye. Confocal microscopy was performed
 172 using laser scanning Fluoview Olympus microscope (FV-1000, Olympus Lifesciences) at 60X
 173 magnification using z-stacks. Sequential scanning mode was used to detect fluorophores in two
 174 different phases to avoid crosstalk. Images were processed using ImageJ software.

175

176 **rMATS splicing analysis**

177 For splicing analysis, clean reads from Input samples were aligned to the *Drosophila melanogaster*
 178 genome (Ensembl version BDGP6) using STAR (Dobin et al., 2013). Splice isoform switching
 179 events were detected using replicate Multivariate Analysis of Transcript Splicing (rMATS) (Shen et
 180 al., 2014). Alternative splicing was quantified using the percent spliced in (PSI) metric that reports
 181 inclusion or splicing of an event such that $PSI = \text{Inclusion} / (\text{Inclusion} + \text{Exclusion})$. For genotypic
 182 comparisons, differences in relative isoform abundance were calculated as ΔPSI values: $\Delta PSI(\text{APP}$
 183 $\text{vs. wildtype}) = PSI_{\text{APP}} - PSI_{\text{wildtype}}$; and $\Delta PSI(\text{APP;Tip60 vs. APP}) = PSI_{\text{APP;Tip60}} - PSI_{\text{APP}}$. Positive
 184 ΔPSI values indicate higher inclusion in APP over wildtype and APP;Tip60 over APP, respectively.
 185 Significant splicing events were identified using the cutoffs: $FDR < 0.1$ and $|\Delta PSI| \geq 0.1$. Conserved
 186 human orthologs were predicted using best match from DRSC Integrative Ortholog Prediction Tool
 187 (DIOPT) (Hu et al., 2011).

188

189 **RNA Immunoprecipitation and Sequencing (RIP-Seq)**

190 Magna RIP RNA-binding protein immunoprecipitation kit (Millipore) was used for native, more
 191 direct RNA immunoprecipitation without protein cross-linking. 200 *Drosophila* third instar larval
 192 brains were dissected in ice-cold PBS and teased apart with a Dounce homogenizer. The tissue was
 193 resuspended in RIP lysis buffer post centrifugation at 1,500 rpm for 5 minutes. In each tissue lysate
 194 sample, 10% fraction was kept aside for total RNA purification (INPUT RNA) and the remaining
 195 90% were used for RNA immunoprecipitation (IP RNA). Magnetic beads were prepared according to
 196 the protocol using rabbit-Tip60 antibody (Abcam ab23886, 7.5µg), and normal rabbit IgG (7.5µg)
 197 was used as a negative control. The pretreated beads and tissue lysate were mixed and incubated with
 198 rotation overnight at 4°C. After washing with RIP wash buffer for five times, protein was digested
 199 using proteinase K treatment. RNA was phenol– chloroform precipitated from IP and INPUT
 200 samples in parallel. RNA purity and integrity were assessed using Nanodrop spectrophotometer
 201 (Thermo Fisher Scientific, MA, USA) and RNA 6000 Nano assay on 2100 Bioanalyzer (Agilent
 202 Technologies, CA, USA). Whole transcriptome sequencing was performed on IP and INPUT RNA
 203 samples using DNBSEQ sequencing technology platform (BGI Genomics, China) with 100-bp
 204 paired-end reads. Low-quality raw reads were filtered out using in-house BGI genomics pipeline on
 205 SOAPnuke (BGI-flexlab) (Chen et al., 2018). Clean RNA reads were aligned to the *Drosophila*
 206 *melanogaster* genome (Ensembl version BDGP6) using HISAT2 (Kim et al., 2019). Reads were
 207 mapped using Bowtie2 (Langmead and Salzberg, 2012) and gene expression was quantified using
 208 RNA-Seq by Expectation-Maximization (RSEM) (Li and Dewey, 2011). Principal component
 209 analysis (PCA) and heatmap clustering (Euclidean distance) were performed to cluster the samples
 210 and identify the batch effects and sample heterogeneity. All plots were constructed using R/
 211 Bioconductor. Gene ontology biological processes and human disease relevance was assessed using
 212 FlyEnrichr, a gene list enrichment analysis tool for *Drosophila melanogaster* (Chen et al., 2013).

213 Read distribution was assessed using Resect RNA-seq Quality Control package (Wang et al., 2012)
 214 on individual BAM files and *Drosophila* dm6 RefSeq genome bed file (O'Leary et al., 2016), and the
 215 output was visualized using MultiQC modular tool (Ewels et al., 2016).

216

217 **RNA Immunoprecipitation and RT-qPCR (RIP-qPCR) on human hippocampal tissues**

218 For all human studies, human hippocampal samples were obtained from the National Disease
 219 Research Interchange (NDRI), with informed consent by all donors. The control brains included
 220 three males with an age range of 70–85 years. The AD brains were from one male and two females
 221 with an age range of 73–87 years. For RNA Immunoprecipitation, frozen hippocampal tissues were
 222 disrupted in liquid nitrogen using Cryo-Cup Grinder (BioSpec Products). Lysate were processed with
 223 either rabbit-Tip60 antibody (Abcam ab23886, 7.5µg) or normal rabbit IgG (7.5µg). Protein was
 224 digested using proteinase K treatment and RNA was phenol–chloroform precipitated. For RT-qPCR
 225 analysis, cDNA was prepared using the SuperScript II reverse transcriptase kit (Invitrogen) according
 226 to the manufacturer's instructions with 1µg of total RNA. RT-qPCRs were performed in a 10µl
 227 reaction volume containing cDNA, 1µM Power SYBR Green PCR Master Mix (Applied
 228 Biosystems), and 10µM forward and reverse primers. Primers are listed in **Table 1**. RT-qPCR was
 229 performed using an ABI 7500 Real-Time PCR system (Applied Biosystems) following the
 230 manufacturer's instructions. Fold enrichment for all the respective genes was calculated relative to
 231 the non- specific Rabbit IgG antibody control.

232

233 **Splice-specific qPCR**

234 Total RNA was isolated from 40 staged third instar larval brains using the Quick-RNA Miniprep kit
 235 (Zymo research). cDNA was prepared using the SuperScript II reverse transcriptase kit (Invitrogen)
 236 according to the manufacturer's instructions with 1µg of total RNA. Isoform specific exon-exon
 237 junction primers were designed using NCBI Primer-BLAST. The primer pair specificity was

238 analyzed using the reference sequence database of *Drosophila melanogaster* (taxid: 7227). RT-
239 qPCRs were performed in a 10 μ l reaction volume containing cDNA, 1 μ M Power SYBR Green PCR
240 Master Mix (Applied Biosystems), and 10 μ M forward and reverse primers. Primers are listed in
241 **Table 2**. RT-qPCR was performed using an ABI 7500 Real-Time PCR system (Applied Biosystems)
242 following the manufacturer's instructions. Fold change in mRNA expression was determined by the
243 delta-deltaCt method relative to wildtype using Rpl32 as housekeeping gene.

244

245 **Experimental Design and Statistical analysis**

246 All statistical analysis were performed using GraphPad Prism version 9.4.0 software package.
247 Statistical analysis of RNA-Seq data differences between two groups were considered statistically
248 significant with $q < 0.05$ (false discovery rate [FDR] < 0.05 , controlled by Benjamini–Hochberg).
249 For identification of Tip60-RNA targets significantly enriched in IP over Input, a threshold cutoff of
250 adjusted p-value < 0.05 was used. Volcano plots comparing Tip60's RNA targets significantly
251 enriched in wildtype, APP and APP;Tip60 were generated using a threshold cutoff of adjusted p-
252 value < 0.05 and \log_2 Fold Change of ≤ -0.583 and ≥ 0.583). Alternative splicing events significantly
253 altered between genotypes were identified using FDR < 0.1 . Volcano plots depicting difference in
254 relative isoform abundance between genotypes were generated using a threshold cutoff of FDR < 0.1
255 and $|\Delta\text{PSI}| \geq 0.1$, where PSI = percent spliced in. For splice-specific RT-qPCR, statistical
256 significance between the two groups was calculated using unpaired Student's t-test with $p < 0.05$. For
257 Tip60 IP fold enrichment in healthy vs AD human tissues, two-way ANOVA with Sidak's multiple
258 comparison test was used with $p < 0.05$.

259

260

261

262 RESULTS

263 I. Structural homology and evolutionary conservation of *Drosophila* Tip60 RNA binding 264 residues across mammalian species supports their critical functional significance.

265 Chromodomains are protein–RNA interaction modules (Akhtar et al., 2000), yet it remains to
266 be determined if the Tip60 chromodomain structure is primed for an RNA-binding function.
267 Structural studies on Esa1 HAT, the common ortholog of Tip60 and MOF HATs in yeast, have
268 mapped its RNA-binding activity to a specific helical turn structural motif (η 2) in its chromodomain
269 (Shimojo et al., 2008). Using protein secondary structure predictions, we found structural
270 conservation between Tip60 and Esa1 chromodomains, especially at the RNA-binding helical turn
271 motif (η 2) (**Figure 1A**). Similarly, protein structure superimposition shows Tip60 chromodomain
272 folds into an almost identical 3D structure as the Esa1 chromodomain with minimal structural
273 divergence of 1.02 root mean square deviation (**Figure 2A**). Importantly, Tip60 chromodomain
274 contains the predicted tudor-knot conformation and the RNA-binding helical turn motif essential for
275 RNA-binding in Esa1 (Shimojo et al., 2008), supporting functional similarity for putative Tip60-
276 RNA binding. Since Tip60 plays a crucial role in synaptic plasticity (Sarathi and Elefant, 2011; Beaver
277 et al., 2020), we next assessed whether key mRNA involved in synaptic plasticity are predicted to
278 interact with the Tip60 chromodomain and full protein. Using the *in silico* RNA-protein interaction
279 prediction server (Muppirala et al., 2011), we identified several mRNA candidates strongly predicted
280 to interact with the Tip60 chromodomain (**Figure 1B**). These results support an RNA-binding
281 function for Tip60's chromodomain that is predicted to target mRNA enriched for synaptic plasticity.

282
283 Prior work using Esa1 mutational screens identified four precise RNA-binding residues in the
284 chromodomain that completely abolished Esa1's RNA-binding ability when mutated (Shimojo et al.,
285 2008). Notably, these four RNA-binding residues were found to be conserved in Tip60's
286 chromodomain and are exposed at the surface near the RNA-binding turn (**Figure 2B**). The polar

287 nature of all four amino acids- Tyr 57, Tyr 60, Asn64 and Arg66, suggests these residues interact
 288 with RNA via hydrogen bonding, which is a typical characteristic of protein-RNA interactions
 289 (Teplova et al., 2011;Corley et al., 2020). Additionally, the positively charged Arg66 is able to
 290 complement the negatively charged RNA for ionic bonding, another common observation with
 291 protein-RNA binding (Chen and Varani, 2005). In contrast, the proven and predicted Tip60's
 292 histone-binding residues- Trp39, Phe56, Val58, His59, Tyr60, Val61, Phe63, Leu67, Val71, Asp75,
 293 Leu76 (Sun et al., 2009;Letunic and Bork, 2018;Zhang et al., 2018) are mostly non-polar amino acid
 294 residues positioned inside the chromodomain core. Specifically, Tyr60 and Phe63 amino acids
 295 together form an aromatic cage in the Tip60 chromodomain that recognizes methylated lysine
 296 residues for histone acetylation (Zhang et al., 2018). The close proximity of RNA-binding residues
 297 with this aromatic cage and the indispensable role of Tyr60 in both, RNA-binding (Shimojo et al.,
 298 2008) and histone-binding functions (Sun et al., 2009), suggests that these two functions do not occur
 299 simultaneously. Lastly, all RNA-binding residues and most histone binding residues were found to be
 300 evolutionary conserved across mammalian species, indicating their functional importance (**Figure**
 301 **2C**). Together, these results strongly support a novel, conserved RNA-binding function for Tip60
 302 chromodomain that is likely mutually exclusive from its well-studied histone-binding function.

303

304 **II. Tip60 interacts with protein encoding RNAs enriched for neuronal processes implicated in** 305 **cognition and neurodegenerative disorders *in vivo***

306 Since our structural and molecular findings support an RNA-binding function for the Tip60
 307 chromodomain, we asked whether Tip60 directly interacts with RNA molecules *in vivo*. For genome-
 308 centric identification of Tip60-RNA interactions, we utilized a non-crosslinking, native RNA
 309 immunoprecipitation (RIP) technique to extract Tip60-bound RNA from wildtype *Drosophila* larval
 310 brains. We confirmed the presence of RNA molecules in the Tip60-immunoprecipitate that revealed
 311 RNAs at specific nucleotide size (~100-2000 base pairs) in different biological replicates (**Figure**

312 **3A).** Notably, RNA was not detected with non-specific Rabbit IgG and less RNA was
 313 immunoprecipitated with RNAi-mediated Tip60 knockdown, indicating Tip60's RNA binding is
 314 specific *in vivo* (**Figure 3B**). Further, nucleic acid bands were completely lost post RNase treatment,
 315 confirming presence of RNA in the immunoprecipitate samples. Our results uncover a specific and
 316 reproducible RNA-binding function for Tip60 in *Drosophila* brain, *in vivo*.

317
 318 To identify Tip60's RNA targets *in vivo*, we performed whole transcriptome sequencing
 319 (RIP-Seq) on both the Tip60-immunoprecipitated RNA (IP RNA) and total RNA present in tissue
 320 before immunoprecipitation (Input RNA) for enrichment comparison (**Figure 4A**). Heatmap of RNA
 321 enrichment across samples shows two important observations (**Figure 4B**). First, similar RNAs are
 322 immunoprecipitated in all three IP RNA samples, indicative of highly specific Tip60-RNA
 323 interaction. Second, several RNAs enriched in the Input RNA were not immunoprecipitated in the IP
 324 RNA, suggesting Tip60 does not equally favor binding to all RNA molecules. Next, we performed a
 325 principal component analysis (PCA) to observe variation between the samples (**Figure 5A**). As
 326 expected, the IP RNA and Input RNA samples clustered in two separate groups, suggesting limited
 327 sample-to-sample variation. In contrast, there was major variation between the IP and Input RNA
 328 clusters, validating that Tip60's RNA binding function is highly selective and reproducible in
 329 different biological samples. To further confirm Tip60's RNA-binding selectivity, we used the MA
 330 scatter plot that shows log fold change of IP over Input RNA (**Figure 5B**). Using a threshold cutoff
 331 of adjusted p-value <0.05, we identified RNAs significantly different between IP and Input (red
 332 scatters). We then selected for RNAs significantly enriched in IP over input, which we refer to as
 333 'Tip60 RNA targets'. Our RIP-Sequencing identified a total of 2884 Tip60-RNA targets, of which 35
 334 are non-coding RNAs and 2849 are protein encoding RNAs (**Figure 4C, Extended Table 2-1**). To
 335 study biological pathways and disease relevance of the top 2000 Tip60 RNA targets, we used
 336 FlyEnrichr, a gene list enrichment analysis tool for *Drosophila melanogaster* (Chen et al., 2013). Our

analysis revealed that Tip60 RNA targets were enriched for critical dynamic neuronal processes that included axon guidance and axonogenesis, transcription and development (**Figure 4D**). Notable, the majority of these processes are linked to several human diseases with tauopathy and Alzheimer's Disease displaying highest prevalence (**Figure 4E, Extended Table 2-2**). Together, our results identify a highly specific RNA-binding function for Tip60 in the brain *in vivo* that favors interaction with protein encoding RNAs that mediate critical neuronal processes linked to neurodegenerative diseases.

III. Increased Tip60 partially rescues Tip60-RNA targeting alterations in the APP AD associated neurodegenerative brain.

We previously showed that early-preclinical mild cognitive impairments (MCI) and late-stage AD pathologies in humans are tightly conserved both epigenetically and pathologically in the extensively characterized AD associated human amyloid precursor protein (APP) *Drosophila* model (APP AD) (Zhu et al., 2007; Pirooznia et al., 2012; Johnson et al., 2013; Pirooznia and Elefant, 2013; Xu et al., 2014; Xu et al., 2016; Panikker et al., 2018; Karnay et al., 2019; Beaver et al., 2020; Zhang et al., 2020; Beaver et al., 2021; Bhatnagar et al., 2023). This high degree of disease conservation allows for general principles learned from the AD APP fly to be applied to mammalian systems. Our prior studies revealed reduced Tip60 HAT levels with concomitant altered patterns of chromatin histone acetylation and neuronal gene expression in the brains of our APP AD *Drosophila* model that contribute to cognitive deficits and are prevented by increased Tip60 levels. Thus, we asked whether Tip60's RNA-binding function is also perturbed in APP AD flies and that this defect can be ameliorated by genetically increasing Tip60 levels. To address this question, we assessed Tip60-RNA interactions under pan-neuronally expressed human APP⁶⁹⁵ isoform alone (APP AD model) or in combination with Tip60 wildtype protein (APP;Tip60 model) using RIP-Seq on *Drosophila* larval brains. Transcriptomic sequencing of Tip60-IP RNA and Input RNA revealed that

362 similar to wildtype, Tip60-RNA binding is specific and selective for only certain RNA molecules
 363 from the entire Input RNA pool in APP and APP;Tip60 genotypes (**Figure 6A,B**). Further, using a
 364 threshold cutoff of adjusted p-value <0.05 , we identified Tip60 RNA targets enriched in IP that
 365 clustered separately between genotypes, suggesting variations in Tip60-RNA binding in different
 366 genotypes (**Figure 6C, Extended Table 2-1**). Although the majority of RNA targets are shared by all
 367 three genotypes, we found certain RNAs that are uniquely targeted only in wildtype, APP, or
 368 APP;Tip60, supporting Tip60 RNA target divergence in different genotypes (**Figure 6D**). Together,
 369 these results demonstrate that although specificity and selectivity of Tip60's RNA binding functions
 370 remains unaltered, Tip60 targets partially different sets of RNA in wildtype, APP and APP;Tip60
 371 *Drosophila* models.

372

373 To better understand how Tip60's RNA-binding function is altered in different genotypes, we
 374 compared the distribution and intersection of Tip60's RNA targets between APP vs. wildtype and
 375 APP versus APP;Tip60 (**Extended Table 3-1**). Using volcano plot analysis, we first identified
 376 Tip60's RNA targets that are significantly enriched in IP in APP (red scatters), wildtype (blue
 377 scatters), or both (black scatters) (**Figure 7A, left**) and APP;Tip60 (red scatters), APP (blue scatters),
 378 or both (black scatters) (**Figure 7A, right**). We found similar number of Tip60-RNA targets that are
 379 either significantly enriched or depleted in binding in APP vs. wildtype (192 and 171, respectively)
 380 and APP;Tip60 vs. APP (554 and 607, respectively). Next, we used an UpSet plot to visualize
 381 intersections between these four differential Tip60-RNA target comparisons that are represented as
 382 individual rows (**Figure 7B**). Out of the 171 RNA that interacted with Tip60 in wildtype but not in
 383 APP brains (row 1), increased Tip60 in the APP;Tip60 genotype restored Tip60-RNA interactions
 384 with 56 (32.8%) of these RNAs (row 1 and row 3 overlap, purple bar). Similarly, out of the 192 RNA
 385 that Tip60 mistargeted in APP but not in wildtype (row 2), increased Tip60 in the APP;Tip60
 386 genotype resulted in reduced inappropriate interactions in 43 (22.4%) of these RNAs (row 2 and row

387 4 overlap, purple bar). Together, increased Tip60 in the APP;Tip60 genotype restored 27.6%
 388 (99/363) Tip60-RNA target interactions that were altered in the APP brain that we refer to as ‘Tip60
 389 rescued RNA targets’. To identify the biological processes these Tip60 rescued RNA targets are
 390 involved in, we performed functional annotation clustering on this set of RNAs using FlyEnrichr
 391 gene ontology analysis (**Figure 7C**). Top enriched cellular processes included chromatin assembly
 392 and remodeling, axon and dendrite guidance, protein modification, intracellular transport, and
 393 proteolysis, and intriguingly, RNA transport and splicing. Together, our results point to a functional
 394 role for Tip60-RNA binding in the brain that is disrupted under APP neurodegenerative conditions
 395 and is partially protected against by increased Tip60.

396

397 **IV. Tip60 interacts with pre-mRNAs that emanate from Tip60’s chromatin gene targets**

398 We previously reported that Tip60 displays a nuclear cytoplasmic distribution pattern in both
 399 the *Drosophila* and mammalian brain. Thus, we asked whether Tip60 primarily interacts with
 400 unspliced pre-mRNA in the nucleus or mature spliced mRNA in the cytoplasm. We performed
 401 RSEQC read distribution analysis (Wang et al., 2012) on our Tip60-IP RNA and Input RNA samples
 402 from RIP-Seq to calculate the distribution pattern of mapped reads over different genome features,
 403 such as like coding DNA sequence (CDS) exon, 5’UTR exon, 3’ UTR exon, intron, and intergenic
 404 regions (**Figure 8A**). As expected from the Input samples containing both pre-mRNA and mature
 405 mRNA, the majority of the reads mapped to CDS exonic regions and UTR regions, while the
 406 remaining mapped to introns and intergenic regions. Strikingly, we observed similar read distribution
 407 in Tip60-IP RNA samples, including mapping to intronic regions, suggesting the presence of pre-
 408 mRNA in the RNA population that Tip60 specifically interacts with. Further, read mapping at
 409 intronic regions revealed higher enrichment of RNAs from Tip60-RIP samples when compared to
 410 their respective Inputs for all genotypes, indicating that Tip60 preferentially targets unspliced pre-
 411 mRNAs that reside in the nucleus. Finally, since RNA splicing is predominantly co-transcriptional

and occurs in close proximity with the chromatin loci it originates with, we asked whether there is any overlap between Tip60 target RNAs and chromatin gene loci. To address this question, we compared our Tip60 RNA targets from RIP-Seq with Tip60 chromatin gene targets we previously published using ChIP-Seq (Beaver et al., 2021). Importantly, RIP-Seq and CHIP-Seq were performed using identical staged larval brains for wildtype, APP and APP;Tip60 genotypes. Remarkably, we observed a significant overlap (78-79%) between Tip60's RNA and gene targets for wildtype ($p < 2.263e-06$), APP ($p < 7.115e-17$) and APP;Tip60 ($p < 6.523e-28$, hypergeometric test) (**Figure 8B, Extended Table 4-1**). These results suggest that Tip60 regulates identical genes at both the chromatin and RNA level, potentially by interacting with nascent RNA as it is transcribed.

The significant overlap between Tip60's gene targets at the chromatin and RNA level prompted us to ask whether Tip60's interaction with RNA is required for its chromatin interaction. To address this question, we assessed if RNase treatment mislocalizes Tip60 in polytene chromosomes (PCs) within fly salivary glands. PCs are a well-established model to study functional chromosomes due to large size and prominent banding pattern (Johansen et al., 2009; Vatolina et al., 2011). As expected, we found that *Drosophila* Tip60 localizes to the less-compact interbands in PCs, representing regions of highly active gene transcription (**Figure 9**) (Schirling et al., 2010) and accordingly, co-localizes with RNA Pol II. Treatment of PCs with RNase reduced Tip60 staining, supporting a putative role for Tip60-RNA interaction occurring in close proximity to chromatin (**Figure 8C, 10**). Together, our results demonstrate that Tip60 primarily targets identical gene loci at both the chromatin and RNA level and that Tip60's RNA binding function is at least in part, required for Tip60's chromatin interaction.

V. Tip60 mediates alternative splicing selection of neural pre-mRNA targets associated with Alzheimer's Disease

437 Our published ChIP studies showing Tip60 chromatin enrichment at intergenic and intronic
 438 regions within genes (Beaver et al., 2021) in conjunction with our RNA read map analysis revealing
 439 enrichment of RNAs within intronic regions of these same genes in Tip60- RIP samples support an
 440 interaction between Tip60 and unspliced pre-mRNAs. In neurons, AS of pre-mRNA is a central
 441 mechanism used to increase the genetic plasticity and proteomic diversity required for dynamic
 442 neuronal processes, making these tissues particularly susceptible to splicing defects (Li et al.,
 443 2007; Su and Tarn, 2018). Given that AS is primarily co-transcriptional and that AS defects hallmark
 444 AD, we hypothesized that Tip60-RNA interaction mediates AS of pre-mRNA targets emanating from
 445 Tip60's chromatin gene loci and that this process is disrupted in the APP AD larval brain. To assess
 446 Tip60's involvement in potential AS defects in the APP brain, we applied replicate multivariate
 447 analysis of transcript splicing (rMATS) analysis on RNA-Sequencing data from *Drosophila*
 448 wildtype, APP and APP;Tip60 Input samples (**Extended Tables 5-1, 5-2**). The relative abundance of
 449 each isoform was quantified as percentage spliced in (PSI); Δ PSI quantified the difference in relative
 450 isoform abundance between genotypes. Our analysis uncovered a multitude of differential
 451 mammalian-like AS alteration events including skipped exons (SE), alternative 5' splice site (A5SS),
 452 alternative 3' splice site (A3SS), mutually exclusive exons (MXE) and retained introns (RI) between
 453 genotypes (**Figure 11A**). We identified a total of 698 and 517 significant splicing defects between
 454 APP vs. wildtype and APP;Tip60 vs. APP comparisons, respectively, that affected every AS event
 455 category, suggesting genotype-dependent splicing modifications at a global level (**Figure 11B**).
 456 Although MXE accounts for most significant AS alterations, about 80% of these alterations are
 457 present in *Dscam1* gene that encodes for 38,106 distinct proteins via AS of 95 variable exons
 458 (Graveley, 2005). Strikingly, a comparison of RNAs showing altered splicing in APP or
 459 APP;Tip60 with Tip60 wildtype RNA targets identified from RNA-IP Sequencing data reveal
 460 that >50% of RNA undergoing significant AS alterations in APP (186/358) and APP;Tip60

461 (162/284) brains are bona-fide Tip60-RNA targets in the wild-type brain (**Figure 11C**). Moreover,
 462 about 30% of human orthologues for these Tip60-targeted AS genes in APP (54/177) and APP;Tip60
 463 (44/152) were found to be enriched for AD in the DisGeNET curated database of gene-disease
 464 associations (Piñero et al., 2016) (**Tables 3, 4**). Therefore, our results strongly suggest that Tip60
 465 possesses the ability to influence AS decisions of unspliced pre-mRNA targets implicated in AD
 466 pathogenesis.

467
 468 We next investigated if restoring Tip60 levels in APP;Tip60 is sufficient to protect against
 469 AD-associated AS defects observed in *Drosophila* APP neurodegeneration. To test this, we screened
 470 the 54 Tip60-targeted AD-associated AS defects in APP for reversal in APP;Tip60 such that
 471 $(\Delta\text{PSI})_{\text{APPTip60}} \equiv -(\Delta\text{PSI})_{\text{APP}}$ at the same or a nearby genomic location. Remarkably, we identified 15
 472 triaged Tip60-rescued AS events mapping to 12 genes that are altered in APP and rescued by
 473 restoration of Tip60 levels in APP;Tip60 (**Table 5**). Only 1 out of the 34 MXE events in *Dscam1*
 474 gene were included in the main list to avoid repetition (**Table 6**). These triaged Tip60-rescued AS
 475 events are distributed over all five types of AS and have no preference towards exon inclusion or
 476 exclusion, suggesting Tip60 is acting as a global splicing regulator (**Figure 12A**). Individual
 477 schematic representations show splicing defects for each AS type that is reversed at the exact
 478 exonic/intronic genomic locations (**Figure 12B**). For example, exon 6 in the *heph* gene is
 479 preferentially included in wildtype (PSI= 0.81), skipped in APP (PSI= 0.39), and included back again
 480 in APP;Tip60 (PSI= 0.69). Similarly, long isoforms of *Dlg1* exon 1 (A5SS) and *Rab3-GEF* exon 4
 481 (A3SS) are favored in wildtype (PSI= 0.96; 0.44), relatively excluded in APP (PSI= 0.71; 0.00) and
 482 restored in APP;Tip60 (PSI= 1.00; 0.34). Likewise, *Dscam1* gene contains mutually exclusive exons
 483 at position 6 where a specific exon in wildtype (PSI= 0.88) is skipped for another exon in APP (PSI=
 484 0.05) but included again in APP;Tip60 (PSI= 0.67). Lastly, the intron between exons 3 and 4 in *Adar*

gene is less included in wildtype (PSI= 0.77) as compared to APP (PSI= 0.96) that is restored in APP;Tip60 (PSI= 0.60). Finally, to test if the AS defects we observed in the APP neurodegenerative fly brain are modulated by Tip60-RNA targeting, we utilized splice-specific RT-qPCR on larval brains from wildtype and RNAi-mediated Tip60 neural knockdown samples (**Figure 12C-E**). Remarkably, the expression of predominant RNA isoform for *heph* ($t_{(4)}=6.797$, $p=0.0012$, unpaired Student's t-test), *Dscam1* ($t_{(4)}=7.707$, $p=0.0008$, unpaired Student's t-test), and *Adar* ($t_{(4)}=2.530$, $p=0.0323$, unpaired Student's t-test) in the wildtype larval brain was found to be significantly reduced upon Tip60 RNAi-mediated knockdown. In conclusion, neural Tip60 knockdown is sufficient for inducing the exact AS defects identified in *heph*, *Dscam1* and *Adar* under APP neurodegeneration., therefore validating the role of Tip60 in modulating AS decisions of its pre-mRNA targets.

VI. Tip60's RNA-binding function is conserved in the human brain and altered under AD pathology

The human orthologues of the 12 triaged Tip60-rescued AS genes perform diverse yet critical neuronal functions that go awry in AD pathogenesis (**Figure 13A**). For example, ADAM10 (fly *kuz*) is a α -secretase that cleaves APP to promote the non-amyloidogenic pathway and reduce A β plaque load (Niemitz, 2013;Yuan et al., 2017). Accordingly, ADAM10 is the third most significant AD-associated gene in DisGeNET database (Piñero et al., 2016) and is currently being tested as a potential AD treatment (Manzine et al., 2019). Likewise, DLG1 (fly *dlg1*) is a scaffolding protein known to interact with APP intracellular C-terminal domain (AICD) (Silva et al., 2020) and regulate APP metabolism by recruiting ADAM10 to the synapse (Marcello et al., 2013). Additionally, RBFOX1 (fly *Rbfox1*) and PTBP1 (fly *heph*) are two key splicing regulators of neuronal-specific AS in the mammalian brain (Li et al., 2021) that directly regulate AS of APP exon 7 (Smith et al.,

2011;Alam et al., 2014) and therefore, control APP⁶⁹⁵ production and A β plaque load (Belyaev et al., 2010). Similarly, ADARB1 (fly *Adar*) is a major adenosine to inosine RNA editing enzyme in mammals that also regulates splicing (Solomon et al., 2013) and its function is reduced in human AD hippocampus (Khmermesh et al., 2016;Annese et al., 2018). Moreover, HSPG2 (fly *trol*) extracellular matrix protein is observed to be co-deposited with A β plaques in the brains of AD patients (Van Gool et al., 1993;Zhang et al., 2014) where it accelerates A β oligomerization and aggregation (Liu et al., 2016). Besides, MADD (fly *Rab3-GEF*) and HDAC4 show altered expression in AD pathology (Del Villar and Miller, 2004;Shen et al., 2016) and have been proposed to serve as novel AD pharmacological targets (Mielcarek et al., 2015;Hassan et al., 2021).

Importantly, and consistent with our data, several studies have previously reported AS defects in post-mortem human AD-brains in 7 out of these 12 triaged Tip60-rescued AS genes (Tollervy et al., 2011;Raj et al., 2018;Adusumalli et al., 2019;Marques-Coelho et al., 2021). To test if Tip60's RNA binding function is conserved in the human brain and whether such putative Tip60-RNA binding is altered under human AD pathology, we performed RIP-qPCR on RNA isolated from post-mortem human hippocampal tissues obtained from healthy controls and AD patients (**Figure 13B**). Remarkably, we found that Tip60 interacted with RNAs corresponding to the 7 human Tip60-rescued AS *Drosophila* orthologs that exhibit known AS defects in the human AD brain. Importantly, as compared to healthy controls, Tip60 enrichment for RNA transcripts encoded by each of these 7 loci was significantly reduced in AD patients ($F_{(7,32)}=3.775$, $p=0.0043$, two-way ANOVA with Sidak's multiple comparison test). Notably, Tip60 enrichment for ADAM10 transcripts in the healthy brain is most significantly reduced in AD brain ($t_{(32)}=5.756$, $p=1.10045E-06$), supporting a role for Tip60 in mediating RNA processing of genes critical for keeping AD neurodegeneration in check. Together, our results reveal a novel RNA splicing regulatory function for Tip60 that mediates

AS decisions for its unspliced pre-mRNA targets enriched for AS impairments that hallmark AD etiology.

DISCUSSION

I. The selective interaction of Tip60 with protein coding neural mRNAs is disrupted in AD brain

Tip60, the second most highly expressed HAT in the mammalian brain, drives neural function and neuroprotection in AD but studies to date have conventionally focused on its role in chromatin dynamics and neural gene control, leaving additional mechanistic functions unexplored. Here, we report a highly specific, selective, and reproducible RNA-binding function for Tip60's chromodomain in the *Drosophila* brain *in vivo*. Our findings are not unprecedented as chromodomains within multiple chromatin regulatory proteins have been shown to directly interact with RNA (Akhtar et al., 2000; Morales et al., 2005; Bernstein et al., 2006; Shimojo et al., 2008; Ishida et al., 2012; Akoury et al., 2019). Chromodomains within MOF HAT and chromobox-7 achieve dosage compensation by targeting roX noncoding RNA at the male X chromosome and *Xist* noncoding RNA at the female X chromosome in *Drosophila* and mammalian cells, respectively (Akhtar et al., 2000; Bernstein et al., 2006). Our findings confirm and extend these studies by being the first to sequence and characterize a complex array of neural RNAs that are specifically bound to Tip60 in the fly brain. We find that Tip60 primarily targets protein encoding RNAs that mediate dynamic neuronal processes and are enriched for human diseases such as tauopathy and AD, indicating disruption of Tip60-RNA binding is involved in these cognitive disorders. In line with these findings, we observe that Tip60-RNA targeting is disrupted in the AD fly brain and in AD human hippocampal samples supporting a functional role for Tip60-RNA binding in AD pathology. Remarkably, increasing Tip60 levels in the AD fly brain partially protects against Tip60-RNA targeting alterations that are enriched for dynamic neuronal processes including chromatin assembly

558 and remodeling, axonal guidance, protein modification processes, and RNA splicing and transport.
 559 We speculate that such Tip60-RNA binding disruptions lead to transcriptomic alterations that
 560 ultimately contribute significantly to AD pathologies but can be protected against by increased Tip60
 561 levels.

562

563 **II. Tip60's bi-level gene regulation at the chromatin and RNA level mediates rapid fine-tuning** 564 **of neural gene expression**

565 Tip60 is a key mediator of activity-dependent gene expression underlying dynamic neuronal
 566 processes and is shuttled from cytoplasm into nucleus upon neuronal stimulation for histone
 567 acetylation (Xu et al., 2016;Karnay et al., 2019). This raises the possibility that Tip60 could be
 568 binding with RNA emanating from its activity-dependent genes at various stages of RNA processing
 569 to dictate ultimate protein isoforms and function in the brain. However, whether Tip60 interacts with
 570 nascent RNAs in the nucleus or mature RNA in the cytoplasm and whether Tip60's interacting RNAs
 571 are transcribed directly from Tip60 chromatin targets remains unclear. Here, we show enrichment of
 572 intronic regions in the Tip60-IP bound RNA samples, indicative of Tip60 primarily targeting
 573 unspliced pre-mRNAs that reside in the nucleus. Further, we found reduced Tip60 staining on
 574 polytene chromosomes post RNase treatment, strongly suggesting that Tip60 interacts with newly
 575 transcribed pre-mRNA in close proximity to chromatin. Consistent with this finding, we identified a
 576 significant overlap between Tip60's RNA targets and its chromatin gene targets, suggesting Tip60 is
 577 regulating expression and function of identical neural targets via targeting at both the chromatin and
 578 RNA levels respectively. Although our findings are unprecedented for a histone acetyltransferase,
 579 HP1 chromosomal protein has been shown to dissociate with heterochromatin to bind with newly
 580 synthesized RNA owing to its greater affinity for RNA over histones (Keller et al., 2012). In support
 581 of this concept, we find Tip60 is unlikely to bind with both histone and RNA concurrently due to
 582 steric hindrance at interacting sites. Therefore, we are the first to propose a model by which Tip60

583 rapidly fine-tunes its neural targets for dynamic gene regulation by orchestrating a bi-level switching
 584 mechanism such that Tip60 recruitment to chromatin allows for histone acetylation mediated gene
 585 activation as well as targeting of newly synthesized RNA that may further stabilize binding in a
 586 positive feedback loop (**Figure 14**).

587
 588

589 **III. Tip60 mediated alternative splicing selection may underly splicing defects characterized as** 590 **hallmarks of Alzheimer's Disease**

591 RNA splicing abnormalities have recently emerged as a widespread hallmark in AD and AS
 592 defects in major disease candidate genes – including APP, Tau, PSEN, and ApoE, have since been
 593 linked to AD pathology (Love et al., 2015; Jakubauskienė and Kanopka, 2021; Li et al., 2021).
 594 Although causes remain unclear, dysregulation of epigenetic mechanisms under AD pathology (Liu
 595 et al., 2018; Nativio et al., 2018) and their recent convergence with co-transcriptional AS regulation
 596 (Luco et al., 2011; Rahhal and Seto, 2019; Xu et al., 2021) strongly suggest a causative role for
 597 epigenetic regulators/modifications in AS defects underlying AD pathology. In support of this
 598 concept, here we show that the Tip60 HAT doubles as an RNA splicing modulator and mediates AS
 599 selection of its pre-mRNA targets associated with AD. We discovered a multitude of differential
 600 mammalian-like AS alteration events in the APP AD fly brain, with over half of these altered RNAs
 601 identified as bona-fide Tip60-RNA targets enriched for AD that are partially protected against by
 602 increasing Tip60 levels. Moreover, consistent with a previous finding that shows Tip60 knockdown
 603 in epithelial cells alters AS of a key integrin subunit (Bhatia et al., 2020), we find Tip60 neural
 604 knockdown is sufficient for inducing AS defects identified under APP neurodegeneration, therefore
 605 underscoring criticality of Tip60 mediated AS regulation in AD pathogenesis. Further, since several
 606 Tip60-rescued fly AS genes show splicing defects in post-mortem AD human brains (Tollervey et
 607 al., 2011; Raj et al., 2018; Adusumalli et al., 2019; Marques-Coelho et al., 2021) and we find Tip60-

RNA binding is altered in AD hippocampus, we propose that Tip60 mediated AS modulation is a conserved critical post-transcriptional step that is disrupted early in AD etiology. In particular, we find Tip60-RNA binding of ADAM10, a constitutive α -secretase, is significantly lost under AD pathology. Interestingly, reduced ADAM10 activity in the post-mortem human AD brain has been linked to AS induced isoform change without a change in the overall gene expression (Marques-Coelho et al., 2021), suggesting Tip60 modulated ADAM10 splicing could be central to AD pathogenesis. Thus, we are the first to uncover distinct histone and RNA binding capabilities for Tip60 that mediate its function in neural gene control and RNA splicing, respectively, and may underly the chromatin packaging and splicing defects that are now characterized as hallmarks of AD.

IV. One target, two functions: Tip60 HAT as a novel therapeutic target for Alzheimer's Disease

Pharmacological treatments aiming to restore histone acetylation via HDAC inhibition are currently a research hotspot for developing AD cognition enhancing drugs (Gräff and Tsai, 2013; Simões-Pires et al., 2013; Mielcarek et al., 2015). Although promising in reinstating cognition, HDAC inhibitors are known to exhibit side effects due to non-specific global hyperacetylation (Didonna and Opal, 2015; Yang et al., 2017). Alternatively, enhancing activity of specific HATs in promoting cognition associated histone acetylation serves as an exciting new therapeutic strategy that remains to be fully explored (Caccamo et al., 2010; Selvi et al., 2010; Valor et al., 2013). In support of this concept, here we identify a novel splicing modulation function for Tip60 that likely complements its histone function for neuroprotection, therefore highlighting Tip60 as unique dual-functioning therapeutic target for ameliorating both, histone and splicing aberrations in AD. Strikingly, mutations only in RNA-binding and not histone-binding residues in the Esa1 HAT chromodomain are lethal (Shimojo et al., 2008), strongly supporting that the RNA function of HATs are non-redundant and critical for viability. Although precise mechanisms underlying Tip60 mediated AS regulation remain to be elucidated, we propose three probable mechanisms. First, similar to RNA-binding proteins

633 (Herzel et al., 2017;Rachez et al., 2021), Tip60 could be binding at a splice site or an accessory site
634 influencing transient RNA folding, and therefore, may modulate the timing of splice site exposure to
635 the splicing machinery. Second, since Tip60 typically interacts with additional proteins in a complex
636 for gene regulation (Ikura et al., 2000;Frank et al., 2003), Tip60-RNA binding could trigger assembly
637 of a secondary complex that ultimately modulates AS decisions. Third, since histone acetylation
638 modifications have been implicated in AS regulation (Hnilicová et al., 2011;Rahhal and Seto, 2019),
639 Tip60's HAT function might modulate AS decisions while it tethers the target pre-mRNA to the
640 chromatin. Further, we observed Tip60-rescued AS events in two major splicing regulators,
641 RBFOX1 and PTBP1 that could in turn impact splicing of other neural genes. Nevertheless, we do
642 not rule out potential additional mechanisms. Our findings strongly underscore supplementing
643 current histone acetylation targeted therapeutics with splice-switching strategies, such as the use of
644 antisense oligonucleotides (AO) that for desired pre-mRNA processing (Quemener et al., 2020;Li et
645 al., 2021). Currently, six splice-switching AO have been approved by the US FDA for mRNA
646 manipulation in rare diseases (Li et al., 2021;Raguraman et al., 2021). Although successful in
647 reducing A β production and ameliorating cognition in AD pre-clinical models (Huynh et al.,
648 2017;Chang et al., 2018), further studies are needed to corroborate the effectiveness and safety of
649 splice-switching AO in AD. Dissecting apart Tip60's histone versus RNA function and further
650 elucidation of mechanisms underlying Tip60 mediated AS modulation should provide earlier, safer,
651 and more selective ways for AD therapeutics in the clinical setting.

652

References

- Adusumalli, S., Ngian, Z.K., Lin, W.Q., Benoukraf, T., and Ong, C.T. (2019). Increased intron retention is a post-transcriptional signature associated with progressive aging and Alzheimer's disease. *Aging cell* 18, e12928.
- Agirre, E., Oldfield, A.J., Bellora, N., Segelle, A., and Luco, R.F. (2021). Splicing-associated chromatin signatures: a combinatorial and position-dependent role for histone marks in splicing definition. *Nature Communications* 12, 682.
- Akhtar, A., Zink, D., and Becker, P.B. (2000). Chromodomains are protein-RNA interaction modules. *Nature* 407, 405.
- Akoury, E., Ma, G., Demolin, S., Brönnner, C., Zocco, M., Cirilo, A., Ivic, N., and Halic, M. (2019). Disordered region of H3K9 methyltransferase Clr4 binds the nucleosome and contributes to its activity. *Nucleic Acids Res* 47, 6726-6736.
- Alam, S., Suzuki, H., and Tsukahara, T. (2014). Alternative splicing regulation of APP exon 7 by RBFOX proteins. *Neurochem Int* 78, 7-17.
- Annese, A., Manzari, C., Lionetti, C., Picardi, E., Horner, D.S., Chiara, M., Caratozzolo, M.F., Tullo, A., Fosso, B., Pesole, G., and D'Erchia, A.M. (2018). Whole transcriptome profiling of Late-Onset Alzheimer's Disease patients provides insights into the molecular changes involved in the disease. *Scientific Reports* 8, 4282.
- Beaver, M., Bhatnagar, A., Panikker, P., Zhang, H., Snook, R., Parmar, V., Vijayakumar, G., Betini, N., Akhter, S., and Elephant, F. (2020). Disruption of Tip60 HAT mediated neural histone acetylation homeostasis is an early common event in neurodegenerative diseases. *Sci Rep* 10, 18265.
- Beaver, M., Karisetty, B.C., Zhang, H., Bhatnagar, A., Armour, E., Parmar, V., Brown, R., Xiang, M., and Elephant, F. (2021). Chromatin and transcriptomic profiling uncover dysregulation of the Tip60 HAT/HDAC2 epigenomic landscape in the neurodegenerative brain. *Epigenetics*, 1-22.
- Belyaev, N.D., Kellett, K.A., Beckett, C., Makova, N.Z., Revett, T.J., Nalivaeva, N.N., Hooper, N.M., and Turner, A.J. (2010). The transcriptionally active amyloid precursor protein (APP) intracellular domain is preferentially produced from the 695 isoform of APP in a {beta}-secretase-dependent pathway. *J Biol Chem* 285, 41443-41454.
- Bernstein, E., and Allis, C.D. (2005). RNA meets chromatin. *Genes & development* 19, 1635-1655.
- Bernstein, E., Duncan, E.M., Masui, O., Gil, J., Heard, E., and Allis, C.D. (2006). Mouse polycomb proteins bind differentially to methylated histone H3 and RNA and are enriched in facultative heterochromatin. *Molecular and cellular biology* 26, 2560-2569.
- Bhatia, S.S., Koeffler, H.P., and Jha, S. (2020). Abstract 4670: TIP60 regulates alternative splicing of Integrin subunit alpha 6. *Cancer Research* 80, 4670-4670.
- Bhatnagar, A., Karnay, A.M., and Elephant, F. (2023). "Drosophila Epigenetics," in *Handbook of Epigenetics*. Elsevier), 215-247.
- Caccamo, A., Maldonado, M.A., Bokov, A.F., Majumder, S., and Oddo, S. (2010). CBP gene transfer increases BDNF levels and ameliorates learning and memory deficits in a mouse model of Alzheimer's disease. *Proceedings of the National Academy of Sciences* 107, 22687-22692.
- Chang, J.L., Hinrich, A.J., Roman, B., Norrbom, M., Rigo, F., Marr, R.A., Norstrom, E.M., and Hastings, M.L. (2018). Targeting amyloid- β precursor protein, APP, splicing with antisense oligonucleotides reduces toxic amyloid- β production. *Molecular Therapy* 26, 1539-1551.
- Chen, E.Y., Tan, C.M., Kou, Y., Duan, Q., Wang, Z., Meirelles, G.V., Clark, N.R., and Ma'ayan, A. (2013). Enrichr: interactive and collaborative HTML5 gene list enrichment analysis tool. *BMC Bioinformatics* 14, 128.
- Chen, Y., Chen, Y., Shi, C., Huang, Z., Zhang, Y., Li, S., Li, Y., Ye, J., Yu, C., Li, Z., Zhang, X., Wang, J., Yang, H., Fang, L., and Chen, Q. (2018). SOAPnuke: a MapReduce acceleration-supported software for integrated quality control and preprocessing of high-throughput sequencing data. *Gigascience* 7, 1-6.
- Chen, Y., and Varani, G. (2005). Protein families and RNA recognition. *Febs j* 272, 2088-2097.

- 704 Consortium, T.U. (2020). UniProt: the universal protein knowledgebase in 2021. *Nucleic Acids Research*
705 49, D480-D489.
- 706 Corley, M., Burns, M.C., and Yeo, G.W. (2020). How RNA-Binding Proteins Interact with RNA:
707 Molecules and Mechanisms. *Mol Cell* 78, 9-29.
- 708 Del Villar, K., and Miller, C.A. (2004). Down-regulation of DENN/MADD, a TNF receptor binding
709 protein, correlates with neuronal cell death in Alzheimer's disease brain and hippocampal neurons.
710 *Proc Natl Acad Sci U S A* 101, 4210-4215.
- 711 Delano, W.L. (2002). Pymol: An open-source molecular graphics tool. *CCP4 Newsl. Protein Crystallogr*
712 40, 82-92.
- 713 Deture, M.A., and Dickson, D.W. (2019). The neuropathological diagnosis of Alzheimer's disease.
714 *Molecular Neurodegeneration* 14, 32.
- 715 Didonna, A., and Opal, P. (2015). The promise and perils of HDAC inhibitors in neurodegeneration.
716 *Annals of clinical and translational neurology* 2, 79-101.
- 717 Dobin, A., Davis, C.A., Schlesinger, F., Drenkow, J., Zaleski, C., Jha, S., Batut, P., Chaisson, M., and
718 Gingeras, T.R. (2013). STAR: ultrafast universal RNA-seq aligner. *Bioinformatics* 29, 15-21.
- 719 Ewels, P., Magnusson, M., Lundin, S., and Källér, M. (2016). MultiQC: summarize analysis results for
720 multiple tools and samples in a single report. *Bioinformatics* 32, 3047-3048.
- 721 Francis, Y.I., Fà, M., Ashraf, H., Zhang, H., Staniszewski, A., Latchman, D.S., and Arancio, O. (2009).
722 Dysregulation of histone acetylation in the APP/PS1 mouse model of Alzheimer's disease. *Journal*
723 *of Alzheimer's Disease* 18, 131-139.
- 724 Frank, S.R., Parisi, T., Taubert, S., Fernandez, P., Fuchs, M., Chan, H.M., Livingston, D.M., and Amati,
725 B. (2003). MYC recruits the TIP60 histone acetyltransferase complex to chromatin. *EMBO reports*
726 4, 575-580.
- 727 Graff, J., Rei, D., Guan, J.S., Wang, W.Y., Seo, J., Hennig, K.M., Nieland, T.J., Fass, D.M., Kao, P.F.,
728 Kahn, M., Su, S.C., Samiei, A., Joseph, N., Haggarty, S.J., Delalle, I., and Tsai, L.H. (2012). An
729 epigenetic blockade of cognitive functions in the neurodegenerating brain. *Nature* 483, 222-226.
- 730 Gräff, J., and Tsai, L.-H. (2013). The potential of HDAC inhibitors as cognitive enhancers. *Annual review*
731 *of pharmacology and toxicology* 53, 311-330.
- 732 Graveley, B.R. (2005). Mutually exclusive splicing of the insect Dscam pre-mRNA directed by
733 competing intronic RNA secondary structures. *Cell* 123, 65-73.
- 734 Hassan, M., Zahid, S., Alashwal, H., Kloczkowski, A., and Moustafa, A.A. (2021). Mechanistic insights
735 into TNFR1/MADD death domains in Alzheimer's disease through conformational molecular
736 dynamic analysis. *Scientific Reports* 11, 12256.
- 737 Herzel, L., Ottoz, D.S.M., Alpert, T., and Neugebauer, K.M. (2017). Splicing and transcription touch
738 base: co-transcriptional spliceosome assembly and function. *Nature Reviews Molecular Cell*
739 *Biology* 18, 637-650.
- 740 Hnilicová, J., Hozeifi, S., Dušková, E., Icha, J., Tománková, T., and Staněk, D. (2011). Histone
741 deacetylase activity modulates alternative splicing. *PloS one* 6, e16727.
- 742 Hu, Y., Flockhart, I., Vinayagam, A., Bergwitz, C., Berger, B., Perrimon, N., and Mohr, S.E. (2011). An
743 integrative approach to ortholog prediction for disease-focused and other functional studies. *BMC*
744 *bioinformatics* 12, 1-16.
- 745 Huynh, T.V., Liao, F., Francis, C.M., Robinson, G.O., Serrano, J.R., Jiang, H., Roh, J., Finn, M.B.,
746 Sullivan, P.M., Esparza, T.J., Stewart, F.R., Mahan, T.E., Ulrich, J.D., Cole, T., and Holtzman,
747 D.M. (2017). Age-Dependent Effects of apoE Reduction Using Antisense Oligonucleotides in a
748 Model of β -amyloidosis. *Neuron* 96, 1013-1023.e1014.
- 749 Ikura, T., Ogryzko, V.V., Grigoriev, M., Groisman, R., Wang, J., Horikoshi, M., Scully, R., Qin, J., and
750 Nakatani, Y. (2000). Involvement of the TIP60 histone acetylase complex in DNA repair and
751 apoptosis. *Cell* 102, 463-473.
- 752 Ishida, M., Shimojo, H., Hayashi, A., Kawaguchi, R., Ohtani, Y., Uegaki, K., Nishimura, Y., and
753 Nakayama, J.-I. (2012). Intrinsic nucleic acid-binding activity of Chp1 chromodomain is required
754 for heterochromatic gene silencing. *Molecular cell* 47, 228-241.

- 755 Jakubauskienė, E., and Kanopka, A. (2021). Alternative Splicing and Hypoxia Puzzle in Alzheimer's and
756 Parkinson's Diseases. *Genes* 12, 1272.
- 757 Johansen, K.M., Cai, W., Deng, H., Bao, X., Zhang, W., Girton, J., and Johansen, J. (2009). Polytene
758 chromosome squash methods for studying transcription and epigenetic chromatin modification in
759 *Drosophila* using antibodies. *Methods* 48, 387-397.
- 760 Johnson, A.A., Sarthi, J., Pirooznia, S.K., Reube, W., and Elefant, F. (2013). Increasing Tip60 HAT
761 levels rescues axonal transport defects and associated behavioral phenotypes in a *Drosophila*
762 Alzheimer's disease model. *J Neurosci* 33, 7535-7547.
- 763 Karnay, A., Karisetty, B.C., Beaver, M., and Elefant, F. (2019). Hippocampal stimulation promotes
764 intracellular Tip60 dynamics with concomitant genome reorganization and synaptic gene
765 activation. *Molecular and Cellular Neuroscience* 101, 103412.
- 766 Keller, C., Adaixo, R., Stunnenberg, R., Woolcock, K.J., Hiller, S., and Bühler, M. (2012). HP1Swi6
767 mediates the recognition and destruction of heterochromatic RNA transcripts. *Molecular cell* 47,
768 215-227.
- 769 Khmeresh, K., D'erchia, A.M., Barak, M., Anese, A., Wachtel, C., Levanon, E.Y., Picardi, E., and
770 Eisenberg, E. (2016). Reduced levels of protein recoding by A-to-I RNA editing in Alzheimer's
771 disease. *Rna* 22, 290-302.
- 772 Killin, L.O., Starr, J.M., Shiue, I.J., and Russ, T.C. (2016). Environmental risk factors for dementia: a
773 systematic review. *BMC Geriatr* 16, 175.
- 774 Kim, C.H., Kim, J.W., Jang, S.M., An, J.H., Seo, S.B., and Choi, K.H. (2015). The chromodomain-
775 containing histone acetyltransferase TIP60 acts as a code reader, recognizing the epigenetic codes
776 for initiating transcription. *Biosci Biotechnol Biochem* 79, 532-538.
- 777 Kim, D., Paggi, J.M., Park, C., Bennett, C., and Salzberg, S.L. (2019). Graph-based genome alignment
778 and genotyping with HISAT2 and HISAT-genotype. *Nature biotechnology* 37, 907-915.
- 779 Knopman, D.S., Amieva, H., Petersen, R.C., Chételat, G., Holtzman, D.M., Hyman, B.T., Nixon, R.A.,
780 and Jones, D.T. (2021). Alzheimer disease. *Nature Reviews Disease Primers* 7, 33.
- 781 Krieger, E., Joo, K., Lee, J., Lee, J., Raman, S., Thompson, J., Tyka, M., Baker, D., and Karplus, K.
782 (2009). Improving physical realism, stereochemistry, and side-chain accuracy in homology
783 modeling: Four approaches that performed well in CASP8. *Proteins* 77 Suppl 9, 114-122.
- 784 Langmead, B., and Salzberg, S.L. (2012). Fast gapped-read alignment with Bowtie 2. *Nature Methods* 9,
785 357-359.
- 786 Laskowski, R.A., Macarthur, M.W., Moss, D.S., and Thornton, J.M. (1993). PROCHECK: a program to
787 check the stereochemical quality of protein structures. *Journal of applied crystallography* 26, 283-
788 291.
- 789 Letunic, I., and Bork, P. (2018). 20 years of the SMART protein domain annotation resource. *Nucleic
790 acids research* 46, D493-D496.
- 791 Li, B., and Dewey, C.N. (2011). RSEM: accurate transcript quantification from RNA-Seq data with or
792 without a reference genome. *BMC Bioinformatics* 12, 323.
- 793 Li, D., McIntosh, C.S., Mastaglia, F.L., Wilton, S.D., and Aung-Htut, M.T. (2021). Neurodegenerative
794 diseases: a hotbed for splicing defects and the potential therapies. *Translational Neurodegeneration*
795 10, 16.
- 796 Li, Q., Lee, J.-A., and Black, D.L. (2007). Neuronal regulation of alternative pre-mRNA splicing. *Nature
797 Reviews Neuroscience* 8, 819-831.
- 798 Liu, C.C., Zhao, N., Yamaguchi, Y., Cirrito, J.R., Kanekiyo, T., Holtzman, D.M., and Bu, G. (2016).
799 Neuronal heparan sulfates promote amyloid pathology by modulating brain amyloid- β clearance
800 and aggregation in Alzheimer's disease. *Sci Transl Med* 8, 332ra344.
- 801 Liu, X., Jiao, B., and Shen, L. (2018). The Epigenetics of Alzheimer's Disease: Factors and Therapeutic
802 Implications. *Frontiers in genetics* 9, 579-579.
- 803 Love, J.E., Hayden, E.J., and Rohn, T.T. (2015). Alternative Splicing in Alzheimer's Disease. *J
804 Parkinsons Dis Alzheimers Dis* 2.

- Lu, X., Deng, Y., Yu, D., Cao, H., Wang, L., Liu, L., Yu, C., Zhang, Y., Guo, X., and Yu, G. (2014). Histone Acetyltransferase p300 Mediates Histone Acetylation of PS1 and BACE1 in a Cellular Model of Alzheimer's Disease. *PLOS ONE* 9, e103067.
- Luco, R.F., Allo, M., Schor, I.E., Kornblihtt, A.R., and Misteli, T. (2011). Epigenetics in alternative pre-mRNA splicing. *Cell* 144, 16-26.
- Manzine, P.R., Ettcheto, M., Cano, A., Busquets, O., Marcello, E., Pelucchi, S., Di Luca, M., Endres, K., Olloquequi, J., and Camins, A. (2019). ADAM10 in Alzheimer's disease: Pharmacological modulation by natural compounds and its role as a peripheral marker. *Biomedicine & Pharmacotherapy* 113, 108661.
- Marcello, E., Saraceno, C., Musardo, S., Vara, H., De La Fuente, A.G., Pelucchi, S., Di Marino, D., Borroni, B., Tramontano, A., Pérez-Otaño, I., Padovani, A., Giustetto, M., Gardoni, F., and Di Luca, M. (2013). Endocytosis of synaptic ADAM10 in neuronal plasticity and Alzheimer's disease. *J Clin Invest* 123, 2523-2538.
- Marques-Coelho, D., Iohan, L.D.C.C., Melo De Farias, A.R., Flaig, A., Lambert, J.-C., and Costa, M.R. (2021). Differential transcript usage unravels gene expression alterations in Alzheimer's disease human brains. *NPJ aging and mechanisms of disease* 7, 1-15.
- Mielcarek, M., Zielonka, D., Carnemolla, A., Marcinkowski, J.T., and Guidez, F. (2015). HDAC4 as a potential therapeutic target in neurodegenerative diseases: a summary of recent achievements. *Front Cell Neurosci* 9, 42.
- Morales, V., Regnard, C., Izzo, A., Vetter, I., and Becker, P.B. (2005). The MRG domain mediates the functional integration of MSL3 into the dosage compensation complex. *Molecular and cellular biology* 25, 5947-5954.
- Muppirla, U.K., Honavar, V.G., and Dobbs, D. (2011). Predicting RNA-protein interactions using only sequence information. *BMC bioinformatics* 12, 489.
- Nativio, R., Donahue, G., Berson, A., Lan, Y., Amlie-Wolf, A., Tuzer, F., Toledo, J.B., Gosai, S.J., Gregory, B.D., Torres, C., Trojanowski, J.Q., Wang, L.-S., Johnson, F.B., Bonini, N.M., and Berger, S.L. (2018). Dysregulation of the epigenetic landscape of normal aging in Alzheimer's disease. *Nature Neuroscience* 21, 497-505.
- Niemitz, E. (2013). ADAM10 and Alzheimer's disease. *Nature Genetics* 45, 1273-1273.
- O'leary, N.A., Wright, M.W., Brister, J.R., Ciufo, S., Haddad, D., Mcveigh, R., Rajput, B., Robbertse, B., Smith-White, B., and Ako-Adjei, D. (2016). Reference sequence (RefSeq) database at NCBI: current status, taxonomic expansion, and functional annotation. *Nucleic acids research* 44, D733-D745.
- Panikker, P., Xu, S.J., Zhang, H., Sarthi, J., Beaver, M., Sheth, A., Akhter, S., and Elefant, F. (2018). Restoring Tip60 HAT/HDAC2 Balance in the Neurodegenerative Brain Relieves Epigenetic Transcriptional Repression and Reinstates Cognition. *J Neurosci* 38, 4569-4583.
- Peixoto, L., and Abel, T. (2013). The role of histone acetylation in memory formation and cognitive impairments. *Neuropsychopharmacology : official publication of the American College of Neuropsychopharmacology* 38, 62-76.
- Piñero, J., Bravo, À., Queralt-Rosinach, N., Gutiérrez-Sacristán, A., Deu-Pons, J., Centeno, E., García-García, J., Sanz, F., and Furlong, L.I. (2016). DisGeNET: a comprehensive platform integrating information on human disease-associated genes and variants. *Nucleic acids research*, gkw943.
- Pirooznia, S.K., and Elefant, F. (2013). Targeting specific HATs for neurodegenerative disease treatment: translating basic biology to therapeutic possibilities. *Frontiers in cellular neuroscience* 7, 30.
- Pirooznia, S.K., Sarthi, J., Johnson, A.A., Toth, M.S., Chiu, K., Koduri, S., and Elefant, F. (2012). Tip60 HAT activity mediates APP induced lethality and apoptotic cell death in the CNS of a Drosophila Alzheimer's disease model. *PLoS One* 7, e41776.
- Quemener, A.M., Bachelot, L., Forestier, A., Donnou-Fournet, E., Gilot, D., and Galibert, M.D. (2020). The powerful world of antisense oligonucleotides: From bench to bedside. *Wiley Interdiscip Rev RNA* 11, e1594.

- 855 Rachez, C., Legendre, R., Costallat, M., Varet, H., Yi, J., Kornobis, E., and Muchardt, C. (2021). HP1 γ
856 binding pre-mRNA intronic repeats modulates RNA splicing decisions. *EMBO reports* 22, e52320.
- 857 Raguraman, P., Balachandran, A.A., Chen, S., Diermeier, S.D., and Veedu, R.N. (2021). Antisense
858 Oligonucleotide-Mediated Splice Switching: Potential Therapeutic Approach for Cancer
859 Mitigation. *Cancers (Basel)* 13.
- 860 Rahhal, R., and Seto, E. (2019). Emerging roles of histone modifications and HDACs in RNA splicing.
861 *Nucleic Acids Res* 47, 4911-4926.
- 862 Raj, T., Li, Y.I., Wong, G., Humphrey, J., Wang, M., Ramdhani, S., Wang, Y.-C., Ng, B., Gupta, I., and
863 Haroutunian, V. (2018). Integrative transcriptome analyses of the aging brain implicate altered
864 splicing in Alzheimer's disease susceptibility. *Nature genetics* 50, 1584-1592.
- 865 Robert, X., and Gouet, P. (2014). Deciphering key features in protein structures with the new ENDscript
866 server. *Nucleic acids research* 42, W320-W324.
- 867 Sanchez-Mut, J.V., and Gräff, J. (2015). Epigenetic alterations in Alzheimer's disease. *Frontiers in*
868 *Behavioral Neuroscience* 9.
- 869 Sarthi, J., and Elefant, F. (2011). dTip60 HAT activity controls synaptic bouton expansion at the
870 Drosophila neuromuscular junction. *PLoS One* 6, e26202.
- 871 Schirling, C., Heseding, C., Heise, F., Kesper, D., Klebes, A., Klein-Hitpass, L., Vortkamp, A.,
872 Hoffmann, D., Saumweber, H., and Ehrenhofer-Murray, A.E. (2010). Widespread regulation of
873 gene expression in the Drosophila genome by the histone acetyltransferase dTip60. *Chromosoma*
874 119, 99-113.
- 875 Selvi, B.R., Cassel, J.-C., Kundu, T.K., and Boutillier, A.-L. (2010). Tuning acetylation levels with HAT
876 activators: therapeutic strategy in neurodegenerative diseases. *Biochimica et Biophysica Acta*
877 *(BBA)-Gene Regulatory Mechanisms* 1799, 840-853.
- 878 Shen, S., Park, J.W., Lu, Z.-X., Lin, L., Henry, M.D., Wu, Y.N., Zhou, Q., and Xing, Y. (2014). rMATS:
879 Robust and flexible detection of differential alternative splicing from replicate RNA-Seq data.
880 *Proceedings of the National Academy of Sciences* 111, E5593-E5601.
- 881 Shen, X., Chen, J., Li, J., Kofler, J., and Herrup, K. (2016). Neurons in Vulnerable Regions of the
882 Alzheimer's Disease Brain Display Reduced ATM Signaling. *eNeuro* 3.
- 883 Shimojo, H., Sano, N., Moriwaki, Y., Okuda, M., Horikoshi, M., and Nishimura, Y. (2008). Novel
884 structural and functional mode of a knot essential for RNA binding activity of the Esa1 presumed
885 chromodomain. *Journal of molecular biology* 378, 987-1001.
- 886 Sievers, F., Wilm, A., Dineen, D., Gibson, T.J., Karplus, K., Li, W., Lopez, R., McWilliam, H., Remmert,
887 M., and Söding, J. (2011). Fast, scalable generation of high-quality protein multiple sequence
888 alignments using Clustal Omega. *Molecular systems biology* 7, 539.
- 889 Silva, B., Niehage, C., Maglione, M., Hoflack, B., Sigrist, S.J., Wassmer, T., Pavlowsky, A., and Preat, T.
890 (2020). Interactions between amyloid precursor protein-like (APPL) and MAGUK scaffolding
891 proteins contribute to appetitive long-term memory in Drosophila melanogaster. *J Neurogenet* 34,
892 92-105.
- 893 Simões-Pires, C., Zwick, V., Nurisso, A., Schenker, E., Carrupt, P.-A., and Cuendet, M. (2013). HDAC6
894 as a target for neurodegenerative diseases: what makes it different from the other HDACs?
895 *Molecular Neurodegeneration* 8, 7.
- 896 Smith, P., Al Hashimi, A., Girard, J., Delay, C., and Hébert, S.S. (2011). In vivo regulation of amyloid
897 precursor protein neuronal splicing by microRNAs. *J Neurochem* 116, 240-247.
- 898 Solomon, O., Oren, S., Safran, M., Deshet-Unger, N., Akiva, P., Jacob-Hirsch, J., Cesarkas, K., Kabesa,
899 R., Amariglio, N., Unger, R., Rechavi, G., and Eyal, E. (2013). Global regulation of alternative
900 splicing by adenosine deaminase acting on RNA (ADAR). *Rna* 19, 591-604.
- 901 Su, C.-H., and Tarn, W.-Y. (2018). Alternative splicing in neurogenesis and brain development. *Frontiers*
902 *in molecular biosciences* 5, 12.
- 903 Sun, Y., Jiang, X., Xu, Y., Ayrapetov, M.K., Moreau, L.A., Whetstine, J.R., and Price, B.D. (2009).
904 Histone H3 methylation links DNA damage detection to activation of the tumour suppressor Tip60.
905 *Nature cell biology* 11, 1376.

- 906 Teplova, M., Malinina, L., Darnell, J.C., Song, J., Lu, M., Abagyan, R., Musunuru, K., Teplov, A.,
 907 Burley, S.K., Darnell, R.B., and Patel, D.J. (2011). Protein-RNA and protein-protein recognition by
 908 dual KH1/2 domains of the neuronal splicing factor Nova-1. *Structure (London, England : 1993)*
 909 19, 930-944.
- 910 Tollervey, J.R., Wang, Z., Hortobágyi, T., Witten, J.T., Zarnack, K., Kayikci, M., Clark, T.A.,
 911 Schweitzer, A.C., Rot, G., and Curk, T. (2011). Analysis of alternative splicing associated with
 912 aging and neurodegeneration in the human brain. *Genome research* 21, 1572-1582.
- 913 Valor, L.M., Viosca, J., Lopez-Atalaya, J.P., and Barco, A. (2013). Lysine acetyltransferases CBP and
 914 p300 as therapeutic targets in cognitive and neurodegenerative disorders. *Curr Pharm Des* 19,
 915 5051-5064.
- 916 Van Gool, D., David, G., Lammens, M., Baro, F., and Dom, R. (1993). Heparan sulfate expression
 917 patterns in the amyloid deposits of patients with Alzheimer's and Lewy body type dementia.
 918 *Dementia* 4, 308-314.
- 919 Vatolina, T.Y., Boldyreva, L.V., Demakova, O.V., Demakov, S.A., Kokoza, E.B., Semeshin, V.F.,
 920 Babenko, V.N., Goncharov, F.P., Belyaeva, E.S., and Zhimulev, I.F. (2011). Identical functional
 921 organization of nonpolytene and polytene chromosomes in *Drosophila melanogaster*. *PloS one* 6,
 922 e25960.
- 923 Wang, L., Wang, S., and Li, W. (2012). RSeQC: quality control of RNA-seq experiments. *Bioinformatics*
 924 28, 2184-2185.
- 925 Waterhouse, A., Bertoni, M., Bienert, S., Studer, G., Tauriello, G., Gumienny, R., Heer, F.T., De Beer,
 926 T.a.P., Rempfer, C., and Bordoli, L. (2018). SWISS-MODEL: homology modelling of protein
 927 structures and complexes. *Nucleic acids research* 46, W296-W303.
- 928 Waterhouse, A.M., Procter, J.B., Martin, D.M.A., Clamp, M., and Barton, G.J. (2009). Jalview Version
 929 2—a multiple sequence alignment editor and analysis workbench. *Bioinformatics* 25, 1189-1191.
- 930 Xu, S., Panikker, P., Iqbal, S., and Elephant, F. (2016). Tip60 HAT action mediates environmental
 931 enrichment induced cognitive restoration. *PloS one* 11.
- 932 Xu, S., Wilf, R., Menon, T., Panikker, P., Sarthi, J., and Elephant, F. (2014). Epigenetic control of learning
 933 and memory in *Drosophila* by Tip60 HAT action. *Genetics* 198, 1571-1586.
- 934 Xu, S.J., Lombroso, S.I., Fischer, D.K., Carpenter, M.D., Marchione, D.M., Hamilton, P.J., Lim, C.J.,
 935 Neve, R.L., Garcia, B.A., Wimmer, M.E., Pierce, R.C., and Heller, E.A. (2021). Chromatin-
 936 mediated alternative splicing regulates cocaine-reward behavior. *Neuron* 109, 2943-2966.e2948.
- 937 Yang, S.-S., Zhang, R., Wang, G., and Zhang, Y.-F. (2017). The development prospect of HDAC
 938 inhibitors as a potential therapeutic direction in Alzheimer's disease. *Translational*
 939 *neurodegeneration* 6, 19-19.
- 940 Yuan, X.-Z., Sun, S., Tan, C.-C., Yu, J.-T., and Tan, L. (2017). The Role of ADAM10 in Alzheimer's
 941 Disease. *Journal of Alzheimer's Disease* 58, 303-322.
- 942 Zhang, G.L., Zhang, X., Wang, X.M., and Li, J.P. (2014). Towards understanding the roles of heparan
 943 sulfate proteoglycans in Alzheimer's disease. *Biomed Res Int* 2014, 516028.
- 944 Zhang, H., Karisetty, B.C., Bhatnagar, A., Armour, E.M., Beaver, M., Roach, T.V., Mortazavi, S.,
 945 Mandloi, S., and Elephant, F. (2020). Tip60 protects against amyloid- β -induced transcriptomic
 946 alterations via different modes of action in early versus late stages of neurodegeneration. *Molecular*
 947 *and Cellular Neuroscience* 109, 103570.
- 948 Zhang, Y., Lei, M., Yang, X., Feng, Y., Yang, Y., Loppnau, P., Li, Y., Yang, Y., Min, J., and Liu, Y.
 949 (2018). Structural and histone binding studies of the chromo barrel domain of TIP 60. *FEBS letters*
 950 592, 1221-1232.
- 951 Zhu, X., Singh, N., Donnelly, C., Boimel, P., and Elephant, F. (2007). The cloning and characterization of
 952 the histone acetyltransferase human homolog Dmel\TIP60 in *Drosophila melanogaster*:
 953 Dmel\TIP60 is essential for multicellular development. *Genetics* 175, 1229-1240.
- 954
- 955

956 **FIGURE LEGENDS**

957 **Figure 1: Tip60 secondary structure conservation with Esa1 HAT and putative RNA targets.**

958 **(A)** Tip60 chromodomain is predicted to fold in a similar secondary structure as Esa1 chromodomain
 959 with conserved RNA-binding helical turn ($\eta 2$) and four proven RNA-binding residues from Esa1.
 960 *Drosophila melanogaster* Tip60 (Q960X4) and *Saccharomyces cerevisiae* Esa1 (Q08649) sequence
 961 similarities and secondary structure information were analyzed using ESPript. **(B)** Several key
 962 mRNA involved in synaptic plasticity are putative Tip60 targets. RNA-protein interactions prediction
 963 (RPISeq) server was used to score *Drosophila* Tip60 (Q960X4) protein interactions with mRNA
 964 candidates. A probability of >0.5 suggests a strong possibility of the mRNA candidates being a target
 965 of the Tip60 chromodomain or the full protein, respectively.

966

967 **Figure 2: Tip60's structural homology with known RNA-binding Esa1 HAT uncovers distinct**

968 **conserved RNA-binding and histone-binding sites.** **(A)** Structural homology between *Drosophila*
 969 Tip60 chromodomain (cyan, SWISS-MODEL) and known RNA-binding yeast Esa1 chromodomain
 970 (orange, PDB: 2Ro0). **(B)** Amino acid residues in the *Drosophila* Tip60 chromodomain predicted for
 971 RNA binding (red), histone binding (green) or both functions (magenta) **(C)** Evolutionary
 972 conservation of chromodomain RNA-binding and histone-binding residues across mammalian
 973 species. Multiple sequence alignment with Clustal Omega was used to align *Drosophila* Tip60
 974 chromodomain (UniProt: Q960X4) with Esa1 yeast (Q08649) and Tip60 from *Homo sapiens*
 975 (Q92993), *Pongo abelii* (Sumatran orangutan) (Q5RBG4), *Mus musculus* (Q8CHK4), and *Rattus*
 976 *norvegicus* (Q99MK2). Refer to Table 2-1 for Tip60 RNA targets significantly enriched in IP and
 977 Table 2-2 for Gene Ontology analysis and human disease relevance.

978

979 **Figure 3: Tip60-RNA immunoprecipitation (RIP) assay controls. (A)** Bioanalyzer gel shows

980 immunoprecipitated RNA at specific nucleotide sizes with increasing Tip60 antibody concentrations

981 of 5 μ g (lanes 1,2), 7.5 μ g (lanes 3,4) and 10 μ g (lanes 5,6). RNA is not immunoprecipitated with
 982 Rabbit IgG control (lanes 7,8). RNA is separated based on nucleotide sizes from larger molecules at
 983 top to smaller molecules at bottom. **(B)** Tip60-RNAi mediated knockdown reduces amount of RNA
 984 immunoprecipitated (red) when compared to wild type (blue). Sample peak is lost post RNase
 985 treatment of wild type sample (magenta), confirming presence of RNA in the immunoprecipitate
 986 samples. RNA migration time (seconds, X-axis) of constant marker dye and samples are plotted
 987 against fluorescence intensity (Y-axis). RNA concentration is determined based on the time corrected
 988 area underneath each sample peak and the upper marker in each sample. [nt]: nucleotide sizes; [FU]:
 989 fluorescence intensity. See Table 3-1 for Tip60's RNA targets comparison between *Drosophila*
 990 wildtype, APP and APP;Tip60 conditions.

991

992 **Figure 4: RNA Immunoprecipitation and Sequencing (RIP-Seq) reveals a highly specific,**
 993 **selective, and reproducible RNA-binding function for Tip60 in the *Drosophila* brain.** (A) RIP-
 994 Seq schematic: Tip60-bound RNA molecules are immunoprecipitated and extracted (IP RNA) along
 995 with the total RNA (INPUT RNA) from *Drosophila* larval brains for RNA Sequencing. **(B)**
 996 Hierarchically clustered heatmap depicting RNA homogeneity within replicates and variability
 997 between IP and INPUT groups from three wildtype (WT) biological replicates. **(C)** Classification of
 998 Tip60 RNA targets as protein coding or non-coding RNA. **(D)** Gene ontology biological processes
 999 and **(E)** human diseases enriched for the top 2000 Tip60 RNA targets. Refer to Table 4-1 for overlap
 1000 between Tip60's RNA targets and gene targets at the chromatin level.

1001

1002 **Figure 5: Tip60-RNA target identification in the wildtype (WT) samples.** (A) Principal
 1003 component analysis (PCA) plot showing samples variation between RNA enriched in the IP samples
 1004 (triangles) and respective Input samples (circles) from three wildtype (WT) *Drosophila* biological
 1005 replicates. **(B)** MA scatter plot shows log fold change of IP RNA over Input RNA (Y-axis) and

1006 average expression between the groups (X-axis). Red scatters are present below the threshold cutoff
 1007 of adjusted p-value <0.05. WT: wildtype; IP: immunoprecipitate RNA; INPUT: Input RNA. See
 1008 Tables 5-1 and 5-2 for complete splicing results from rMATS analysis between APP vs. wildtype and
 1009 APP;Tip60 vs APP

1010

1011 **Figure 6: Tip60 RNA targets are altered in *Drosophila* APP neurodegenerative model and**
 1012 **partially rescued by Tip60 overexpression. (A)** Volcano plots depicting Tip60's RNA targets
 1013 specifically enriched in immunoprecipitate RNA (IP RNA) between APP vs. wildtype (left) and
 1014 APP;Tip60 vs. APP (right) *Drosophila* larval brains. Tip60-RNA targets with significantly enriched
 1015 binding (red), reduced binding (blue) or non-significant binding alterations (black) between
 1016 genotypes are depicted (cutoff: adjusted p-value <0.05; log₂ Fold Change of ≤-0.583 and ≥0.583).
 1017 **(B)** UpSet plot representing the distribution and intersection of Tip60's RNA target alterations
 1018 between APP vs. wildtype and APP;Tip60 vs APP. Rows represent the total number of Tip60-RNA
 1019 targets in each comparison that are either unique (black dots) or overlapping (connecting line) with
 1020 other comparisons. Purple columns represent Tip60 rescued RNA targets. **(C)** Biological pathways
 1021 enriched for Tip60-rescued RNA targets that are either excluded in wildtype, targeted in APP, and
 1022 excluded again in APP;Tip60 (left) or targeted in wildtype, excluded in APP, and targeted again in
 1023 APP;Tip60 (right). Some genes appear in more than one GO category. WT: wildtype; NS: Not
 1024 significant.

1025

1026 **Figure 7: Tip60's RNA targets comparison between *Drosophila* wildtype, APP and APP;Tip60**
 1027 **conditions.** Heatmap depicting RNA enriched in IP and INPUT biological replicates from **(A)** APP,
 1028 and **(B)** APP;Tip60 *Drosophila* larval brains. **(C)** Principal component analysis (PCA) plot showing
 1029 variation between Tip60's RNA targets that are specifically enriched in the immunoprecipitate RNA
 1030 (IP RNA) between the wildtype (square), APP (circles), and APP;Tip60 (triangles). **(D)** Venn

1031 diagram shows distribution of Tip60's RNA targets that are unique or shared between wildtype
 1032 (blue), APP (purple), and APP;Tip60 (red). WT: wildtype; IP: immunoprecipitate RNA; Input: Input
 1033 RNA.

1034

1035 **Figure 8: Tip60 targets identical gene loci at chromatin and RNA levels. (A)** Reads from Tip60-
 1036 immunoprecipitated RNA (IP) and total RNA (Input) samples in wildtype, APP and APP;Tip60 were
 1037 mapped to corresponding genomic features in the following priority order: CDS exons (blue) > UTR
 1038 exons (black /green) > Introns (orange) > Intergenic regions. CDS: coding DNA sequence; TSS:
 1039 transcription start site; TES: transcription end site. **(B)** Overlap between Tip60's RNA targets and its
 1040 gene targets identified via Chromatin Immunoprecipitation and Sequencing (ChIP-Seq) in wildtype,
 1041 APP and APP;Tip60 *Drosophila* larval brains. **(C)** *Drosophila* salivary polytene chromosomes
 1042 stained for DAPI (blue), Histone H3 pan-acetyl (yellow), RNA polymerase-II (green), and Tip60
 1043 (red) antibodies wither in the presence or absence of RNase.

1044

1045 **Figure 9: Tip60 localizes to the actively transcribed gene regions on polytene chromosomes.**
 1046 Polytene chromosomes from wildtype *Drosophila* salivary glands are squashed and co-stained with
 1047 DAPI (blue), RNA polymerase-II (green), and Tip60 (red). Tip60 co-localizes with RNA polymerase
 1048 II in the interbands region (merged yellow) representing sites of active gene transcription between
 1049 densely packed heterochromatin. RNAPII: RNA-polymerase II.

1050

1051 **Figure 10: Tip60's chromatin recruitment is sensitive to RNase treatment.** Polytene
 1052 chromosomes from wildtype *Drosophila* salivary glands were squashed and co-stained with DAPI
 1053 (blue), histone H3 pan-acetyl (yellow), RNA polymerase-II (green), and Tip60 (red) antibodies. (A)
 1054 In absence of RNase treatment, polytene chromosomes are saturated with Histone H3 pan-acetyl,
 1055 RNA polymerase-II and Tip60 staining. (B) After RNase treatment, RNA polymerase-II and Tip60

1056 staining are partially lost while histone H3 pan-acetylation staining remains unaffected on polytene
1057 chromosomes. RNAPII: RNA-polymerase II; H3Ac: Histone H3 pan-acetylation.

1058

1059 **Figure 11: Tip60-RNA targets differentially spliced in *Drosophila* APP and APP;Tip60 models**
1060 **are implicated in Alzheimer's Disease (AD).** (A) Summary of total differential alternative splicing
1061 events detected between APP vs. wildtype and APP;Tip60 vs. APP using rMATS. Alternative
1062 splicing events are classified as Skipped Exons (SE), Alternative 5' Splice Site (A5SS), Alternative
1063 3' Splice Site (A3SS), Mutually Exclusive Exons (MXE) and Retained Intron (RI). (B) Volcano plot
1064 depicting splicing events significantly altered between APP vs. wildtype (left) and APP;Tip60 vs.
1065 APP (right) *Drosophila* larval brains. The relative abundance of each isoform was quantified as
1066 percentage spliced in (PSI) for every genotype; Δ PSI (X-axis) quantified the difference in relative
1067 isoform abundance between different genotypes. All events are significant (false discovery rate, FDR
1068 <0.1 and $|\Delta$ PSI ≥ 0.1). (C) Significantly altered splicing events were mapped to fly genome and
1069 filtered for direct Tip60 RNA targets identified via RIP-Seq in wildtype. Conserved human orthologs
1070 were predicted using DIOPT and compared with DisGeNET database for AD relevance.

1071

1072 **Figure 12: Tip60 modulates alternative splicing decisions of Alzheimer's Disease (AD)-**
1073 **associated genes.** (A) The 15 triaged Tip60-rescued splicing defects in AD-associated genes. X-axis
1074 represents differences in relative isoform abundance (Δ PSI, where PSI= Percent Spliced In) between
1075 APP vs. wildtype (red) and APP;Tip60 vs. APP (black). (B) Schematic representation of Tip60-
1076 rescued splicing events from every type of alternative splicing. Percentage represents the relative
1077 isoform abundance for the indicated genotype obtained via rMATS analysis. (C-E) Splice specific
1078 RT-qPCR on *Drosophila* larval brains from wildtype and Tip60 RNAi mediated knockdown (n=3) to
1079 detect alternatively spliced isoforms in heph, Dscam1 and Adar genes. Histogram represents relative
1080 fold change in mRNA expression calculated using ddCT method using Rpl32 as the housekeeping

1081 gene. Statistical significance was calculated using unpaired Student's t-test. * $p < 0.05$, ** $p < 0.01$,
 1082 *** $p < 0.001$. Error bars indicate SEM.

1083

1084 **Figure 13: Tip60-RNA targeting is conserved in human hippocampus and impaired in**
 1085 **Alzheimer's Disease (AD) patient hippocampus. (A)** Conserved human orthologs for the 12
 1086 triaged AD-associated Tip60-rescued genes were predicted using DIOPT. Previously reported
 1087 splicing defects in post-mortem human AD brain tissues were identified in the literature: [†](Marques-
 1088 Coelho et al., 2021); ^{*}(Adusumalli et al., 2019); [^](Tollervey et al., 2011); ^ˆ(Raj et al., 2018). **(B)**
 1089 Tip60-bound RNA Immunoprecipitation and RT-qPCR (RIP-qPCR) was performed on hippocampus
 1090 obtained from healthy controls or AD patients (n=3 brains). Histogram represents Tip60 IP fold
 1091 enrichment for each gene relative to Rabbit IgG (negative control). Statistical significance was
 1092 calculated using two-way ANOVA with Sidak's multiple comparison test. **** $p < 0.001$. Error bars
 1093 indicate SEM.

1094

1095 **Figure 14: Model for Tip60's novel bi-level gene regulation at the chromatin and RNA level.**
 1096 Our results support a model by which Tip60 regulates both, the expression and splicing of a similar
 1097 set of neural targets via its functions at the chromatin and the RNA, respectively. **(A)** Tip60 promotes
 1098 neural gene expression via histone acetylation at the chromatin that increases chromatin accessibility
 1099 for the transcriptional machinery. **(B)** Tip60 targets the newly transcribed pre-mRNA to modulate its
 1100 alternative splicing decision by either altering splice site accessibility, assembling a complex that
 1101 affects splicing, or tethering it to the chromatin for splicing regulation via histone acetylation. The
 1102 model figure was created using BioRender.com.

1103

1104

1105 TABLE LEGENDS

1106 **Table 1:** Primer sequences used for Human RIP-qPCR.

1107

1108 **Table 2:** Primer sequences used for splice-specific qPCR in Tip60 RNAi mediated knockdown.

1109

1110 **Table 3: Mammalian conservation of Tip60-RNA targets with altered splicing in *Drosophila***

1111 **APP and APP;Tip60 models.** Significantly altered splicing events in **(A)** APP vs. wildtype and **(B)**

1112 APP;Tip60 vs APP were mapped to fly genome and filtered for Tip60 RNA targets

1113 immunoprecipitated in *Drosophila* wildtype genotype. Conserved human orthologs were predicted

1114 using best match from the DRSC Integrative Ortholog Prediction Tool (DIOPT). Human ortholog

1115 match were found for 177/186 and 152/162 splicing targets in the APP vs. wildtype and APP;tip60 vs

1116 APP comparisons, respectively.

1117

1118 **Table 4: Tip60-RNA targets with altered splicing enriched in DisGeNET Alzheimer's Disease**

1119 **database.** Conserved human orthologs of Tip60-RNA targets with significantly altered splicing

1120 events in **(A)** APP vs. wildtype and **(B)** APP;Tip60 vs APP were compared with the curated

1121 DisGeNET gene-disease association database for Alzheimer's Disease (AD). 54 genes and 44 genes

1122 were found to be associated with AD from the APP vs. wildtype and APP;Tip60 vs APP splicing

1123 comparisons, respectively.

1124

1125 **Table 5: Genomic coordinates of the triaged Tip60-rescued splicing events from rMATS**

1126 **analysis.**

1127 Differential splicing isoforms were quantified as Percent Spliced In (PSI) using rMATS. Difference

1128 in isoform abundance between genotypes APP vs. wildtype and APP;Tip60 vs. APP is reported as

1129 Delta PSI. Alternative splicing events include: **(A)** skipped exon (SE), **(B)** alternative 5' splice site

1130 (A5SS), **(C)** alternative 3' splice site (A3SS), **(D)** mutually exclusive exons (MXE) and **(E)** retained

1131 intron (RI).

1132

1133 **Table 6: Tip60-rescued mutually exclusive splicing events in *Dscam1*.** Differential splicing
 1134 isoforms were quantified as Percent Spliced In (PSI) using rMATS. Difference in MXE isoform
 1135 abundance between genotypes APP vs. wildtype and APP;Tip60 vs. APP is reported as Delta PSI.

1136

1137 **EXTENDED DATA**

1138 **Extended Table 2-1: Tip60-RNA targets significantly enriched in the immunoprecipitate**
 1139 **fraction of *Drosophila* wildtype, APP and APP;tip60 larval brains.** Using a threshold cutoff of
 1140 Benjamini-Hochberg adjusted p-value (padj) <0.05, RNA significantly enriched in Tip60-
 1141 immunoprecipitated RNA (IP RNA) over the total RNA (Input RNA) were identified for (A)
 1142 wildtype, (B) APP, and (C) APP;Tip60. The Tip60 RNA targets were classified as coding mRNA
 1143 (RefSeq category: NM) or non-coding RNA (RefSeq category: NR).

1144

1145 **Extended Table 2-2: Gene Ontology and human disease relevance for Tip60 RNA targets in**
 1146 ***Drosophila* wildtype larval brains.** (A) Gene ontology biological processes and (B) human disease
 1147 relevance was assessed using FlyEnrichr gene list enrichment analysis tool for *Drosophila*
 1148 *melanogaster*. Top 2000 Tip60 RNA targets significantly enriched in the immunoprecipitate fraction
 1149 of wildtype *Drosophila* larval brains were used as input query.

1150

1151 **Extended Table 3-1: Tip60-RNA target alterations between *Drosophila* wildtype, APP and**
 1152 **APP;Tip60 larval brains.** Tip60-RNA targets selectively enriched in immunoprecipitate that were
 1153 either significantly enriched or depleted in binding between genotypes were identified as: (A)
 1154 Enriched targeting in APP over wildtype (up APP vs. WT); (B) Less targeting in APP over wildtype
 1155 (down APP vs. WT); (C) Enriched targeting in APP;Tip60 over APP (up APPTip60 vs. APP); (D)
 1156 Less targeting in APP;Tip60 over APP (down APPTip60 vs. APP).

1157

1158 **Extended Table 4-1: Overlap between Tip60's RNA targets and gene targets at the chromatin**
 1159 **level.** Tip60's RNA targets identified via RNA-immunoprecipitation and sequencing (RIP-Seq) were
 1160 compared to its gene targets identified via chromatin immunoprecipitation and sequencing (ChIP-
 1161 Seq) in (A) wildtype, (B) APP, and (C) APP;Tip60 *Drosophila* larval brains.

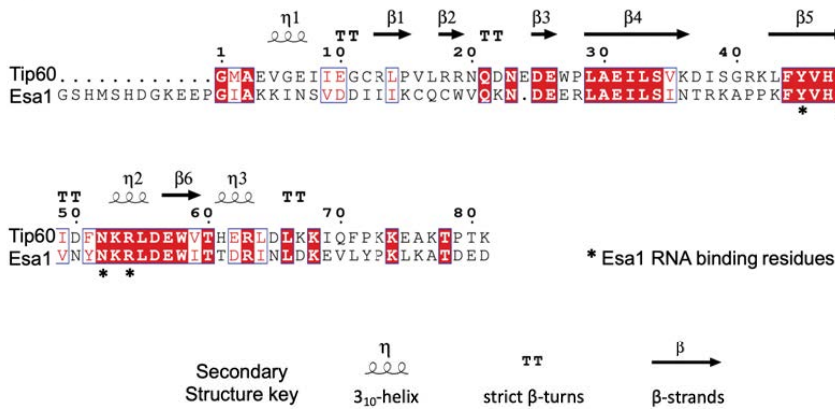
1162

1163 **Extended Table 5-1: Alternative splicing results from rMATS analysis on *Drosophila* APP vs.**
 1164 **wildtype larval brains.** Differential splicing isoforms were identified and compared between total
 1165 RNA samples from APP and wildtype genotypes using rMATS. Junctions Counts (JC) are quantified
 1166 for each type of alternative splicing event: (A) skipped exon (SE), (B) alternative 5' splice site
 1167 (A5SS), (C) alternative 3' splice site (A3SS), (D) mutually exclusive exons (MXE) and (E) retained
 1168 intron (RI). The Percent Spliced In (PSI) values are reported as Inclusion Level for APP (Sample 1)
 1169 and wildtype (Sample 2). Significant splicing events were identified using the following cutoffs:
 1170 false discovery rate (FDR) <0.1 and Inclusion Level Difference (Δ PSI) ≥ 0.1 or ≤ 0.1 .

1171

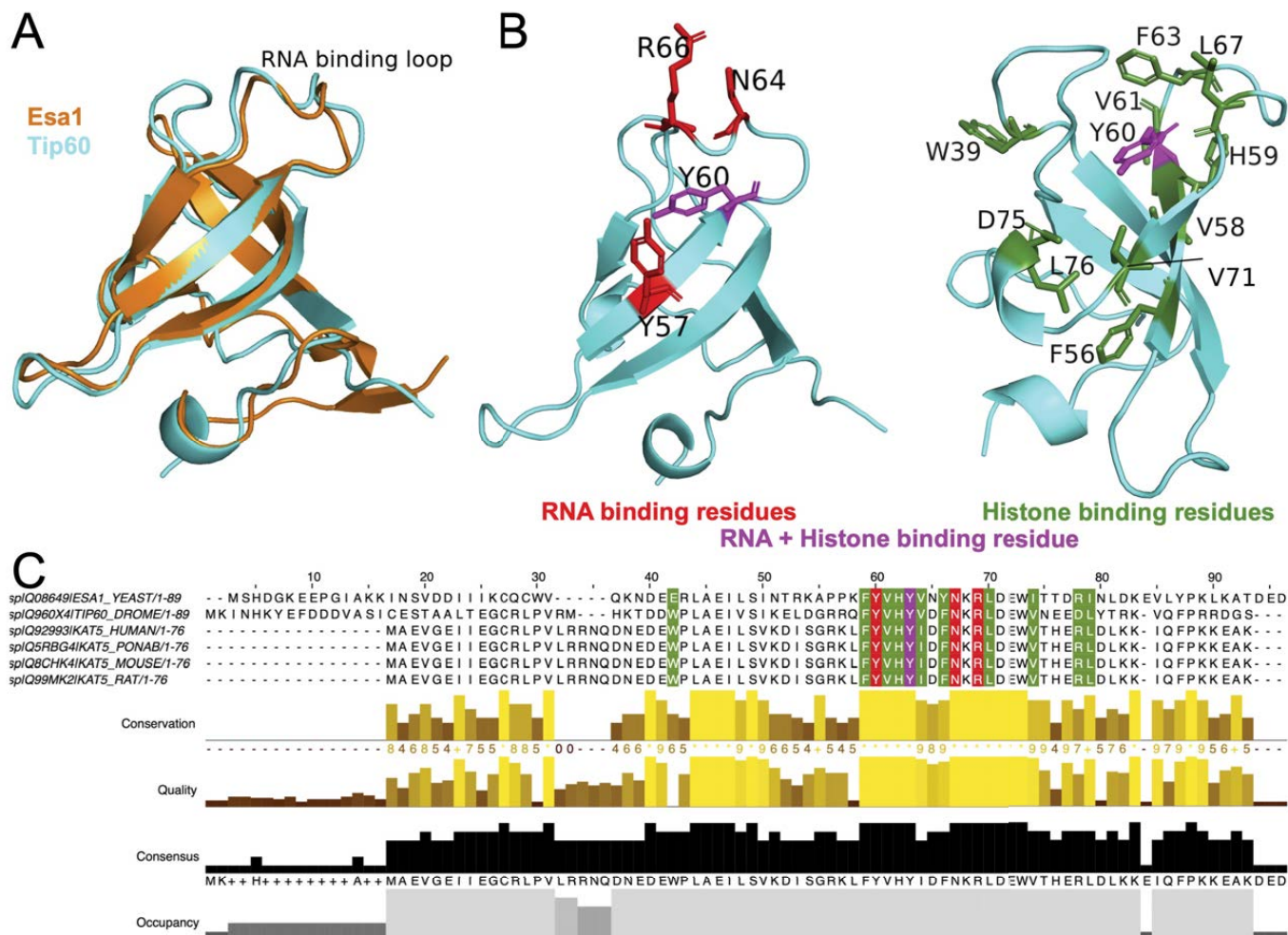
1172 **Extended Table 5-2: Alternative splicing results from rMATS analysis on *Drosophila***
 1173 **APP;Tip60 vs. APP larval brains.** Differential splicing isoforms were identified and compared
 1174 between total RNA samples from APP;Tip60 and APP genotypes. Junctions Counts (JC) are
 1175 quantified for each type of alternative splicing event: (A) skipped exon (SE), (B) alternative 5' splice
 1176 site (A5SS), (C) alternative 3' splice site (A3SS), (D) mutually exclusive exons (MXE) and (E)
 1177 retained intron (RI). The Percent Spliced In (PSI) values are reported as Inclusion Level for
 1178 APP;Tip60 (Sample 1) and APP (Sample 2). Significant splicing events were identified using the
 1179 following cutoffs: false discovery rate (FDR) < 0.1 and Inclusion Level Difference (Δ PSI) ≥ 0.1 or \leq
 1180 0.1.

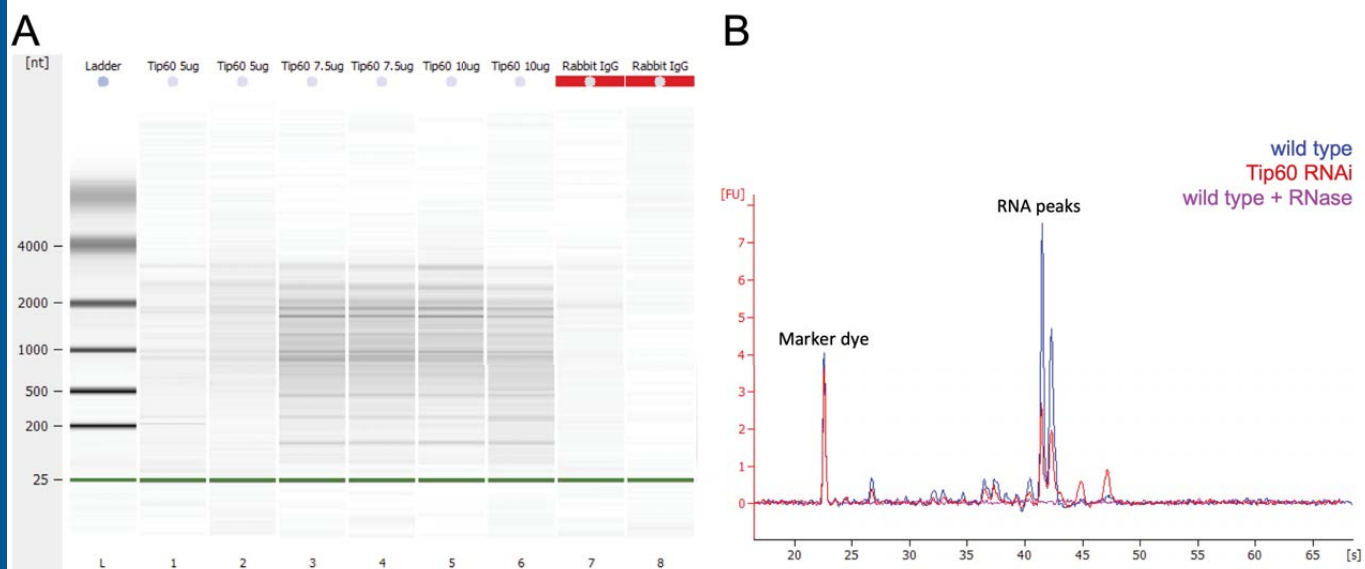
A

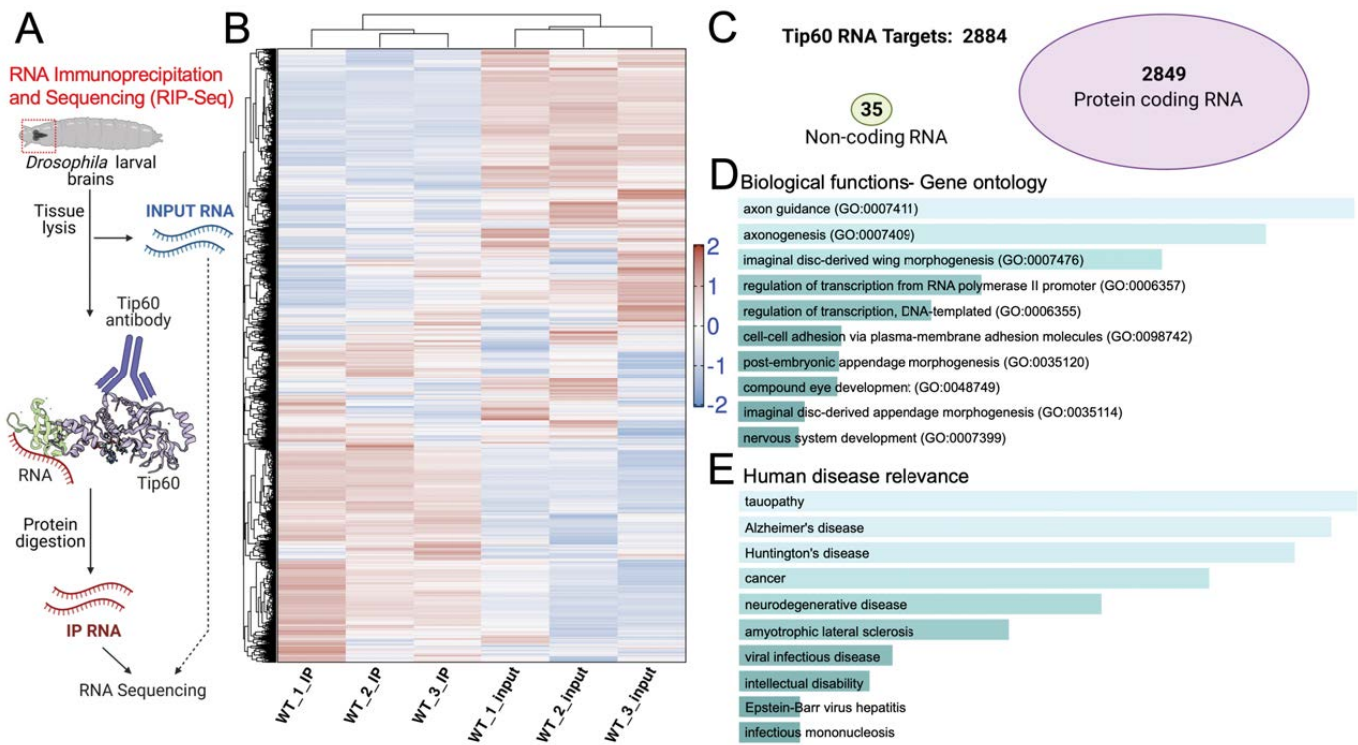


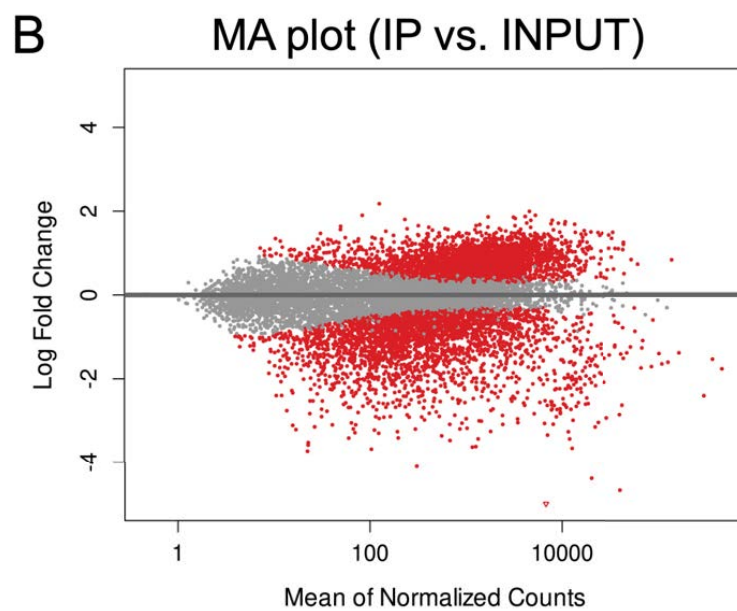
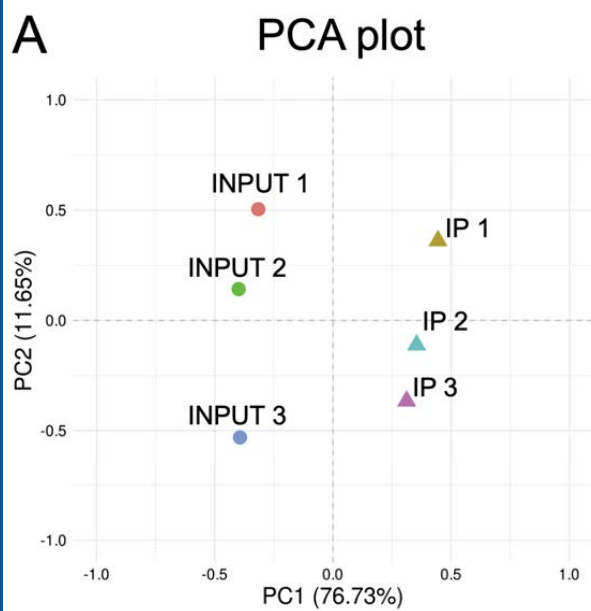
B

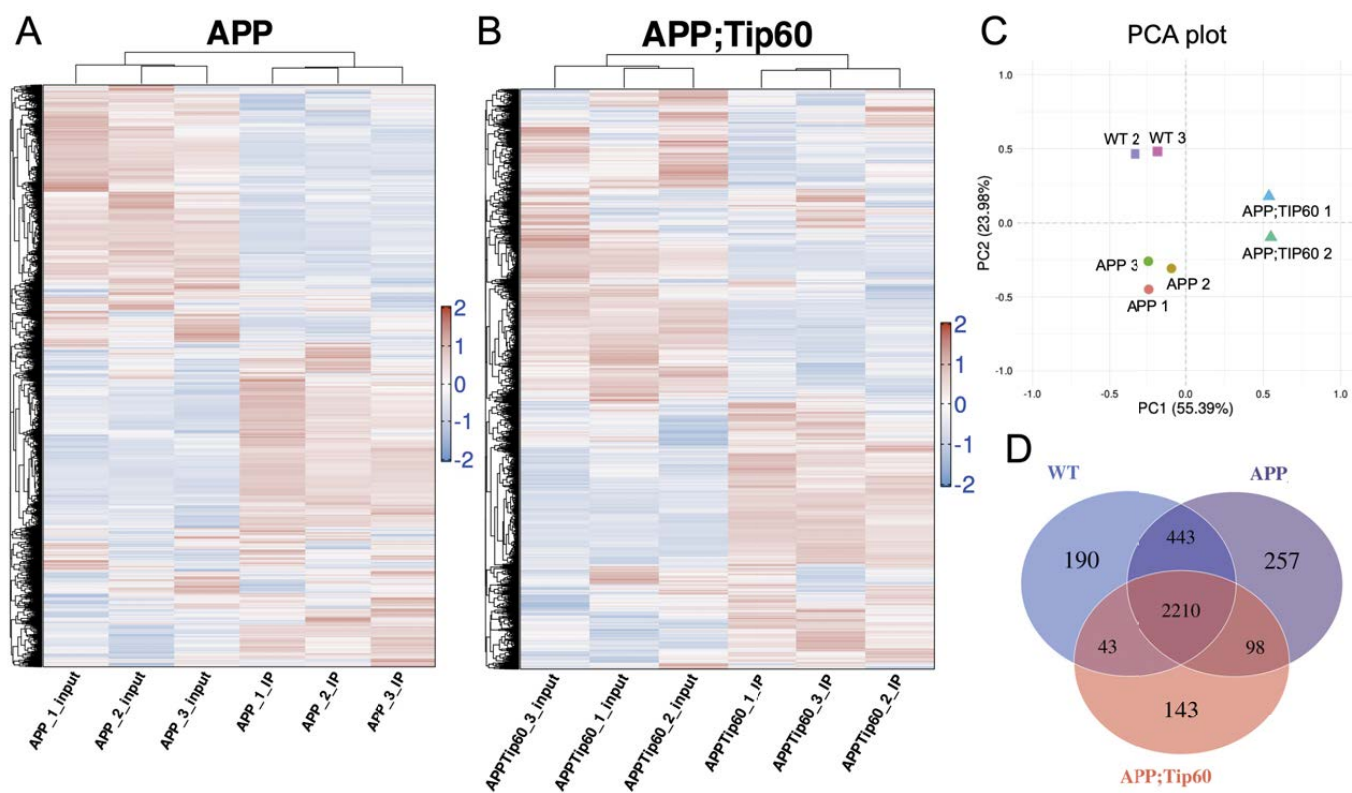
| RNA-Protein Interaction (RPI) Prediction | | | |
|--|-----------------------|----------------------------|---------------------------|
| <i>Drosophila</i> RNA target | Mammalian ortholog | Tip60 chromo- domain | Tip60 whole protein |
| Arm | β -catenin | 0.92 | 0.96 |
| Bruchpilot | CAST | 0.88 | 0.97 |
| CASK | CASK | 0.88 | 0.93 |
| Futsch | MAP1A/B | 0.69 | 0.9 |
| GluRIIA | GluK1-4 | 0.97 | 0.98 |
| GluRIIB | GluK1-4 | 0.86 | 0.97 |
| GluRIIC | GRID2 | 0.89 | 0.93 |
| Neurologin 2 | Neurologin | 0.94 | 0.97 |
| Shaker | KCNA1 | 0.88 | 0.98 |
| Shibire | Dynamin 1 | 0.94 | 0.98 |
| Synapsin | SYN3 | 0.93 | 0.99 |

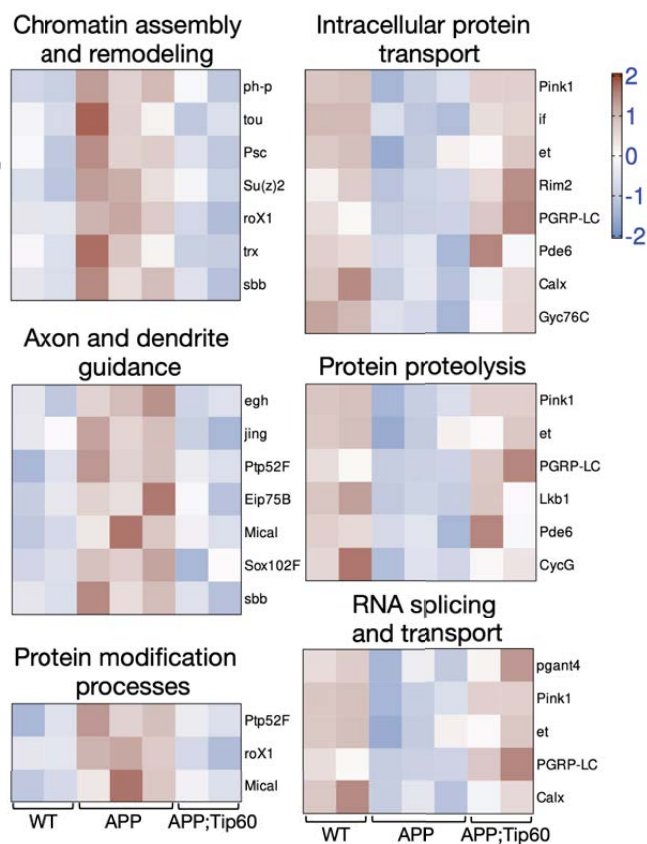


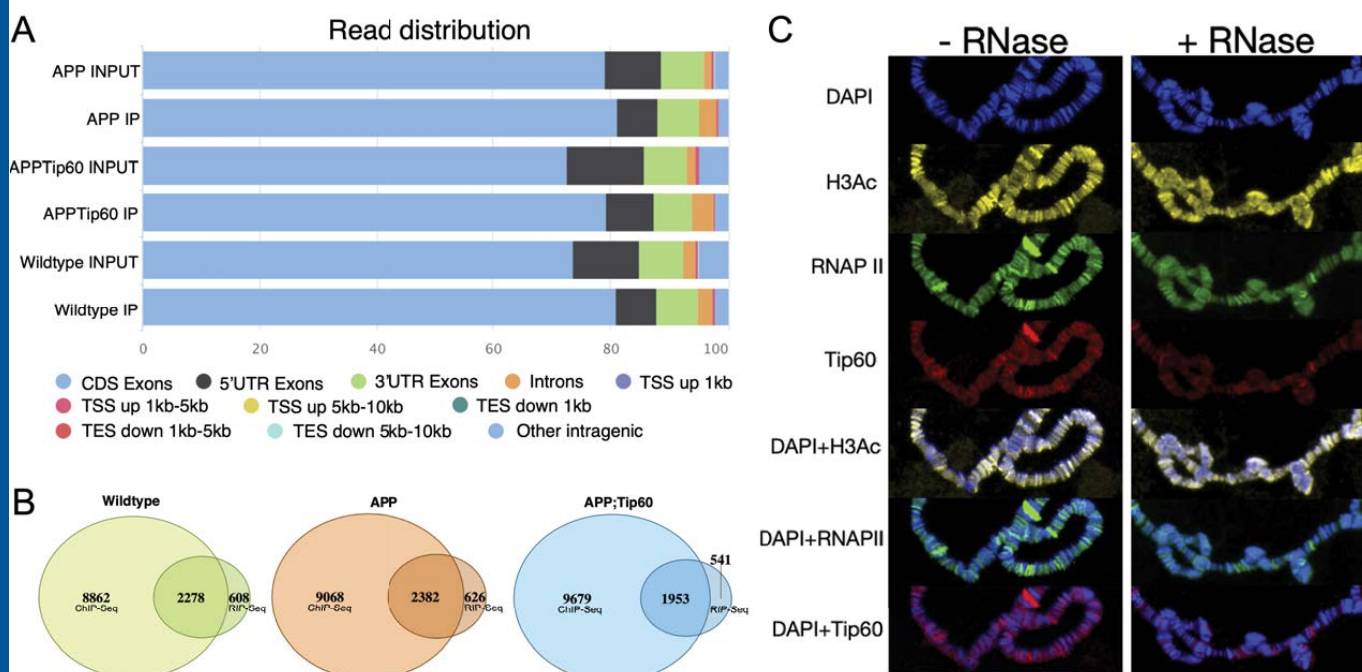


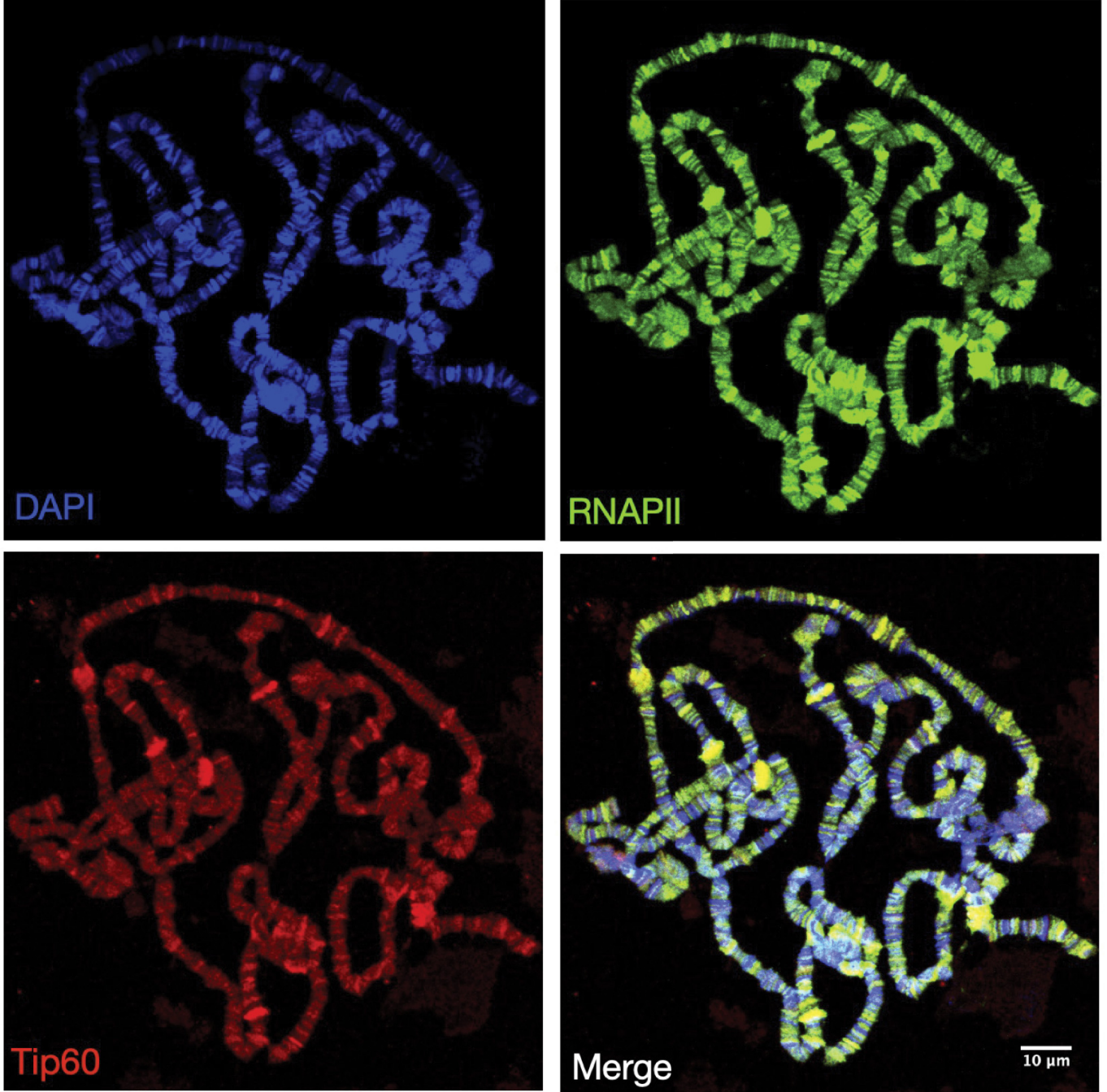




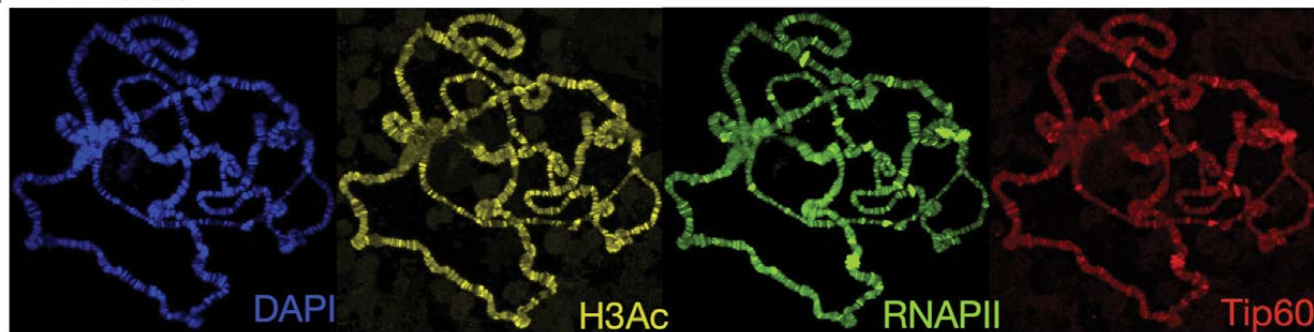




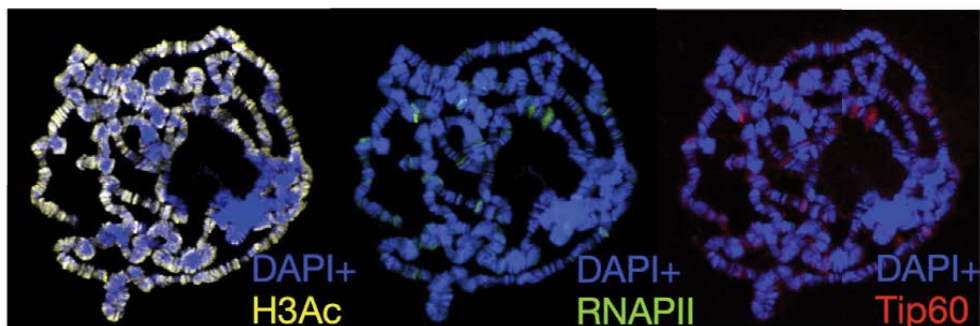
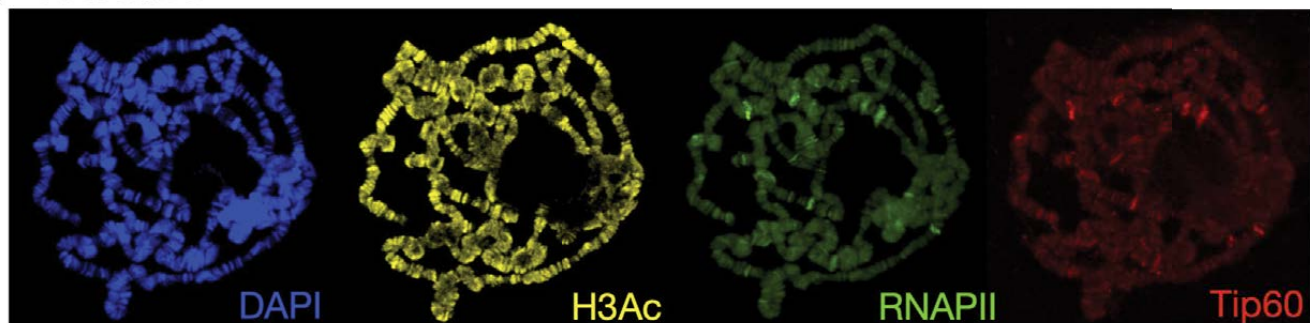


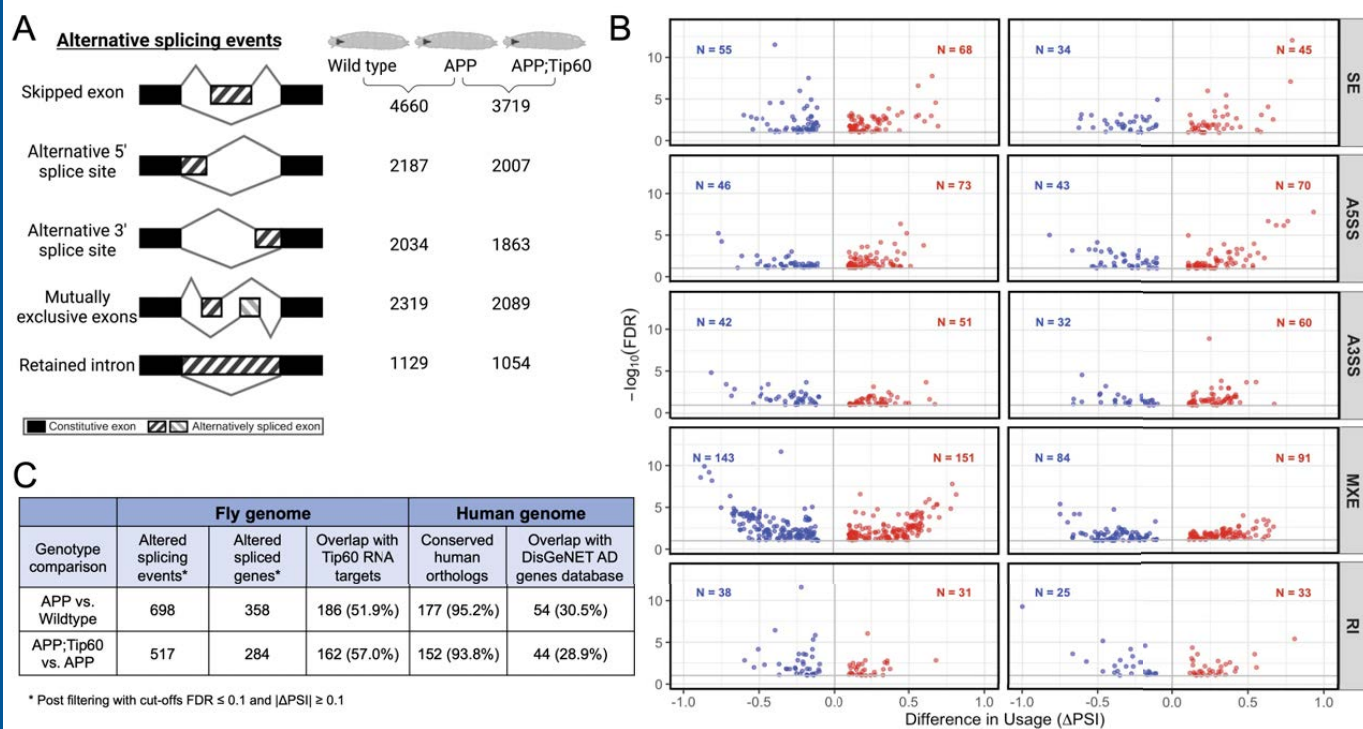


A -RNase

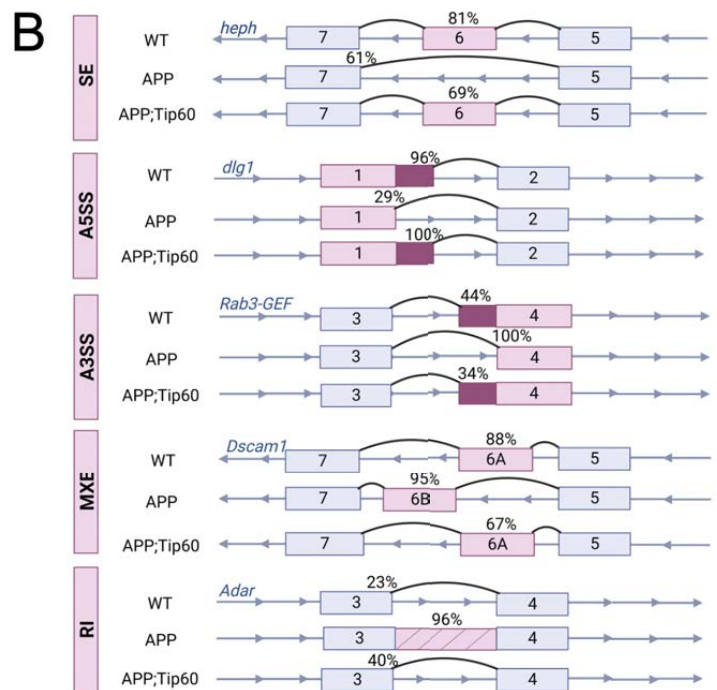
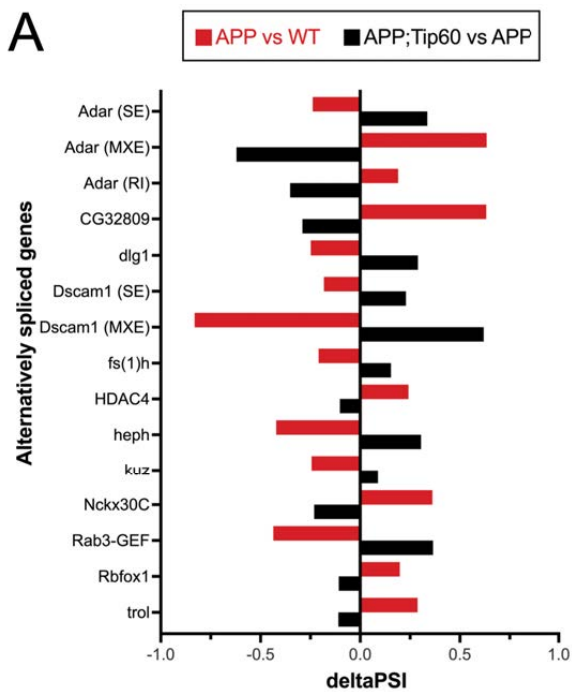


B +RNase

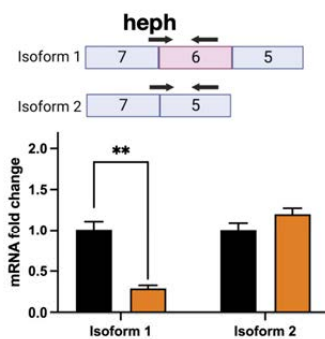




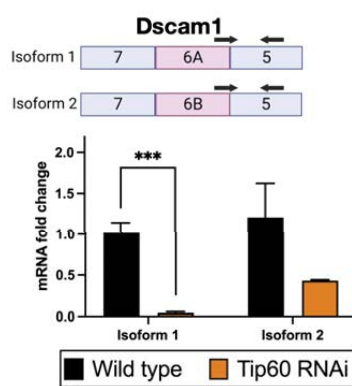
A



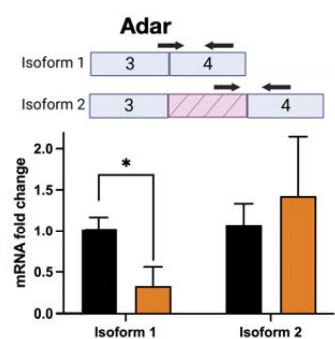
C



D



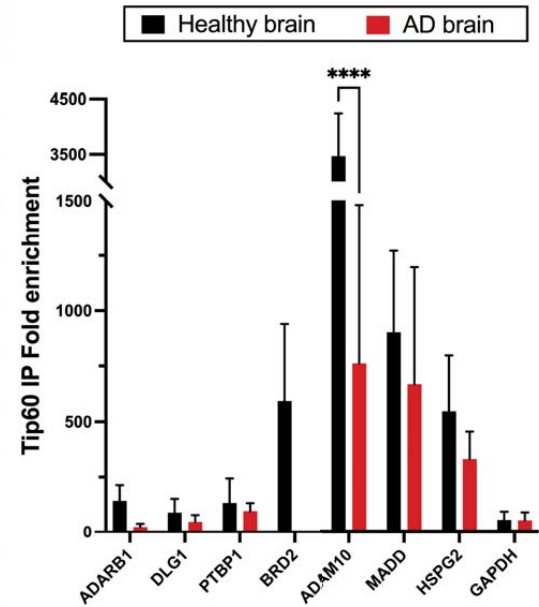
E



A

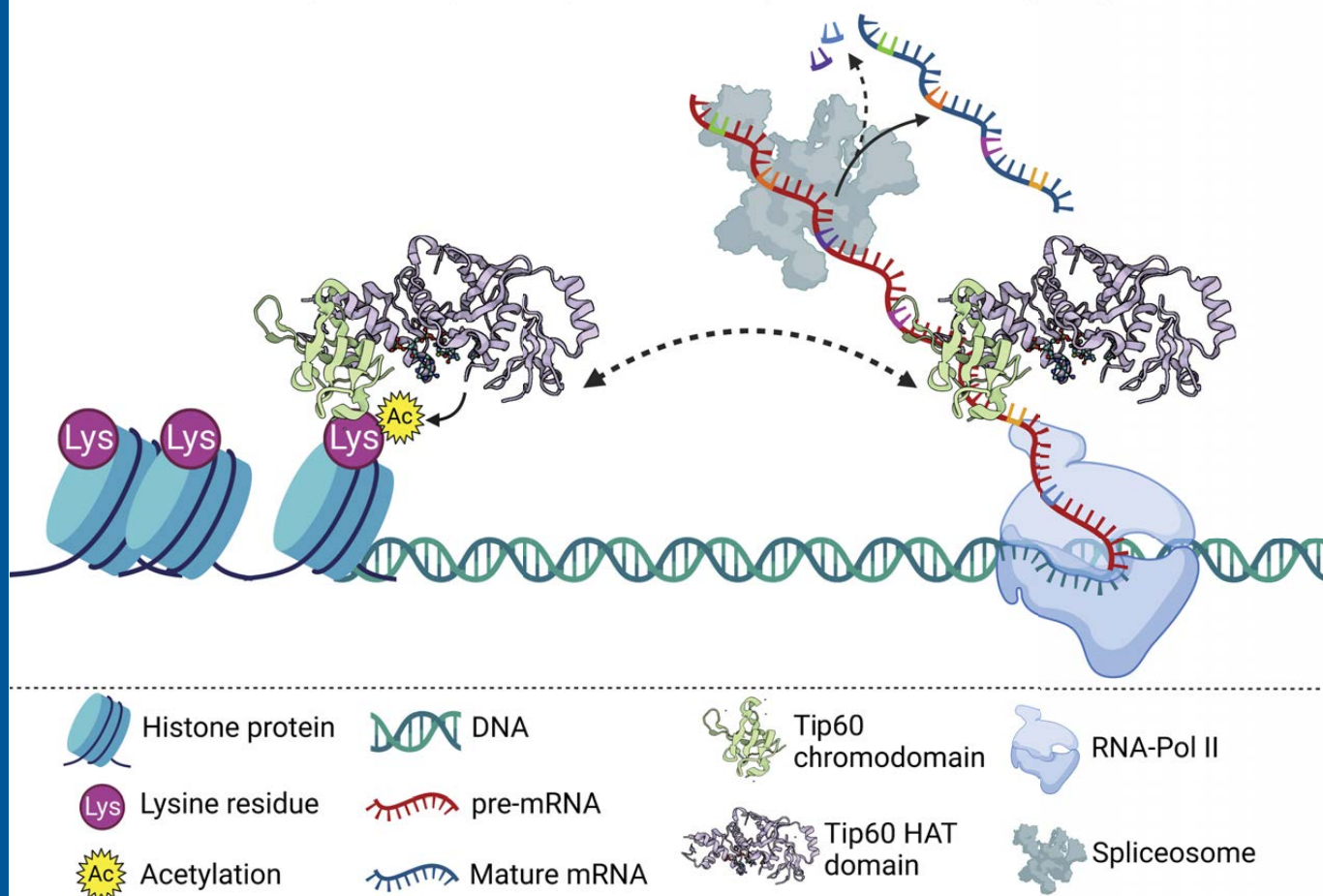
| No. | <i>Drosophila</i> | | | Human ortholog | | |
|-----|-------------------|----------------|----------------|----------------|---|------------------------------|
| | Gene | Splicing event | Splice site | Gene | Biological function | Splicing defects in AD brain |
| 1. | Adar | SE | Exon 3 | ADARB1 | Adenosine to inosine RNA editing and alternative splicing | Yes ⁺ |
| | | MXE | Exon at 2 | | | |
| | | RI | Between 3 & 4 | | | |
| 2. | CG32809 | A5SS or A3SS | Exon 1 or 3 | KIAA1217 | Skeletal system development | -- |
| 3. | dlg1 | A5SS | Exon 1 | DLG1 | Synaptic scaffolding; APP metabolism | Yes ⁺⁺ |
| 4. | Dscam1 | SE | Exon 9 | DSCAML1 | Neuron cell adhesion and axon guidance | -- |
| | | MXE | Exon at 6 | | | |
| 5. | fs(1)h | A5SS | Exon 1 | BRD2 | Chromatin remodeling and regulation of transcription | Yes ⁺ |
| 6. | HDAC4 | A3SS or MXE | Exon 3 or 5 | HDAC4 | Histone deacetylation mediated gene repression | -- |
| 7. | heph | SE | Exon 6 | PTBP1 | RNA alternative splicing and mRNA processing | Yes ⁺⁺ |
| 8. | kuz | SE | Exon 3 or 12 | ADAM10 | α -secretase; Non-amyloidogenic APP cleavage | Yes ⁺ |
| 9. | Nckx30C | A3SS | Exon 1 or 2 | SLC24A2 | Calcium signaling for learning and memory | -- |
| 10. | Rab3-GEF | A3SS | Exon 4 | MADD | Rab3 GDP to GTP activation; Cell apoptosis | Yes ⁺⁺ |
| 11. | Rbfox1 | MXE | Exon at 3 or 9 | RBFOX1 | RNA alternative splicing and mRNA processing | -- |
| 12. | trol | SE | Exon 20 | HSPG2 | Cell-surface receptor signaling; amyloid-beta binding | Yes ⁺ |

B



A. Tip60 mediated epigenetic programming

B. Tip60 mediated RNA splicing control



| No. | Tip60 RNA target | Human ortholog | Forward primer | Reverse primer |
|-----|------------------|----------------|-----------------------|------------------------|
| 1 | Adar | ADARB1 | AAGCTGCCTTGGGATCAGAG | GACACGTTGTCCAGATTGCG |
| 2 | CG32809 | KIAA1217 | GCAGAACTCCAGGCATTCCA | TCCATTTGGGGGCCATTTTC |
| 3 | dlg1 | DLG1 | GGTATGTGCGCCTTGGATCT | AAGGTGCAATGCTCTCTGGG |
| 4 | Dscam1 | DSCAML1 | TTTCAACAAGATTGGCCGCAG | AATCTGGTAGCCCCGGATGA |
| 5 | fs(1)h | BRD2 | ATACGGGTGTGCCTTTGGG | TCCTCAAACCTCATTCCGGC |
| 6 | HDAC4 | HDAC4 | TGGAGTGGGGAGAAGCATCA | TCCAACGAGCTCCAACTCC |
| 7 | heph | PTBP1 | CTGCGCATCGACTTTTCCAA | AGGCTGAGATTATACCAGGTGC |
| 8 | kuz | ADAM10 | ACCACAGACTTCTCCGGAATC | GGTCTGTGAAGACATAGGCCA |
| 9 | Nckx30C | SLC24A2 | CTTCCAAACAGCACCAGCAC | GACTTGCTTGCGGGTTTCAG |
| 10 | Rab3-GEF | MADD | AAAGCATCAAACCCGGACCT | ACAAAGACGCCTCGAACTGT |
| 11 | Rbfox1 | RBFOX1 | GAGGGCCGTAATAATCGAGGT | AAGCCTGGCACTGCATAGAA |
| 12 | trol | HSPG2 | ATACGATGGCTTGTCTCTGCC | GTCGTCTCCTGAGATGCTGTC |
| 13 | GAPDH | GAPDH | TCGGAGTCAACGGATTGGT | TTCCCGTTCTCAGCCTTGAC |

| No. | Tip60 RNA target | Splicing event | Transcript | Transcript RefSeq ID | Forward primer | Reverse primer |
|-----|------------------|--------------------------|------------------------|----------------------|--------------------------|--------------------------|
| 1 | heph | Skipped Exon | Exon 6 present | NM_001260470.1 | GCAGTGGGTGGTGGTACAAT | TGTCGTCGATCCTTACCTTTT |
| | | | Exon 6 spliced out | NM_001104522.3 | CAACGTGTGCAAATCAAACGCGAA | GTTCGTCGATCCTTACCTTAAGTC |
| 2 | dlg1 | Alternate 5' Splice Site | Exon 1 long isoform | NM_001272518.1 | TGGGTGTGTTGTTTCGTCG | TTATCCAACCTTTTGCATTGTGTC |
| | | | Exon 1 short isoform | NM_001258694.2 | TCGATTCTACTAGTTGGTGCAA | TGGCGTTCGAGGGTTAAAGT |
| 3 | Rab3-GEF | Alternate 3' Splice Site | Exon 4 long isoform | NM_001103513.3 | TCCGGGTAATGGTGGACCT | GTAAAGAGGCCGTAAGTCTA |
| | | | Exon 4 short isoform | NM_001347809.1 | TCGGCATTAGCAGCGACT | GAGTGGTGTGAGTGTAGGCG |
| 4 | Dscam1 | Mutually Exclusive Exons | First exon 6 included | NM_001043023.1 | ACCGACGCCTATGATGGAAA | ACTTATCTTGGGGCTGACTGTG |
| | | | Second exon 6 included | NM_001259237.1 | AGGCAGCGAATACGATGGAA | GAGTGTCCACTTTGGGAGCC |
| 5 | Adar | Retained Intron | Intron 3_4 spliced out | NM_001258547.2 | ACGCGAGTTACTACATGCCT | TGGTGCACTACCCGGTTTTA |
| | | | Intron 3_4 retained | NM_001258548.2 | TGAGATGCCAAAATACTCTGATCC | GTGTACCGGACCAGTCTGTG |
| 6 | Rpl32 | | | NM_170461.3 | TGGTTCCGGCAAGCTTCAA | TGTTGTCGATACCCTTGGGC |

| (A) Mammalian conservation of genes with altered splicing in APP vs wildtype | | | | | |
|--|------------|---------------|--------------|-----------------|-------------|
| Fly Gene ID | Fly Symbol | Human Gene ID | Human Symbol | Ensembl ID | DIOPT Score |
| 2768716 | mim | 9788 | MTSS1 | ENSG00000170873 | 7 |
| 2768852 | par-1 | 4140 | MARK3 | ENSG00000075413 | 12 |
| 30975 | ewg | 4899 | NRF1 | ENSG00000106459 | 11 |
| 31017 | sdk | 54549 | SDK2 | ENSG00000069188 | 11 |
| 31121 | CG32809 | 56243 | KIAA1217 | ENSG00000120549 | 9 |
| 31130 | Adar | 104 | ADARB1 | ENSG00000197381 | 12 |
| 31353 | CG43689 | 23040 | MYT1L | ENSG00000186487 | 7 |
| 31364 | Fas2 | 4685 | NCAM2 | ENSG00000154654 | 11 |
| 31379 | bi | 6909 | TBX2 | ENSG00000121068 | 11 |
| 31425 | Ptp4E | 5787 | PTPRB | ENSG00000127329 | 12 |
| 31429 | ovo | 5017 | OVOL1 | ENSG00000172818 | 8 |
| 31550 | Ca-alpha1T | 8911 | CACNA1I | ENSG00000100346 | 11 |
| 31722 | fs(1)h | 6046 | BRD2 | ENSG00000204256 | 9 |
| 318206 | Tlk | 11011 | TLK2 | ENSG00000146872 | 11 |
| 318824 | dpy | 2201 | FBN2 | ENSG00000138829 | 4 |
| 32083 | dlg1 | 1739 | DLG1 | ENSG00000075711 | 13 |
| 32115 | Ptp10D | 5787 | PTPRB | ENSG00000127329 | 11 |
| 32217 | Tomosyn | 134957 | STXBP5 | ENSG00000164506 | 14 |
| 32256 | hep | 5609 | MAP2K7 | ENSG00000076984 | 12 |
| 32273 | sno | 55206 | SBNO1 | ENSG00000139697 | 13 |
| 32278 | HDAC4 | 9759 | HDAC4 | ENSG00000068024 | 11 |
| 32406 | rut | 107 | ADCY1 | ENSG00000164742 | 12 |
| 32442 | Rab3-GEF | 8567 | MADD | ENSG00000110514 | 15 |
| 32536 | sd | 7003 | TEAD1 | ENSG00000187079 | 13 |
| 32543 | Myb | 4603 | MYBL1 | ENSG00000185697 | 11 |
| 32547 | tay | 26053 | AUTS2 | ENSG00000158321 | 4 |
| 32561 | mmd | 4185 | ADAM11 | ENSG00000073670 | 9 |
| 32569 | vap | 5921 | RASA1 | ENSG00000145715 | 13 |
| 32589 | CG3632 | 9110 | MTMR4 | ENSG00000108389 | 13 |
| 32619 | para | 6334 | SCN8A | ENSG00000196876 | 12 |
| 32941 | CoRest | 23186 | RCOR1 | ENSG00000089902 | 11 |
| 33156 | l(2)gl | 3996 | LLGL1 | ENSG00000131899 | 15 |
| 33262 | dock | 4690 | NCK1 | ENSG00000158092 | 14 |
| 33807 | CG9171 | 11041 | B4GAT1 | ENSG00000174684 | 7 |
| 33923 | CG11319 | 57628 | DPP10 | ENSG00000175497 | 9 |

| | | | | | |
|-------|-----------|--------|---------|-----------------|----|
| 33989 | Caper | 9584 | RBM39 | ENSG00000131051 | 11 |
| 34096 | Cka | 29966 | STRN3 | ENSG00000196792 | 15 |
| 34112 | Piezo | 63895 | PIEZO2 | ENSG00000154864 | 13 |
| 34127 | Pvr | 3791 | KDR | ENSG00000128052 | 10 |
| 34519 | SCAR | 10810 | WASF3 | ENSG00000132970 | 13 |
| 34686 | MRP | 8714 | ABCC3 | ENSG00000108846 | 14 |
| 34772 | kuz | 102 | ADAM10 | ENSG00000137845 | 14 |
| 34831 | Dyrk2 | 8798 | DYRK4 | ENSG00000010219 | 12 |
| 34844 | eIB | 80139 | ZNF703 | ENSG00000183779 | 9 |
| 35042 | CLIP-190 | 6249 | CLIP1 | ENSG00000130779 | 12 |
| 35071 | CadN2 | 1002 | CDH4 | ENSG00000179242 | 2 |
| 35077 | rdo | 79883 | PODNL1 | ENSG00000132000 | 1 |
| 35090 | CG42750 | 64174 | DPEP2 | ENSG00000167261 | 8 |
| 35107 | Pde11 | 8654 | PDE5A | ENSG00000138735 | 11 |
| 35213 | CG17544 | 8310 | ACOX3 | ENSG00000087008 | 10 |
| 35340 | dia | 1730 | DIAPH2 | ENSG00000147202 | 14 |
| 35359 | sky | 57465 | TBC1D24 | ENSG00000162065 | 14 |
| 35376 | Nhe2 | 6553 | SLC9A5 | ENSG00000135740 | 12 |
| 35400 | CG8671 | 399665 | FAM102A | ENSG00000167106 | 13 |
| 35402 | Mondo | 22877 | MLXIP | ENSG00000175727 | 13 |
| 35420 | Cul2 | 8453 | CUL2 | ENSG00000108094 | 14 |
| 35442 | CG42748 | 389813 | AJM1 | ENSG00000232434 | 6 |
| 35524 | Src42A | 2444 | FRK | ENSG00000111816 | 14 |
| 35539 | Ars2 | 51593 | SRRT | ENSG00000087087 | 14 |
| 35540 | EcR | 10062 | NR1H3 | ENSG00000025434 | 10 |
| 35652 | Dscam1 | 57453 | DSCAML1 | ENSG00000177103 | 13 |
| 35693 | Vps13 | 23230 | VPS13A | ENSG00000197969 | 13 |
| 35771 | lig | 55833 | UBAP2 | ENSG00000137073 | 11 |
| 35846 | Cir1 | 22859 | ADGRL1 | ENSG00000072071 | 10 |
| 35950 | Pkn | 5586 | PKN2 | ENSG00000065243 | 13 |
| 35977 | brp | 26059 | ERC2 | ENSG00000187672 | 7 |
| 36121 | CG11883 | 4907 | NT5E | ENSG00000135318 | 2 |
| 36176 | metro | 143098 | MPP7 | ENSG00000150054 | 13 |
| 36475 | Dh31-R | 10203 | CALCRL | ENSG00000064989 | 14 |
| 36542 | shot | 667 | DST | ENSG00000151914 | 11 |
| 36554 | RN-tre | 9712 | USP6NL | ENSG00000148429 | 11 |
| 36689 | CG8079 | 55109 | AGGF1 | ENSG00000164252 | 13 |
| 36718 | Khc-73 | 63971 | KIF13A | ENSG00000137177 | 13 |
| 36753 | Strn-Mlck | 4638 | MYLK | ENSG00000065534 | 4 |

| | | | | | |
|---------|--------------|--------|----------|-----------------|----|
| 36889 | Psi | 8880 | FUBP1 | ENSG00000162613 | 11 |
| 36924 | CG30460 | 51101 | ZC2HC1A | ENSG00000104427 | 4 |
| 36978 | Patronin | 23271 | CAMSAP2 | ENSG00000118200 | 13 |
| 37038 | grh | 29841 | GRHL1 | ENSG00000134317 | 8 |
| 37129 | CG43066 | 55117 | SLC6A15 | ENSG00000072041 | 10 |
| 37152 | Sik3 | 23387 | SIK3 | ENSG00000160584 | 3 |
| 37165 | Mctp | 79772 | MCTP1 | ENSG00000175471 | 13 |
| 37230 | hts | 118 | ADD1 | ENSG00000087274 | 14 |
| 37254 | sm | 3191 | HNRNPL | ENSG00000104824 | 12 |
| 37422 | ASPP | 23368 | PPP1R13B | ENSG00000088808 | 14 |
| 37552 | Liprin-gamma | 23254 | KAZN | ENSG00000189337 | 13 |
| 37614 | CG42260 | 1260 | CNGA2 | ENSG00000183862 | 4 |
| 37641 | nahoda | 114928 | GPRASP2 | ENSG00000158301 | 1 |
| 3771968 | Msp300 | 23345 | SYNE1 | ENSG00000131018 | 5 |
| 3772382 | Plp | 5116 | PCNT | ENSG00000160299 | 6 |
| 37892 | mAChR-A | 1133 | CHRM5 | ENSG00000184984 | 11 |
| 37981 | NaCP60E | 6334 | SCN8A | ENSG00000196876 | 4 |
| 38027 | rno | 9767 | JADE3 | ENSG00000102221 | 10 |
| 38142 | CG32333 | 57579 | FAM135A | ENSG00000082269 | 13 |
| 38175 | Psa | 9520 | NPEPPS | ENSG00000141279 | 15 |
| 38176 | lml1 | 9681 | DEPDC5 | ENSG00000100150 | 13 |
| 38257 | mu2 | 9656 | MDC1 | ENSG00000137337 | 4 |
| 38327 | MEP-1 | 5326 | PLAGL2 | ENSG00000126003 | 1 |
| 38344 | Atg2 | 55102 | ATG2B | ENSG00000066739 | 14 |
| 38427 | armi | 54456 | MOV10L1 | ENSG00000073146 | 10 |
| 38438 | CG32264 | 221692 | PHACTR1 | ENSG00000112137 | 8 |
| 38487 | CG14995 | 755 | CFAP410 | ENSG00000160226 | 12 |
| 38491 | ens | 9053 | MAP7 | ENSG00000135525 | 4 |
| 38578 | RhoGEF64C | 50650 | ARHGEF3 | ENSG00000163947 | 3 |
| 38755 | tow | 81563 | C1orf21 | ENSG00000116667 | 2 |
| 38844 | CG7546 | 7917 | BAG6 | ENSG00000204463 | 13 |
| 38863 | Ank2 | 287 | ANK2 | ENSG00000145362 | 6 |
| 39004 | Fhos | 80206 | FHOD3 | ENSG00000134775 | 8 |
| 39054 | Rdl | 2568 | GABRP | ENSG00000094755 | 4 |
| 39089 | MTF-1 | 4520 | MTF1 | ENSG00000188786 | 7 |
| 39180 | dpr10 | 1826 | DSCAM | ENSG00000171587 | 1 |
| 39198 | Rbfox1 | 54715 | RBFOX1 | ENSG00000078328 | 9 |
| 39258 | IRSp53 | 10458 | BAIAP2 | ENSG00000175866 | 10 |

| | | | | | |
|-------|------------|--------|---------|-----------------|----|
| 39399 | app | 79683 | ZDHC14 | ENSG00000175048 | 10 |
| 39765 | Taf4 | 6875 | TAF4B | ENSG00000141384 | 10 |
| 39900 | Exn | 25791 | NGEF | ENSG00000066248 | 5 |
| 39902 | CG3764 | 57600 | FNIP2 | ENSG00000052795 | 12 |
| 39999 | Eip75B | 5468 | PPARG | ENSG00000132170 | 4 |
| 40146 | tey | 55182 | RNF220 | ENSG00000187147 | 2 |
| 40167 | Papss | 9061 | PAPSS1 | ENSG00000138801 | 14 |
| 40292 | Pitslre | 984 | CDK11B | ENSG00000248333 | 11 |
| 40414 | CG11247 | 7652 | ZNF99 | ENSG00000213973 | 2 |
| 40461 | SrpK79D | 26576 | SRPK3 | ENSG00000184343 | 9 |
| 40567 | CG31522 | 79993 | ELOVL7 | ENSG00000164181 | 14 |
| 40850 | Alh | 4302 | MLLT6 | ENSG00000275023 | 7 |
| 40924 | CG2993 | 91947 | ARRDC4 | ENSG00000140450 | 6 |
| 40928 | CG17816 | 56890 | MDM1 | ENSG00000111554 | 1 |
| 40933 | EMC1 | 23065 | EMC1 | ENSG00000127463 | 13 |
| 41062 | pyd | 9414 | TJP2 | ENSG00000119139 | 13 |
| 41118 | FER | 2241 | FER | ENSG00000151422 | 12 |
| 41145 | mura | 152006 | RNF38 | ENSG00000137075 | 7 |
| 41749 | cv-c | 10395 | DLC1 | ENSG00000164741 | 9 |
| 41771 | CG14853 | 285141 | ERICH2 | ENSG00000204334 | 6 |
| 41817 | CG42788 | 9758 | FRMPD4 | ENSG00000169933 | 9 |
| 41911 | nsL1 | 284058 | KANSL1 | ENSG00000120071 | 9 |
| 42127 | alt | 6238 | RRBP1 | ENSG00000125844 | 3 |
| 42310 | unc79 | 57578 | UNC79 | ENSG00000133958 | 14 |
| 42327 | Dys | 1756 | DMD | ENSG00000198947 | 11 |
| 42350 | GluClalpha | 2741 | GLRA1 | ENSG00000145888 | 12 |
| 42358 | Ire1 | 10595 | ERN2 | ENSG00000134398 | 13 |
| 42491 | Cortactin | 2017 | CTTN | ENSG00000085733 | 13 |
| 42600 | CG42390 | 8498 | RANBP3 | ENSG00000031823 | 1 |
| 42608 | CG34377 | 389432 | SAMD5 | ENSG00000203727 | 6 |
| 42646 | Nrx-1 | 9378 | NRXN1 | ENSG00000179915 | 12 |
| 42676 | wake | 162282 | ANKFN1 | ENSG00000153930 | 10 |
| 42687 | wge | 84629 | TNRC18 | ENSG00000182095 | 7 |
| 42742 | Irk1 | 3759 | KCNJ2 | ENSG00000123700 | 9 |
| 42840 | CG13604 | 84959 | UBASH3B | ENSG00000154127 | 14 |
| 42848 | Rox8 | 7073 | TIAL1 | ENSG00000151923 | 14 |
| 42935 | puf | 9736 | USP34 | ENSG00000115464 | 14 |
| 42940 | slo | 3778 | KCNMA1 | ENSG00000156113 | 13 |
| 43087 | msi | 124540 | MSI2 | ENSG00000153944 | 5 |

| | | | | | |
|---------|---------|-------|----------|-----------------|----|
| 43277 | CG31064 | 55680 | RUFY2 | ENSG00000204130 | 13 |
| 43673 | dco | 1453 | CSNK1D | ENSG00000141551 | 11 |
| 43788 | Hcf | 29915 | HCFC2 | ENSG00000111727 | 9 |
| 43795 | zfh2 | 79776 | ZFHX4 | ENSG00000091656 | 12 |
| 43803 | Eph | 2047 | EPHB1 | ENSG00000154928 | 13 |
| 43810 | CG11360 | 51320 | MEX3C | ENSG00000176624 | 11 |
| 43841 | unc-13 | 23025 | UNC13A | ENSG00000130477 | 10 |
| 44030 | msn | 23043 | TNIK | ENSG00000154310 | 13 |
| 44100 | Patj | 10207 | PATJ | ENSG00000132849 | 9 |
| 44448 | scrib | 23513 | SCRIB | ENSG00000180900 | 7 |
| 44817 | for | 5592 | PRKG1 | ENSG00000185532 | 13 |
| 44885 | mys | 3688 | ITGB1 | ENSG00000150093 | 14 |
| 45248 | Nckx30C | 25769 | SLC24A2 | ENSG00000155886 | 14 |
| 45320 | trol | 3339 | HSPG2 | ENSG00000142798 | 11 |
| 45775 | mei-P26 | 81844 | TRIM56 | ENSG00000169871 | 4 |
| 45840 | cpo | 11030 | RBPMS | ENSG00000157110 | 9 |
| 45884 | kkv | 3036 | HAS1 | ENSG00000105509 | 4 |
| 47249 | woc | 9202 | ZMYM4 | ENSG00000146463 | 10 |
| 48571 | heph | 5725 | PTBP1 | ENSG00000011304 | 13 |
| 49070 | Mbs | 4660 | PPP1R12B | ENSG00000077157 | 13 |
| 49090 | RyR | 6262 | RYR2 | ENSG00000198626 | 14 |
| 5740528 | CG34354 | 7072 | TIA1 | ENSG00000116001 | 7 |
| 64875 | disco-r | 646 | BNC1 | ENSG00000169594 | 9 |
| 64877 | cpx | 10815 | CPLX1 | ENSG00000168993 | 9 |
| 7354466 | CG42342 | 1305 | COL13A1 | ENSG00000197467 | 3 |
| 8674055 | mgl | 4036 | LRP2 | ENSG00000081479 | 11 |

(B) Mammalian conservation of genes with altered splicing in APP;Tip60 vs APP

| Fly Gene ID | Fly Symbol | Human Gene ID | Human Symbol | Ensembl ID | DIOPT Score |
|-------------|------------|---------------|--------------|-----------------|-------------|
| 14462845 | CG43783 | 55852 | TEX2 | ENSG00000136478 | 7 |
| 2768685 | mld | 51427 | ZNF107 | ENSG00000196247 | 2 |
| 2768852 | par-1 | 4140 | MARK3 | ENSG00000075413 | 12 |
| 31004 | CG13366 | 23384 | SPECC1L | ENSG00000100014 | 11 |
| 31017 | sdk | 54549 | SDK2 | ENSG00000069188 | 11 |
| 31121 | CG32809 | 56243 | KIAA1217 | ENSG00000120549 | 9 |
| 31130 | Adar | 104 | ADARB1 | ENSG00000197381 | 12 |
| 31169 | CG4313 | 53831 | GPR84 | ENSG00000139572 | 5 |

| | | | | | |
|---------|------------------|--------|----------|-----------------|----|
| 31309 | dnc | 5142 | PDE4B | ENSG00000184588 | 12 |
| 31429 | ovo | 5017 | OVOL1 | ENSG00000172818 | 8 |
| 31496 | IntS6 | 203522 | INTS6L | ENSG00000165359 | 12 |
| 31722 | fs(1)h | 6046 | BRD2 | ENSG00000204256 | 9 |
| 31798 | CG12065 | 7378 | UPP1 | ENSG00000183696 | 1 |
| 31826 | rdgA | 8525 | DGKZ | ENSG00000149091 | 14 |
| 31839 | CG7766 | 5256 | PHKA2 | ENSG00000044446 | 13 |
| 318930 | NimA | 375033 | PEAR1 | ENSG00000187800 | 4 |
| 31957 | alpha-Man- la | 10905 | MAN1A2 | ENSG00000198162 | 13 |
| 31991 | CG43347 | 79177 | ZNF576 | ENSG00000124444 | 1 |
| 32083 | dlg1 | 1739 | DLG1 | ENSG00000075711 | 13 |
| 32115 | Ptp10D | 5787 | PTPRB | ENSG00000127329 | 11 |
| 32245 | fne | 1993 | ELAVL2 | ENSG00000107105 | 14 |
| 32256 | hep | 5609 | MAP2K7 | ENSG00000076984 | 12 |
| 32278 | HDAC4 | 9759 | HDAC4 | ENSG00000068024 | 11 |
| 32343 | inaE | 747 | DAGLA | ENSG00000134780 | 13 |
| 32442 | Rab3-GEF | 8567 | MADD | ENSG00000110514 | 15 |
| 32461 | HDAC6 | 10013 | HDAC6 | ENSG00000094631 | 14 |
| 32536 | sd | 7003 | TEAD1 | ENSG00000187079 | 13 |
| 32544 | Gbeta13F | 2782 | GNB1 | ENSG00000078369 | 15 |
| 32589 | CG3632 | 9110 | MTMR4 | ENSG00000108389 | 13 |
| 326128 | Ada2a | 6871 | TADA2A | ENSG00000276234 | 12 |
| 32619 | para | 6334 | SCN8A | ENSG00000196876 | 12 |
| 326215 | SMC5 | 23137 | SMC5 | ENSG00000198887 | 12 |
| 32771 | mnb | 1859 | DYRK1A | ENSG00000157540 | 10 |
| 32930 | kek5 | 340745 | LRIT2 | ENSG00000204033 | 2 |
| 33002 | Nup205 | 23165 | NUP205 | ENSG00000155561 | 13 |
| 33048 | RhoGAP19D | 57636 | ARHGAP23 | ENSG00000275832 | 8 |
| 33137 | l(1)G0196 | 23262 | PIIP5K2 | ENSG00000145725 | 13 |
| 33156 | l(2)gl | 3996 | LLGL1 | ENSG00000131899 | 15 |
| 33158 | Cda5 | 1486 | CTBS | ENSG00000117151 | 1 |
| 33204 | Plc21C | 23236 | PLCB1 | ENSG00000182621 | 13 |
| 33392 | aop | 2120 | ETV6 | ENSG00000139083 | 10 |
| 3346235 | scaf6 | 10523 | CHERP | ENSG00000085872 | 12 |
| 3346237 | nab | 4664 | NAB1 | ENSG00000138386 | 11 |
| 33690 | smog | 57512 | GPR158 | ENSG00000151025 | 7 |
| 33807 | CG9171 | 11041 | B4GAT1 | ENSG00000174684 | 7 |
| 33928 | CG31635 | 284352 | PPP1R37 | ENSG00000104866 | 8 |

| | | | | | |
|---------|------------|--------|----------|-----------------|----|
| 34030 | Ziz | 23348 | DOCK9 | ENSG00000088387 | 12 |
| 34038 | Slob | 54899 | PXK | ENSG00000168297 | 4 |
| 34112 | Piezo | 63895 | PIEZO2 | ENSG00000154864 | 13 |
| 34327 | CG5850 | 55751 | TMEM184C | ENSG00000164168 | 13 |
| 34686 | MRP | 8714 | ABCC3 | ENSG00000108846 | 14 |
| 34701 | CG9932 | 58499 | ZNF462 | ENSG00000148143 | 3 |
| 34831 | Dyrk2 | 8798 | DYRK4 | ENSG00000010219 | 12 |
| 34888 | stc | 4799 | NFX1 | ENSG00000086102 | 14 |
| 34950 | Ca-alpha1D | 776 | CACNA1D | ENSG00000157388 | 13 |
| 34982 | dac | 1602 | DACH1 | ENSG00000276644 | 12 |
| 35042 | CLIP-190 | 6249 | CLIP1 | ENSG00000130779 | 12 |
| 35047 | dl | 5970 | RELA | ENSG00000173039 | 9 |
| 35077 | rdo | 79883 | PODNL1 | ENSG00000132000 | 1 |
| 35107 | Pde11 | 8654 | PDE5A | ENSG00000138735 | 11 |
| 35109 | CG15160 | 23248 | RPRD2 | ENSG00000163125 | 11 |
| 35173 | Acn | 22985 | ACIN1 | ENSG00000100813 | 10 |
| 35340 | dia | 1730 | DIAPH2 | ENSG00000147202 | 14 |
| 35376 | Nhe2 | 6553 | SLC9A5 | ENSG00000135740 | 12 |
| 35402 | Mondo | 22877 | MLXIP | ENSG00000175727 | 13 |
| 35408 | nrv3 | 481 | ATP1B1 | ENSG00000143153 | 14 |
| 35652 | Dscam1 | 57453 | DSCAML1 | ENSG00000177103 | 13 |
| 35715 | LRR | 55604 | CARMIL1 | ENSG00000079691 | 15 |
| 35900 | babo | 7046 | TGFBR1 | ENSG00000106799 | 14 |
| 35950 | Pkn | 5586 | PKN2 | ENSG00000065243 | 13 |
| 36084 | CAP | 10174 | SORBS3 | ENSG00000120896 | 7 |
| 36527 | fl(2)d | 9589 | WTAP | ENSG00000146457 | 11 |
| 36658 | Pcf11 | 51585 | PCF11 | ENSG00000165494 | 11 |
| 36753 | Strn-Mlck | 4638 | MYLK | ENSG00000065534 | 4 |
| 36978 | Patronin | 23271 | CAMSAP2 | ENSG00000118200 | 13 |
| 37038 | grh | 29841 | GRHL1 | ENSG00000134317 | 8 |
| 37152 | Sik3 | 23387 | SIK3 | ENSG00000160584 | 3 |
| 37199 | CG15118 | 338692 | ANKRD13D | ENSG00000172932 | 14 |
| 37254 | sm | 3191 | HNRNPL | ENSG00000104824 | 12 |
| 37288 | Ate1 | 11101 | ATE1 | ENSG00000107669 | 14 |
| 37528 | Fmr1 | 8087 | FXR1 | ENSG00000114416 | 12 |
| 3772382 | Plp | 5116 | PCNT | ENSG00000160299 | 6 |
| 37979 | NKAIN | 154215 | NKAIN2 | ENSG00000188580 | 9 |
| 38063 | CG1233 | 79894 | ZNF672 | ENSG00000171161 | 1 |
| 38173 | hfp | 22827 | PUF60 | ENSG00000179950 | 14 |

| | | | | | |
|-------|---------|--------|---------|-----------------|----|
| 38257 | mu2 | 9656 | MDC1 | ENSG00000137337 | 4 |
| 38327 | MEP-1 | 5326 | PLAGL2 | ENSG00000126003 | 1 |
| 38427 | armi | 54456 | MOV10L1 | ENSG00000073146 | 10 |
| 38963 | Unr | 7812 | CSDE1 | ENSG00000009307 | 15 |
| 39198 | Rbfox1 | 54715 | RBFOX1 | ENSG00000078328 | 9 |
| 39258 | IRSp53 | 10458 | BAIAP2 | ENSG00000175866 | 10 |
| 39262 | GlcAT-P | 27087 | B3GAT1 | ENSG00000109956 | 4 |
| 39533 | dysc | 25861 | WHRN | ENSG00000095397 | 11 |
| 39744 | brm | 6595 | SMARCA2 | ENSG00000080503 | 13 |
| 39902 | CG3764 | 57600 | FNIP2 | ENSG00000052795 | 12 |
| 39919 | Rbp6 | 124540 | MSI2 | ENSG00000153944 | 13 |
| 40167 | Papss | 9061 | PAPSS1 | ENSG00000138801 | 14 |
| 40171 | Su(Tpl) | 22936 | ELL2 | ENSG00000118985 | 10 |
| 40220 | CG17233 | 79780 | CCDC82 | ENSG00000149231 | 5 |
| 40433 | Nopp140 | 9221 | NOLC1 | ENSG00000166197 | 3 |
| 40461 | SrpK79D | 26576 | SRPK3 | ENSG00000184343 | 9 |
| 40515 | nrm | 84033 | OBSCN | ENSG00000154358 | 1 |
| 40560 | CG32944 | 55351 | STK32B | ENSG00000152953 | 13 |
| 40567 | CG31522 | 79993 | ELOVL7 | ENSG00000164181 | 14 |
| 40793 | gpp | 84444 | DOT1L | ENSG00000104885 | 12 |
| 40928 | CG17816 | 56890 | MDM1 | ENSG00000111554 | 1 |
| 41145 | mura | 152006 | RNF38 | ENSG00000137075 | 7 |
| 41225 | Mical | 9645 | MICAL2 | ENSG00000133816 | 8 |
| 41592 | CG31342 | 6386 | SDCBP | ENSG00000137575 | 4 |
| 41612 | sim | 6492 | SIM1 | ENSG00000112246 | 9 |
| 41737 | trx | 9757 | KMT2B | ENSG00000272333 | 9 |
| 41817 | CG42788 | 9758 | FRMPD4 | ENSG00000169933 | 9 |
| 41911 | nsI1 | 284058 | KANSL1 | ENSG00000120071 | 9 |
| 42150 | Rim | 22999 | RIMS1 | ENSG00000079841 | 10 |
| 42413 | CG4360 | 7637 | ZNF84 | ENSG00000198040 | 1 |
| 42601 | SKIP | 54440 | SASH3 | ENSG00000122122 | 6 |
| 42687 | wge | 84629 | TNRC18 | ENSG00000182095 | 7 |
| 42824 | sba | 55777 | MBD5 | ENSG00000204406 | 7 |
| 42845 | Miro | 55288 | RHOT1 | ENSG00000126858 | 14 |
| 42854 | Syx1A | 6804 | STX1A | ENSG00000106089 | 15 |
| 42935 | puf | 9736 | USP34 | ENSG00000115464 | 14 |
| 43105 | LpR2 | 7436 | VLDLR | ENSG00000147852 | 12 |
| 43126 | CG5890 | 30820 | KCNIP1 | ENSG00000182132 | 13 |
| 43130 | Lnk | 10603 | SH2B2 | ENSG00000160999 | 11 |

| | | | | | |
|---------|---------|-------|----------|-----------------|----|
| 43317 | Tusp | 56995 | TULP4 | ENSG00000130338 | 13 |
| 43399 | CG1646 | 55015 | PRPF39 | ENSG00000185246 | 10 |
| 43469 | Ptp99A | 5793 | PTPRG | ENSG00000144724 | 9 |
| 43505 | Wdr24 | 84219 | WDR24 | ENSG00000127580 | 14 |
| 43535 | CG31038 | 23625 | FAM89B | ENSG00000176973 | 2 |
| 43710 | PNPase | 87178 | PNPT1 | ENSG00000138035 | 15 |
| 43788 | Hcf | 29915 | HCFC2 | ENSG00000111727 | 9 |
| 43809 | Slip1 | 23024 | PDZRN3 | ENSG00000121440 | 11 |
| 43856 | nej | 2033 | EP300 | ENSG00000100393 | 12 |
| 43923 | axo | 26047 | CNTNAP2 | ENSG00000174469 | 5 |
| 43924 | jim | 10794 | ZNF460 | ENSG00000197714 | 2 |
| 43997 | jbug | 2316 | FLNA | ENSG00000196924 | 3 |
| 44018 | cas | 54897 | CASZ1 | ENSG00000130940 | 7 |
| 44039 | Pak | 5058 | PAK1 | ENSG00000149269 | 14 |
| 44160 | sw | 1781 | DYNC1I2 | ENSG00000077380 | 13 |
| 44448 | scrib | 23513 | SCRIB | ENSG00000180900 | 7 |
| 44861 | sdt | 64398 | MPP5 | ENSG00000072415 | 12 |
| 45248 | Nckx30C | 25769 | SLC24A2 | ENSG00000155886 | 14 |
| 45320 | trol | 3339 | HSPG2 | ENSG00000142798 | 11 |
| 45380 | spin | 83985 | SPNS1 | ENSG00000169682 | 13 |
| 46194 | Spn | 55607 | PPP1R9A | ENSG00000158528 | 11 |
| 48571 | heph | 5725 | PTBP1 | ENSG00000011304 | 13 |
| 48973 | Src64B | 6714 | SRC | ENSG00000197122 | 9 |
| 49070 | Mbs | 4660 | PPP1R12B | ENSG00000077157 | 13 |
| 49968 | Cadps | 8618 | CADPS | ENSG00000163618 | 14 |
| 50225 | Prosap | 50944 | SHANK1 | ENSG00000161681 | 11 |
| 7354466 | CG42342 | 1305 | COL13A1 | ENSG00000197467 | 3 |
| 7354470 | CG42402 | 59271 | EVA1C | ENSG00000166979 | 8 |

| (A) Alzheimer's Disease enrichment for genes with altered splicing in APP vs wildtype | | | | | |
|---|-------------|--------------|--------------|---------------|--|
| No. | Fly Gene ID | Fly Symbol | Human Symbol | Human Gene ID | Gene Full Name |
| 1 | 2768852 | par-1 | MARK3 | 4140 | microtubule affinity regulating kinase 3 |
| 2 | 30975 | ewg | NRF1 | 4899 | nuclear respiratory factor 1 |
| 3 | 31121 | CG32809 | KIAA1217 | 56243 | KIAA1217 |
| 4 | 31130 | Adar | ADARB1 | 104 | adenosine deaminase RNA specific B1 |
| 5 | 31353 | CG43689 | ST18 | 9705 | ST18 C2H2C-type zinc finger transcription factor |
| 6 | 31364 | Fas2 | NCAM2 | 4685 | neural cell adhesion molecule 2 |
| 7 | 31379 | bi | TBX2 | 6909 | T-box transcription factor 2 |
| 8 | 31722 | fs(1)h | BRD2 | 6046 | bromodomain containing 2 |
| 9 | 32083 | dlg1 | DLG1 | 1739 | discs large MAGUK scaffold protein 1 |
| 10 | 32273 | sno | SBNO1 | 55206 | strawberry notch homolog 1 |
| 11 | 32278 | HDAC4 | HDAC4 | 9759 | histone deacetylase 4 |
| 12 | 32442 | Rab3-GEF | MADD | 8567 | MAP kinase activating death domain |
| 13 | 32569 | vap | RASA1 | 5921 | RAS p21 protein activator 1 |
| 14 | 32941 | CoRest | RCOR1 | 23186 | REST corepressor 1 |
| 15 | 34127 | Pvr | KDR | 3791 | kinase insert domain receptor |
| 16 | 34519 | SCAR | WASF3 | 10810 | WASP family member 3 |
| 17 | 34772 | kuz | ADAM10 | 102 | ADAM metallopeptidase domain 10 |
| 18 | 35071 | CadN2 | CDH1 | 999 | cadherin 1 |
| 19 | 35077 | rdo | IGFALS | 3483 | insulin like growth factor binding protein acid labile subunit |
| 20 | 35090 | CG42750 | DPEP2 | 64174 | dipeptidase 2 |
| 21 | 35107 | Pde11 | PDE5A | 8654 | phosphodiesterase 5A |
| 22 | 35524 | Src42A | FRK | 2444 | fyn related Src family tyrosine kinase |
| 23 | 35540 | EcR | NR1H3 | 10062 | nuclear receptor subfamily 1 group H member 3 |
| 24 | 35652 | Dscam1 | DSCAML1 | 57453 | DS cell adhesion molecule like 1 |
| 25 | 36121 | CG11883 | NT5E | 4907 | 5'-nucleotidase ecto |
| 26 | 36542 | shot | DST | 667 | dystonin |
| 27 | 37129 | CG43066 | SLC6A15 | 55117 | solute carrier family 6 member 15 |
| 28 | 37552 | Liprin-gamma | KAZN | 23254 | kazrin, periplakin interacting protein |
| 29 | 37641 | nahoda | GPRASP2 | 114928 | G protein-coupled receptor associated sorting protein 2 |
| 30 | 3771968 | Msp300 | SYNE1 | 23345 | spectrin repeat containing nuclear envelope protein 1 |
| 31 | 37892 | mAChR-A | CHRM1 | 1128 | cholinergic receptor muscarinic 1 |
| 32 | 38175 | Psa | NPEPPS | 9520 | aminopeptidase puromycin sensitive |
| 33 | 38487 | CG14995 | CFAP410 | 755 | cilia and flagella associated protein 410 |

| 34 | 39198 | Rbfox1 | RBFOX1 | 54715 | RNA binding fox-1 homolog 1 |
|---|-------------|------------|--------------|---------------|---|
| 35 | 39999 | Eip75B | PPARG | 5468 | peroxisome proliferator activated receptor gamma |
| 36 | 40924 | CG2993 | TXNIP | 10628 | thioredoxin interacting protein |
| 37 | 42327 | Dys | DMD | 1756 | dystrophin |
| 38 | 42491 | Cortactin | CTTN | 2017 | cortactin |
| 39 | 42646 | Nrx-1 | NRXN1 | 9378 | neurexin 1 |
| 40 | 42840 | CG13604 | UBASH3B | 84959 | ubiquitin associated and SH3 domain containing B |
| 41 | 42940 | slo | KCNMA1 | 3778 | potassium calcium-activated channel subfamily M alpha 1 |
| 42 | 43087 | msi | MSI2 | 124540 | musashi RNA binding protein 2 |
| 43 | 43673 | dco | CSNK1D | 1453 | casein kinase 1 delta |
| 44 | 43795 | zfh2 | ZFHX3 | 463 | zinc finger homeobox 3 |
| 45 | 44885 | mys | ITGB1 | 3688 | integrin subunit beta 1 |
| 46 | 45248 | Nckx30C | SLC24A2 | 25769 | solute carrier family 24 member 2 |
| 47 | 45320 | trol | HSPG2 | 3339 | heparan sulfate proteoglycan 2 |
| 48 | 45884 | kkv | HAS1 | 3036 | hyaluronan synthase 1 |
| 49 | 48571 | heph | PTBP1 | 5725 | polypyrimidine tract binding protein 1 |
| 50 | 49090 | RyR | RYR2 | 6262 | ryanodine receptor 2 |
| 51 | 5740528 | CG34354 | TIA1 | 7072 | TIA1 cytotoxic granule associated RNA binding protein |
| 52 | 64875 | disco-r | BNC1 | 54796 | basenuclin 1 |
| 53 | 64877 | cpx | CPLX1 | 10815 | complexin 1 |
| 54 | 8674055 | mgl | LRP2 | 4036 | LDL receptor related protein 2 |
| (B) Alzheimer's Disease enrichment for genes with altered splicing in APP;Tip60 vs APP | | | | | |
| No. | Fly Gene ID | Fly Symbol | Human Symbol | Human Gene ID | Gene Full Name |
| 1 | 2768852 | par-1 | MARK3 | 4140 | microtubule affinity regulating kinase 3 |
| 2 | 31121 | CG32809 | KIAA1217 | 56243 | KIAA1217 |
| 3 | 31130 | Adar | ADARB1 | 104 | adenosine deaminase RNA specific B1 |
| 4 | 31722 | fs(1)h | BRD2 | 6046 | bromodomain containing 2 |
| 5 | 31826 | rdgA | DGKZ | 8525 | diacylglycerol kinase zeta |
| 6 | 32083 | dlg1 | DLG1 | 1739 | discs large MAGUK scaffold protein 1 |
| 7 | 32245 | fne | ELAVL2 | 1993 | ELAV like RNA binding protein 2 |
| 8 | 32278 | HDAC4 | HDAC4 | 9759 | histone deacetylase 4 |
| 9 | 32442 | Rab3-GEF | MADD | 8567 | MAP kinase activating death domain |
| 10 | 32461 | HDAC6 | HDAC6 | 10013 | histone deacetylase 6 |
| 11 | 32771 | mnb | DYRK1A | 1859 | dual specificity tyrosine phosphorylation |

| | | | | | |
|----|-------|---------|---------|--------|--|
| | | | | | regulated kinase 1A |
| 12 | 33158 | Cda5 | CTBS | 1486 | chitobiase |
| 13 | 33204 | Plc21C | PLCB1 | 23236 | phospholipase C beta 1 |
| 14 | 33928 | CG31635 | PPP1R37 | 284352 | protein phosphatase 1 regulatory subunit 37 |
| 15 | 35047 | dl | RELA | 5970 | RELA proto-oncogene, NF-kB subunit |
| 16 | 35077 | rdo | IGFALS | 3483 | insulin like growth factor binding protein acid labile subunit |
| 17 | 35107 | Pde11 | PDE5A | 8654 | phosphodiesterase 5A |
| 18 | 35652 | Dscam1 | DSCAML1 | 57453 | DS cell adhesion molecule like 1 |
| 19 | 35900 | babo | TGFBR1 | 7046 | transforming growth factor beta receptor 1 |
| 20 | 36084 | CAP | SORBS3 | 10174 | sorbin and SH3 domain containing 3 |
| 21 | 37979 | NKAIN | NKAIN2 | 154215 | sodium/potassium transporting ATPase interacting 2 |
| 22 | 39198 | Rbfox1 | RBFOX1 | 54715 | RNA binding fox-1 homolog 1 |
| 23 | 39262 | GlcAT-P | B3GAT1 | 27087 | beta-1,3-glucuronyltransferase 1 |
| 24 | 39919 | Rbp6 | MSI2 | 124540 | musashi RNA binding protein 2 |
| 25 | 40433 | Nopp140 | NOLC1 | 9221 | nucleolar and coiled-body phosphoprotein 1 |
| 26 | 40515 | nrm | SIRPB1 | 10326 | signal regulatory protein beta 1 |
| 27 | 40560 | CG32944 | STK32B | 55351 | serine/threonine kinase 32B |
| 28 | 41225 | Mical | MICAL2 | 9645 | microtubule associated monooxygenase, calponin and LIM domain containing 2 |
| 29 | 41592 | CG31342 | SDCBP2 | 27111 | syndecan binding protein 2 |
| 30 | 41612 | sim | SIM2 | 6493 | SIM bHLH transcription factor 2 |
| 31 | 42854 | Syx1A | STX1A | 6804 | syntaxin 1A |
| 32 | 43105 | LpR2 | VLDLR | 7436 | very low density lipoprotein receptor |
| 33 | 43317 | Tusp | TULP4 | 56995 | TUB like protein 4 |
| 34 | 43469 | Ptp99A | PTPRG | 5793 | protein tyrosine phosphatase receptor type G |
| 35 | 43856 | nej | EP300 | 2033 | E1A binding protein p300 |
| 36 | 43923 | axo | CNTNAP2 | 26047 | contactin associated protein 2 |
| 37 | 43997 | jbug | FLNA | 2316 | filamin A |
| 38 | 44018 | cas | CASZ1 | 54897 | castor zinc finger 1 |
| 39 | 44039 | Pak | PAK1 | 5058 | p21 (RAC1) activated kinase 1 |
| 40 | 45248 | Nckx30C | SLC24A2 | 25769 | solute carrier family 24 member 2 |
| 41 | 45320 | trol | HSPG2 | 3339 | heparan sulfate proteoglycan 2 |
| 42 | 48571 | heph | PTBP1 | 5725 | polypyrimidine tract binding protein 1 |
| 43 | 48973 | Src64B | FYN | 2534 | FYN proto-oncogene, Src family tyrosine kinase |
| 44 | 50225 | Prosap | SHANK1 | 50944 | SH3 and multiple ankyrin repeat domains 1 |

| (A) Skipped Exon (SE) | | | | | | | | | |
|---------------------------------------|----------|-------|--------|--------------------|----------------------------|--------------------------|----------------------------|--------------------------|-----------|
| Genotype comparison | Gene | chr | strand | Skipped exon | Exon Start | Exon End | Upstream Exon Start | Upstream Exon End | Delta PSI |
| APPvsWT | Adar | chrX | + | 3 | 1778369 | 1778560 | 1775698 | 1775738 | -0.238 |
| APPTip60vsAPP | Adar | chrX | + | 3 | 1778369 | 1778560 | 1775698 | 1775738 | 0.336 |
| APPvsWT | Dscam1 | chr2R | - | 9 | 7344663 | 7344954 | 7344278 | 7344569 | -0.182 |
| APPTip60vsAPP | Dscam1 | chr2R | - | 9 | 7344278 | 7344569 | 7332260 | 7332380 | 0.229 |
| APPvsWT | heph | chr3R | - | 6 | 31931774 | 31932614 | 31921632 | 31921674 | -0.421 |
| APPTip60vsAPP | heph | chr3R | - | 6 | 31931774 | 31932614 | 31921632 | 31921674 | 0.305 |
| APPvsWT | kuz | chr2L | + | 3 | 13558799 | 13558832 | 13551141 | 13551666 | -0.244 |
| APPTip60vsAPP | kuz | chr2L | + | 12 | 13636383 | 13636843 | 13635648 | 13636213 | 0.089 |
| APPvsWT | trol | chrX | - | 20 | 2495040 | 2495238 | 2492987 | 2493215 | 0.287 |
| APPTip60vsAPP | trol | chrX | - | 20 | 2495040 | 2495238 | 2492987 | 2493215 | -0.11 |
| (B) Alternative 5' splice site (A5SS) | | | | | | | | | |
| Genotype comparison | Gene | chr | strand | A5SS exon position | Long Exon Start | Long Exon End | Short Exon Start | Short Exon End | Delta PSI |
| APPvsWT | dlg1 | chrX | + | 1 | 11389667 | 11389781 | 11389667 | 11389697 | -0.248 |
| APPTip60vsAPP | dlg1 | chrX | + | 1 | 11389667 | 11389781 | 11389667 | 11389697 | 0.289 |
| APPvsWT | fs(1)h | chrX | - | 1 | 8056316 | 8056701 | 8056609 | 8056701 | -0.209 |
| APPTip60vsAPP | fs(1)h | chrX | - | 1 | 8056316 | 8056701 | 8056609 | 8056701 | 0.154 |
| APPTip60vsAPP | CG32809 | chrX | - | 1 | 1692296 | 1692768 | 1692438 | 1692768 | -0.29 |
| (C) Alternative 3' splice site (A3SS) | | | | | | | | | |
| Genotype comparison | Gene | chr | strand | A3SS exon position | Long Exon Start | Long Exon End | Short Exon Start | Short Exon End | Delta PSI |
| APPvsWT | CG32809 | chrX | - | 3 | 1685186 | 1685535 | 1685186 | 1685279 | 0.632 |
| APPvsWT | HDAC4 | chrX | - | 5 | 13270390 | 13270693 | 13270390 | 13270612 | 0.242 |
| APPvsWT | Nckx30C | chr2L | - | 2 | 9742374 | 9744230 | 9742374 | 9744226 | 0.362 |
| APPTip60vsAPP | Nckx30C | chr2L | - | 1 | 9746406 | 9746495 | 9746433 | 9746495 | -0.231 |
| APPvsWT | Rab3-GEF | chrX | + | 4 | 15094069 | 15094613 | 15094093 | 15094613 | -0.436 |
| APPTip60vsAPP | Rab3-GEF | chrX | + | 4 | 15094069 | 15094613 | 15094093 | 15094613 | 0.366 |
| (D) Mutually exclusive exons (MXE) | | | | | | | | | |
| Genotype comparison | Gene | chr | strand | MXE exon position | 1 st Exon Start | 1 st Exon End | 2 nd Exon Start | 2 nd Exon End | Delta PSI |

| | | | | | | | | | |
|---------------------------------|-------------|------------|---------------|-----------------------------|----------------------|--------------------|----------------------------|--------------------------|------------------|
| APPvsWT | Adar | chrX | + | 2 | 1775649 | 1775738 | 1778369 | 1778560 | 0.634 |
| APPTip60vsAPP | Adar | chrX | + | 2 | 1775649 | 1775738 | 1778369 | 1778560 | -0.621 |
| APPvsWT | Dscam1 | chr2R | - | 6 | 7357590 | 7357714 | 7359441 | 7359565 | -0.83 |
| APPTip60vsAPP | Dscam1 | chr2R | - | 6 | 7357590 | 7357714 | 7359441 | 7359565 | 0.619 |
| APPTip60vsAPP | HDAC4 | chrX | - | 3 | 13276434 | 13276547 | 13282165 | 13282229 | -0.102 |
| APPvsWT | Rbfox1 | chr3L | + | 9 | 10581841 | 10582118 | 10584815 | 10585539 | 0.198 |
| APPTip60vsAPP | Rbfox1 | chr3L | + | 3 | 10568128 | 10568605 | 10571048 | 10571246 | -0.108 |
| (E) Retained intron (RI) | | | | | | | | | |
| Genotype comparison | Gene | chr | strand | Intron between exons | RI Exon Start | RI Exon End | Upstream Exon Start | Upstream Exon End | Delta PSI |
| APPvsWT | Adar | chrX | + | 3 and 4 | 1778369 | 1778699 | 1778369 | 1778560 | 0.19 |
| APPTip60vsAPP | Adar | chrX | + | 3 and 4 | 1778369 | 1778699 | 1778369 | 1778560 | -0.352 |

| Genotype comparison | Gene | chr | strand | MXE exon position | 1 st Exon Start | 1 st Exon End | 2 nd Exon Start | 2 nd Exon End | Delta PSI |
|---------------------|--------|-------|--------|-------------------|----------------------------|--------------------------|----------------------------|--------------------------|-----------|
| APPvsWT | Dscam1 | chr2R | - | 9 | 7334387 | 7334666 | 7343717 | 7344008 | -0.625 |
| APPTip60vsAPP | Dscam1 | chr2R | - | 9 | 7334387 | 7334666 | 7343717 | 7344008 | 0.292 |
| APPvsWT | Dscam1 | chr2R | - | 9 | 7334387 | 7334666 | 7334933 | 7335218 | -0.238 |
| APPTip60vsAPP | Dscam1 | chr2R | - | 9 | 7334387 | 7334666 | 7334933 | 7335218 | 0.196 |
| APPvsWT | Dscam1 | chr2R | - | 9 | 7334387 | 7334666 | 7335715 | 7336003 | -0.218 |
| APPTip60vsAPP | Dscam1 | chr2R | - | 9 | 7334387 | 7334666 | 7335715 | 7336003 | 0.176 |
| APPvsWT | Dscam1 | chr2R | - | 9 | 7334933 | 7335218 | 7337493 | 7337781 | -0.161 |
| APPTip60vsAPP | Dscam1 | chr2R | - | 9 | 7334933 | 7335218 | 7337493 | 7337781 | 0.353 |
| APPvsWT | Dscam1 | chr2R | - | 9 | 7335715 | 7336003 | 7337493 | 7337781 | -0.164 |
| APPTip60vsAPP | Dscam1 | chr2R | - | 9 | 7335715 | 7336003 | 7337493 | 7337781 | 0.25 |
| APPvsWT | Dscam1 | chr2R | - | 9 | 7337493 | 7337781 | 7344278 | 7344569 | 0.105 |
| APPTip60vsAPP | Dscam1 | chr2R | - | 9 | 7337493 | 7337781 | 7344278 | 7344569 | -0.31 |
| APPvsWT | Dscam1 | chr2R | - | 9 | 7337493 | 7337781 | 7345484 | 7345775 | 0.108 |
| APPTip60vsAPP | Dscam1 | chr2R | - | 9 | 7337493 | 7337781 | 7345484 | 7345775 | -0.347 |
| APPvsWT | Dscam1 | chr2R | - | 9 | 7337493 | 7337781 | 7342582 | 7342881 | 0.265 |
| APPTip60vsAPP | Dscam1 | chr2R | - | 9 | 7337493 | 7337781 | 7342582 | 7342881 | -0.433 |
| APPvsWT | Dscam1 | chr2R | - | 9 | 7337493 | 7337781 | 7341327 | 7341618 | 0.432 |
| APPTip60vsAPP | Dscam1 | chr2R | - | 9 | 7337493 | 7337781 | 7341327 | 7341618 | -0.75 |
| APPvsWT | Dscam1 | chr2R | - | 9 | 7337493 | 7337781 | 7345060 | 7345351 | 0.515 |
| APPTip60vsAPP | Dscam1 | chr2R | - | 9 | 7337493 | 7337781 | 7345060 | 7345351 | -0.75 |
| APPvsWT | Dscam1 | chr2R | - | 9 | 7341327 | 7341618 | 7341707 | 7341995 | -0.423 |
| APPTip60vsAPP | Dscam1 | chr2R | - | 9 | 7341327 | 7341618 | 7341707 | 7341995 | 0.551 |
| APPvsWT | Dscam1 | chr2R | - | 9 | 7341327 | 7341618 | 7343717 | 7344008 | -0.361 |
| APPTip60vsAPP | Dscam1 | chr2R | - | 9 | 7341327 | 7341618 | 7343717 | 7344008 | 0.472 |
| APPvsWT | Dscam1 | chr2R | - | 9 | 7349787 | 7349911 | 7350957 | 7351081 | 0.556 |
| APPTip60vsAPP | Dscam1 | chr2R | - | 9 | 7349787 | 7349911 | 7350957 | 7351081 | -0.222 |
| APPvsWT | Dscam1 | chr2R | - | 6 | 7350781 | 7350905 | 7359441 | 7359565 | -0.861 |
| APPTip60vsAPP | Dscam1 | chr2R | - | 6 | 7350781 | 7350905 | 7359441 | 7359565 | 0.383 |
| APPvsWT | Dscam1 | chr2R | - | 6 | 7352898 | 7353022 | 7360081 | 7360205 | -0.667 |
| APPTip60vsAPP | Dscam1 | chr2R | - | 6 | 7352898 | 7353022 | 7360081 | 7360205 | 0.5 |
| APPvsWT | Dscam1 | chr2R | - | 6 | 7352898 | 7353022 | 7358215 | 7358339 | -0.6 |
| APPTip60vsAPP | Dscam1 | chr2R | - | 6 | 7352898 | 7353022 | 7358215 | 7358339 | 0.378 |
| APPvsWT | Dscam1 | chr2R | - | 6 | 7352898 | 7353022 | 7353244 | 7353365 | -0.489 |
| APPTip60vsAPP | Dscam1 | chr2R | - | 6 | 7352898 | 7353022 | 7353244 | 7353365 | 0.356 |
| APPvsWT | Dscam1 | chr2R | - | 6 | 7353244 | 7353365 | 7359441 | 7359565 | -0.374 |
| APPTip60vsAPP | Dscam1 | chr2R | - | 6 | 7353244 | 7353365 | 7359441 | 7359565 | 0.264 |

| | | | | | | | | | |
|---------------|--------|-------|---|---|---------|---------|---------|---------|--------|
| APPvsWT | Dscam1 | chr2R | - | 6 | 7353244 | 7353365 | 7359015 | 7359139 | 0.367 |
| APPTip60vsAPP | Dscam1 | chr2R | - | 6 | 7353244 | 7353365 | 7359015 | 7359139 | -0.389 |
| APPvsWT | Dscam1 | chr2R | - | 6 | 7353244 | 7353365 | 7356316 | 7356440 | 0.474 |
| APPTip60vsAPP | Dscam1 | chr2R | - | 6 | 7353244 | 7353365 | 7356316 | 7356440 | -0.4 |
| APPvsWT | Dscam1 | chr2R | - | 6 | 7353244 | 7353365 | 7359221 | 7359345 | 0.236 |
| APPTip60vsAPP | Dscam1 | chr2R | - | 6 | 7353244 | 7353365 | 7359221 | 7359345 | -0.48 |
| APPvsWT | Dscam1 | chr2R | - | 6 | 7353244 | 7353365 | 7360525 | 7360649 | 0.427 |
| APPTip60vsAPP | Dscam1 | chr2R | - | 6 | 7353244 | 7353365 | 7360525 | 7360649 | -0.5 |
| APPvsWT | Dscam1 | chr2R | - | 6 | 7353244 | 7353365 | 7357590 | 7357714 | 0.688 |
| APPTip60vsAPP | Dscam1 | chr2R | - | 6 | 7353244 | 7353365 | 7357590 | 7357714 | -0.58 |
| APPvsWT | Dscam1 | chr2R | - | 6 | 7354056 | 7354177 | 7356316 | 7356440 | 0.496 |
| APPTip60vsAPP | Dscam1 | chr2R | - | 6 | 7354056 | 7354177 | 7356316 | 7356440 | -0.407 |
| APPvsWT | Dscam1 | chr2R | - | 6 | 7354881 | 7355005 | 7359441 | 7359565 | -0.309 |
| APPTip60vsAPP | Dscam1 | chr2R | - | 6 | 7354881 | 7355005 | 7359441 | 7359565 | 0.333 |
| APPvsWT | Dscam1 | chr2R | - | 6 | 7355086 | 7355210 | 7359441 | 7359565 | -0.419 |
| APPTip60vsAPP | Dscam1 | chr2R | - | 6 | 7355086 | 7355210 | 7359441 | 7359565 | 0.328 |
| APPvsWT | Dscam1 | chr2R | - | 6 | 7355086 | 7355210 | 7360525 | 7360649 | 0.359 |
| APPTip60vsAPP | Dscam1 | chr2R | - | 6 | 7355086 | 7355210 | 7360525 | 7360649 | -0.396 |
| APPvsWT | Dscam1 | chr2R | - | 6 | 7355086 | 7355210 | 7357590 | 7357714 | 0.578 |
| APPTip60vsAPP | Dscam1 | chr2R | - | 6 | 7355086 | 7355210 | 7357590 | 7357714 | -0.467 |
| APPvsWT | Dscam1 | chr2R | - | 6 | 7357182 | 7357306 | 7357590 | 7357714 | 0.523 |
| APPTip60vsAPP | Dscam1 | chr2R | - | 6 | 7357182 | 7357306 | 7357590 | 7357714 | -0.5 |
| APPvsWT | Dscam1 | chr2R | - | 6 | 7357590 | 7357714 | 7359441 | 7359565 | -0.83 |
| APPTip60vsAPP | Dscam1 | chr2R | - | 6 | 7357590 | 7357714 | 7359441 | 7359565 | 0.619 |
| APPvsWT | Dscam1 | chr2R | - | 6 | 7357590 | 7357714 | 7360081 | 7360205 | -0.606 |
| APPTip60vsAPP | Dscam1 | chr2R | - | 6 | 7357590 | 7357714 | 7360081 | 7360205 | 0.611 |
| APPvsWT | Dscam1 | chr2R | - | 6 | 7358806 | 7358930 | 7359441 | 7359565 | -0.619 |
| APPTip60vsAPP | Dscam1 | chr2R | - | 6 | 7358806 | 7358930 | 7359441 | 7359565 | 0.417 |
| APPvsWT | Dscam1 | chr2R | - | 6 | 7359441 | 7359565 | 7360290 | 7360414 | 0.813 |
| APPTip60vsAPP | Dscam1 | chr2R | - | 6 | 7359441 | 7359565 | 7360290 | 7360414 | -0.458 |